Title
Pericyclases & Pericyclic Reactions in Nature

Author
Jamieson, Cooper

Publication Date
2021

Peer reviewed|Thesis/dissertation

UNIVERSITY OF CALIFORNIA

Los Angeles

Pericyclases & Pericyclic Reactions in Nature

A dissertation submitted in partial satisfaction of the requirements for the degree

Doctor of Philosophy in Chemistry

by

Cooper Stergis Jamieson

2021

ABSTRACT OF THE DISSERTATION

Pericyclases & Pericyclic Reactions in Nature

by

Cooper Stergis Jamieson

Doctor of Philosophy in Chemistry

University of California, Los Angeles, 2021

Professor Kendall N. Houk, Chair

Woodward and Hoffmann introduced the concept of pericyclic reactions in “The Conservation of Orbital Symmetry” and defined them as “reactions in which all first-order changes in bonding relationships take place in concert on a closed curve.” Since this seminal publication, pericyclic reactions like the Diels–Alder reaction, the sigmatropic Claisen rearrangement, or the Alder-ene reaction have been applied to countless syntheses. Such reactions are often referred to as classics in synthesis or as “powerful” synthetic transformations. Herein, pericyclases are defined as those enzymes that catalyze pericyclic reactions. Many researchers have proposed that such enzymes must exist based on primary and secondary metabolite structure, but these cryptic enzymes have remained elusive until now. In Chapters One through Six, I describe enzymes that cannibalize canonical enzyme folds to catalyze classic organic reactions; this fact makes

cannibalize canonical enzyme folds to catalyze classic organic reactions; this fact makes uncovering these enzymes require retro-biosynthetic logic. Using modern genomics, sequence data, retro-biosynthetic and chemical logic, I was able to uncover multiple examples of enzymes that catalyze pericyclic reactions and name these enzymes the pericyclases. This transdisciplinary work led to discoveries of Diels–Alder reactions in varicidin, ilicicolin, leporin, and eupenifeldin biosynthesis, and Alder-ene reactions in pyridoxatin biosynthesis. Such discoveries laid the groundwork for this new enzyme superfamily named the pericyclases. Lastly, these are not isolated examples: genome mining revealed related enzymes to be spread all across the fungi kingdom and indicates nature's utility of pericyclic reactions in all walks of life.

Chapter One is a review article on characterized examples of pericyclic reactions in nature. First, this chapter outlines the class of pericyclic reactions and their utility in synthesis. Then goes on to highlight known examples of enzyme catalyzed pericyclic reactions in natural systems. This chapter closes by showcasing which pericyclic reactions are yet to be discovered in natural systems.

Chapter Two describes the biosynthesis of the varicidins. Computational studies proposed a unique "carboxylative deactivation" strategy where a six-electron oxidation of a terminal methyl group to a carboxylic acid slows the non-enzymatic Diels–Alder reaction by > 10^4-fold. This rate reduction allows for the enzyme PvhB to control the cycloaddition step and catalyze the more challenging *exo* Diels–Alder to form the key *cis*-fused decalin moiety of the varicidins.

Chapter Three describes the biosynthesis of the ilicicolins. Computational studies determined that the key enzymatic Diels–Alder step is an ambimodal reaction in which both *epi*-8 ilicicolin H and ilicicolin I form from a single transition state. The enzyme IccD that catalyzes the Diels–Alder reaction accelerates it by 10^5-fold and selectively forms *epi*-8 ilicicolin H in greater than 99%. This report is the first example of an ambimodal Diels–Alder/Diels–Alder reaction catalyzed by an enzyme. Furthermore, at the time of publication this is the greatest rate acceleration of a pericyclic reaction in a natural system.

Chapter Four describes the biosynthesis of neosetophomone B and eupenifeldin natural products. Calculations verified that this intermolecular Diels–Alder reaction is a concerted process and rationalized how stereoselectivity is achieved. This report is the first example of an enzymatic intermolecular Diels–Alder reaction.

Chapter Five describes how LepI catalyzes a stereoselective dehydration and three pericyclic reactions: a Diels–Alder reaction, a hetero-Diels–Alder reaction, and a retro-Claisen rearrangement. Molecular dynamics simulations revealed how the stereoselective dehydration is achieved. Docking of transition state structures aided in rationalizing *endo*/*exo* selectivity and observed periselectivity. In total, our studies of LepI provide mechanistic insight into enzymatic dehydration-triggered Diels–Alder and hetero-Diels–Alder reactions, as well as hydrogen bonding and electrostatic catalysis of the retro-Claisen rearrangement.

Chapter Six describes the first enzymatic example of the Alder-ene reaction in biology. Computational studies played a crucial role in proposing that the pyridoxatin system would be a good choice to discover an enzymatic Alder-ene reaction. Furthermore, molecular dynamics simulations and 'theozyme' calculations rationalized how catalysis is achieved. These simple quantum mechanical models predicted single point mutations that allowed for the pericyclic reaction type to switch from Alder-ene to hetero-Diels–Alder and *vice versa*.

Chapter Seven is a theoretical investigation on early examples of the [6+4] cycloaddition reaction. Related cycloaddition reactions have recently discovered in spinosyn, heronamide, and streptoseomycin biosynthesis. This study proposes a general postulate that all *endo* higher-order cycloadditions are ambimodal and lead to multiple products from a single transition state.

The dissertation of Cooper Stergis Jamieson is approved.

Neil Kamal Garg

Justin Ryan Caram

Yi Tang

Kendall N. Houk, Committee Chair

University of California, Los Angeles

2021

Table of Contents

List of Schemes

List of Figures

Figure 11
A. The Claisen rearrangement ([3,3]-sigmatropic shift) catalyzed by chorismate mutase; reactions putatively catalyzed by (***B.***) isochorismate-pyrridole lyase, (***C.***) precorrin-8x methyl mutase, and (***D.***) dimethylallyltryptophane synthase.

Figure 12
Intramolecular Diels-Alder reactions to form *cis*- and *trans*-octahydrodecalins.

Figure 13
The MycB-catalyzed Diels-Alder reaction with calculated free energy barriers for spontaneous and model-catalyzed reactions.

Figure 14
SpnF-catalyzed transannular cycloaddition reactions of the macrocyclic precursor via the single ambimodal transition state to form the [4+2] and [6+4] adducts. Ratios given are from MD simulations, although the rapid Cope rearrangement converts the [6+4] adduct to the more stable Diels-Alder adduct for thermodynamic reasons.

Figure 15
A. Reactions catalyzed by LepI in leporin C biosynthesis. ***B.*** Summary of cascade of LepI-catalyzed reactions. ***C.*** Ambimodal transition state structures and asymmetrical bifurcating PES for the formation of leporin C and DA-1 from (*E*)-QM.

Figure 16
A. The Cope rearrangement involved in hapalindole and fischerindole biosynthesis. ***B.*** The likely acid-catalyzed stepwise (nonpericyclic) mechanism.

Figure 17
Proposed pericyclic (***A.***) Alder-ene reaction in catalysis of Ccr; (***B.***) retro-[2,3]-Wittig and Claisen rearrangements catalyzed by AuaG.

Figure 18
Lipocalin-like DAses catalyzes IMDA reactions in biosynthesis of decalin-containing fungal NPs. (***A.***) Characterized DAses and their decalin containing products; (***B.***) Genome mining of a DAse (PvhB) containing cryptic gene cluster from P. variable. Abbreviations: KS, ketosynthase; MAT, malonyl-CoA transferase; DH, dehydratase; MT, methyltransferase; KR, ketoreductase; ACP, acyl carrier protein; C, condensation; A, adenylation; T, thiolation; R, reductase. MFS: major facilitator superfamily; TF: transcription factor; N-MT: N-methyltransferase; ER: enoylreductase; DAse: Diels-Alderase.

Figure 19
Biosynthesis of varicidin A **1**. (***A.***) Product profiles of *A. nidulans* transformed with combinations of pvh genes; (***B.***) The proposed biosynthetic pathway of **1**; (***C.***)

Biochemical characterization of the DAse PvhB *in vitro*. The traces are HPLC with λ = 280 nm. (***D.***) Crystal structure of **2**.

Figure 20
DFT calculated transition states of NEDDA and IEDDA. ***A.*** Transition state structures **TS-1** and **TS-2** with energies shown for nonenzymatic endo-cyclizations of **3** forming **4** and **5**, respectively. ***B.*** *endo* **TS-3** and *exo* **TS-4** of IEDDA reactions in solution as dianions. **TS-4** leads to formation of the *cis*-decalin stereochemistry for varicidin A. ***C.*** *endo* **TS-5** and *exo* **TS-6** of NEDDA reactions when tetramic acid is protonated.

Figure 21
NEDDA and IEDDA reactions. ***A.*** General scheme of both reactions. EWG: electron withdrawing group; EDG: electron donating group; ***B.*** Proposed enzyme-catalyzed IEDDA reaction in ilicicolin H (**8**) biosynthesis, as demonstrated in total synthetic effort towards **8**.

Figure 22
Characterization of ilicicolin H (**8**) biosynthesis. ***A.*** The icc cluster encodes a PKS-NRPS (KS-AT-DH-MT-KR-ERo-ACP-C-A-T-R. KS, ketosynthase; AT, acyltransferase; DH, dehydratase; MT, methyltransferase; KR, ketoreductase; ACP, acyl carrier protein; C, condensation; A, adenylation; PCP, peptidyl carrier protein; R, reductase) IccA, a trans-ER IccB, a ring expansion P450 IccC, a putative C-methyltransferase IccD and a putative old yellow enzyme IccE; ***B.*** Product profiles from heterologous expression of different combinations of icc cluster in *A. nidulans* A1145. Control in trace *i* is *A. nidulans* transformed with empty vectors only; ***C.*** Proposed biosynthetic pathway of **8**; ***D.*** *In vitro* characterization of IccE-catalyzed epimerization. The assays were conducted in 50 mM Tris-HCl at pH 7.0, in the presence of 0.2 mM **9** and 0.1 μM IccE.

Figure 23
Characterization of IccD-catalyzed pericyclic reaction. ***A.*** HPLC profile of time-course reaction of IccD. The assays were conducted at 28°C from 0 to 120 min; ***B.*** Comparison of relative IEDDA and NEDDA product ratio starting from **11**; ***C.*** Calculated reaction surface energies and dynamics results from **11** converting to **9** and **12**. RDY: reaction dynamics yield from **TS-7**.

Figure 24
Representative tropolone-sesquiterpenes probably generated from intermolecular Diels–Alder reactions.

Figure 25
A. Proposed biosynthetic pathways of **13** and **15**. ***B.*** The eupf gene cluster in *P. janthinellum*.

Figure 26
Generation of potential precursors in the biosynthesis of **13**. (***A.,B.,C.***) LCMS traces from heterologous expression of eupfABC/DG in *A. nidulans* or from *in vitro* assay of EupfE. ***D.*** Generation of **17** and **20**.

Figure 27
Biosynthesis of **13** and **14**. ***A.*** LCMS traces from *in vitro* assay of EupF. ***B.*** DFT-computed free energies for hDA reaction between **20** and **18**. ***C.*** Biosynthetic pathway of **13**.

Figure 28
Leporin C biosynthesis pathway highlighting LepI-catalyzed reaction cascade. In the absence of LepI, spontaneous dehydration of alcohol **25** yields a (*E*/*Z*)-mixture of quinone methides (**26**/**27**), which nonenzymatically form Diels-Alder and hetero Diels-Alder adducts. The compounds used in structural study are highlighted by maroon boxes.

Figure 29
LepI structure and the SAM binding site. (***A.***) The overall tertiary structure of LepI is shown in cartoon model, with the N-terminal dimerization domain and C-terminal catalytic domain colored in blue and red, respectively. Simulated-annealing omit map (grey mesh, contoured at 2.5 σ) indicates binding of SAM at the canonical SAM binding site. (***B.***) Intimate LepI homodimer featured by an intertwined dimer interface. (***C.***) Close-up view of SAM binding site. Hydrogen bond interactions are indicated with black dashes. (***D.***) Next to SAM is a large substrate binding cavity and its entrance tunnel (shown together as green surface). The volume of cavity was calculated using POCASA.[9]

Figure 30
Crystal structure of LepI pseudo enzyme-substrate complex and enzyme-product complex. Simulated-annealing omit maps are shown in black mesh and contoured at 3.0 σ. Hydrogen bond interactions are indicated with black dashed lines. ***A.*** Crystal structure of LepI-SAM-**24** (pseudo enzyme-substrate complex). Note that two rotamers of R295 and M45(B) are observed, and two conformations of diene (*s*-trans and *s*-cis) are modeled according to the electron density. Residues from monomer A are colored in salmon, whereas residues from monomer B are colored in light blue and labeled with B in parenthesis. ***B.*** Superposition of LepI-SAM-**24** complex (colored as in (***A.***)) with unliganded LepI-SAM (residues are colored in dark green while SAM is colored in black). Substantial conformational changes are observed for F189, R295, R197, and M45(B). ***C.*** Crystal structure of LepI-SAM-**33 10**. Residues and ligands are color coded as in (***A.***). ***D.*** Superposition of LepI-SAM-**33 10** (residues are colored in white, SAM is colored in gray, ligand is colored in orange) with LepI-SAM-1 (color coded as in (***A.***), note that ethylene glycol is not shown here for clarity).

Figure 31
LepI Mutant activity. ***A.*** In vivo activity of LepI or mutants to synthesize leporin C (**33**) starting from the alcohol substrate **25**. **25** is synthesized by upstream biosynthetic enzymes. ***B.*** *In vitro* retro-Claisen rearrangement activity using **32** as the substrate.

Asterisks indicate mutants with no measurable activity. Error bars show square deviation (s.d.) of three independent experiments (n = 3).

Figure 32
Proposed catalytic mechanism of LepI. Dashed straight lines indicate hydrogen bonds.

Figure 33
Pericyclic reactions in natural product biosynthesis. ***A.*** Known and unknown enzymatic examples of pericyclic reactions. ***B.*** The biosynthesis of leporin B involves a multifunctional O-methyltransferase-like pericyclase LepI. ***C.*** Theoretical investigations indicate that hetero-Diels–Alder **TS-15** is nonenzymatically favored by 1.9 kcal·mol^{-1} over Alder-ene **TS-14** from a common intermediate **40**. Further transformations lead to natural products pyridoxatin **34**, cordypyridones, asperpyridone **35** and fusaricide **36**. ***D.*** The biosynthetic gene cluster (lep) of leporin B from Aspergillus flavus, the putative biosynthetic gene cluster (adx) of pyridoxatin from Albophoma yamanashiensis, the putative biosynthetic gene cluster (pdx) of pyridoxatin from Aspergillus bombycis, and the putative biosynthetic gene cluster (epi) of fusaricide from Epicoccum sorghinum FT1062. PKS-NRPS, polyketide synthase-nonribosomal peptide synthetase; TF, transcription factor; MCT, monocarboxylate transporter; P450, cytochrome P450; SDR, short-chain dehydrogenase/reductase; ER, enoylreductase; PC, pericyclase. ***E.*** The proposed biosynthesis of the Alder-ene product (**41**) and the hetero-Diels–Alder product (**42**) from the common intermediate **40**. ***F.*** One-pot *in vitro* tandem assay of **38** with PdxG and in the presence or absence of selected pericyclases.

Figure 34
Crystal structures of PdxI and HpiI. Simulated annealing omit map shown in grey mesh and contoured at 1.0 σ. Hydrogen bond interactions are indicated with black dashed lines. ***A.*** Cartoon representation of apo-PdxI tertiary structure and binding-cavity (magenta). The C-terminal catalytic domain is shown in green and the N-terminal dimerization domain in lime. ***B.*** Overlay of interlocking homodimer structures of apo-PdxI and apo-HpiI. ***C.*** Active-site view of co-crystal structure of PdxI with substrate analogue ketone **38**. ***D.*** Active-site view of co-crystal structure of HpiI with substrate analogue ketone **38**. In ***C.*** and ***D.***, M76 from Chain B is indicated in different colors.

Figure 35
Mechanism of periselective and regioselective pericyclic reactions. ***A.*** Alder-ene theozyme model based on PdxI structure. ***B.*** O4-Hetero-Diels–Alder theozyme model confirmed by HpiI structure. ***C.*** Analysis of the relative production ratio of the O4-hetero-Diels–Alder adduct **42**, Alder-ene adduct **41**, and the O2-hetero-Diels–Alder adduct **44** from *in vitro* reaction of **38** with PdxG, NADPH, and selected pericyclases. To quantify the ratio, the reaction time of control sample without pericyclases (Cont.) was 12 hours, and reaction times with enzyme were 2 hours. Error bars indicate s.d. of three independent replicates. *Putative cyclized products other than **41**, **42**, and **44** were detected in the control reaction.

Figure 36
Early examples of higher-order [6 + 4] cycloadditions. ***A.*** Independent studies by Cookson and Itô in 1966 and additionally reported in 1970. ***B.*** Verification of Hoffmann and Woodward predictions by Houk in 1966, published in 1970. ***C.*** Synthesis of pentacyclic molecules involving [6 + 4] cycloadditions by Itô and coworkers in 1967. ***D.*** Shapes of the highest-occupied and the lowest-unoccupied molecular orbitals: LUMO of tropone, and HOMOs of cyclopentadiene and cycloheptatriene.

Figure 37
Calculated energy surface for the *exo* (**TS-21**) and *endo* (**TS-22**) reactions of tropone (**45**) and cyclopentadiene (**46**) at the DLPNO-CCSD(T)/cc-pVQZ//ωB97X-D/def2-TZVP level of theory.

Figure 38
Calculated energy surfaces for tropones reacting with cycloheptatriene (**51**). ***A.*** Calculated reaction energetics of tropone **45** and cycloheptatriene **51**. ***B.*** Interconversion Cope (**TS-26**) and Claisen (**TS-27**) pathways of tropone and cycloheptatriene adducts. ***C.*** Diels–Alder TSs (**TS-28** and **TS-29**) leading to pentacyclic adducts. ***D.*** Free energy diagram for tropone (black),chloro tropone (**a**, green), and methoxy tropone (**b**, red) reacting with cycloheptatriene. ***E.*** Summary of quasi-classical reaction dynamics trajectory results indicating ratios of **52**, **53**, and **54** formed from **TS-25**, **TS-25a**, and **TS-25b**. Calculations at the DLPNO-CCSD(T)/cc-pVQZ//ωB97X-D/def2-TZVP level of theory. Dynamics at the optimization level of theory. Energies are quasi-harmonic corrected and reported at 1 M and 25 ºC.

Figure 39
Comparison of tripericyclic TS geometries, energies, and predicted product ratios of **52** and **53** by Yang *et al.*[10] and Lee *et al.*[11] with reaction dynamics yields.

Figure 40
Four-dimensional bond length plots of reaction dynamics trajectories. The color bar maps the common bond (C2–C1, green) among products: separated is grey (4 Å) and formed is blue (1.5 Å). TS ensemble geometries for **TS-25** (red), **TS-26** (gold) and **TS-27** (gold) are overlaid in contrasting colors for clarity. ***A.*** Randomly selected trajectories propagated from **TS-25** leading to each product. ***B.*** Plot of all 135 trajectories propagated from **TS-25**. Calculations are at the ωB97X-D/def2-TZVP level of theory.

Figure 41
Definition of (***A.***) *exo* and *endo* with regards to [6 + 4] cycloadditions, (***B.***) orbital interactions, and (***C***.) parent hydrocarbon transition states of cyclic and acyclic systems. ***D.*** Meta-analysis of complex published examples of *endo*-[6 + 4] transition states.[12–14]

Acknowledgements

I am incredibly humbled by my academic journey. Ken and Yi, none of this would have been possible without your incredible support, openness to collaborate, and willingness to work through my wild ideas. I must acknowledge and thank my PhD advisors, Professor Kendall N. Houk and Professor Yi Tang. You both fostered an environment where I, as someone who did not come to this PhD program from a traditional pathway, felt welcome and able to ask questions until I had exhausted all of my curiosities. Ken, I am very grateful for your advice in how to prepare and give academic presentations. A highlight of my time at UCLA was meeting with you and the weekly visiting lecturer and being given the opportunity to pitch my research to them. Thank you for this opportunity. I feel that this has made me into a clear and confident presenter as well as connected me to academics all over the globe. Yi, I am very grateful for the friendly and casual meeting environment you fostered. I have quite fond memories of our pyridone and pericyclase meetings; it was exhilarating to work together and go through fellow group members, collaborators, and my own results to form a complete picture of each project.

I am very grateful for Masao Ohashi's mentorship in experimental techniques and all of the time we spent together pouring over manuscript drafts or trying to understand some strange results. Thank you. You really pushed me to be the scientist I am today.

I must also acknowledge the Houk laboratory as a whole. I will miss my daily laboratory jobs like maintaining the coffee machine and creating the coffee newsletter. To me, these

duties were just excuses to walk around the office and make small talk with y'all. I already miss this and am looking forward to staying in touch with all of you.

I need to acknowledge my partner, Jan DeLozier, who has supported me throughout the entirety of my PhD. Thank you for your endless support through the good and the bad; thank you for listening to me air my feelings, let me rant, and just ramble about the beauty of nature. Your support and love gave me the confidence to pursue this PhD. I love you, Jan.

Lastly, I need to acknowledge my family who have always pushed me to pursue my own ideas no matter how wild they are. Thank you mom and dad for all that you do for me.

Vita

Education

University of California, Los Angeles

2019	PhD Candidate, Theoretical & Computational Chemistry
2019	MS, Theoretical & Computational Chemistry

Lewis & Clark College

2016	BA, Chemistry (honors)
2016	BA, Art

Teaching Experience

Graduate Level

University of California, Los Angeles

2020 Winter	Teaching Fellow, Physical Organic Chemistry I, Professor Kendall N. Houk
2019 Spring	Teaching Fellow, Physical Organic Chemistry II, Professors Kendall N. Houk & Ellen Sletten

Undergraduate Level

University of California, Los Angeles

2018 Spring	Teaching assistant, Organic Reactions & Pharmaceuticals, Dr. Stephen Hardinger
2018 Winter	Teaching assistant, Organic Reactions & Pharmaceuticals, Dr. Stephen Hardinger
2017 Fall	Teaching assistant, Organic Reactions & Pharmaceuticals, Dr. Stephen Hardinger

Lewis & Clark College

2014–2016	Teaching assistant, Organic Chemistry Lab I & II, Dr. Lisa Holmes
2012–2016	Teaching assistant, Ceramics I, II, III & IV, Professor Ted Vogel

Awards

2021	Royal Society of Chemistry Horizon Prize
2021	Saul and Sylvia Winstein Dissertation Award
2020–2021	UCLA Graduate Education Dissertation Year Fellowship
2020	Michael E. Jung Excellence in Teaching Award
2020	Don C. Atkins Excellence in Research Award
2020	UCLA Chemistry & Biochemistry Excellence in Research Fellowship
2019–2021	Senior Foote Graduate Fellow
2019	Saul Winstein Fellowship

2019	The Future of Research Communications and e-Scholarship
2019	Stanford's CQMD/Pulse Quantum Molecular Design Summer School
2014, 2015	John S. Rogers Science Research Grant
2014 – 2016	Kent Swanson Memorial Scholarship
2013 – 2016	Mellon Funds Research Grant & Lewis & Clark College Presidential Grant

Service

2021	Guest Lecture at Lewis & Clark College, *The Diels–Alder Reaction In Nature*
2021	American Association for the Advancement of Science Member
2020	ACS Reviewer Lab Certificate
2019	UCLA's Exploring Your Universe Science Festival
2018	Sequoia & Kings Canyon National Park Citizen Science Volunteer
2017	Read Marfa Volunteer
2015 – 2021	American Chemical Society (ACS) Member

Chapter 1. The Expanding World of Biosynthetic Pericyclases: Cooperation of Experiment and Theory for Discovery

1.1 Contributions

This is an author manuscript from the publication: Jamieson, C. S.; Ohashi, M.; Liu, F.; Tang, Y.; Houk, K. N. The Expanding World of Biosynthetic Pericyclases: Cooperation of Experiment and Theory for Discovery. *Nat. Prod. Rep*. **2019**, *36* (5), 698–713. https://doi.org/10.1039/c8np00075a. This project was a collaboration between my advisors' laboratories, Kendall N. Houk and Yi Tang. Myself and Postdoctoral fellow Masao Ohashi were co-first authors on this publication. We conducted a thorough literature review. I focused on introducing pericyclic reactions, synthetic examples, and reviewing our laboratories recent findings. Masao Ohashi assisted in editing and finding historical examples of natural pericyclases characterized by other laboratories. Fang Liu assisted us with graphics and editing the manuscript.

1.2 Abstract

Pericyclic reactions are a distinct class of reactions that have wide synthetic utility. Before the recent discoveries described in this review, enzyme-catalyzed pericyclic reactions were not widely known to be involved in biosynthesis. This situation is changing rapidly. We define the scope of pericyclic reactions, give a historical account of their discoveries as biosynthetic reactions, and provide evidence that there are many enzymes in Nature that catalyze pericyclic reactions. These enzymes, the "pericyclases," are the subject of this review.

1.3 Introduction

Woodward and Hoffmann introduced the concept of pericyclic reactions in their classic book, “The Conservation of Orbital Symmetry” that was first published in Angewandte Chemie in 1969.[15] Following the definitions of concerted electrocyclic reactions, cycloadditions, sigmatropic shifts, cheletropic reactions and related processes (Figure 1), Woodward and Hoffmann rationalized previously puzzling experimental data based on what they named the Principle of Conservation of Orbital Symmetry. Woodward and Hoffmann also defined pericyclic reactions: “reactions in which all first-order changes in bonding relationships take place in concert on a closed curve.”[16]

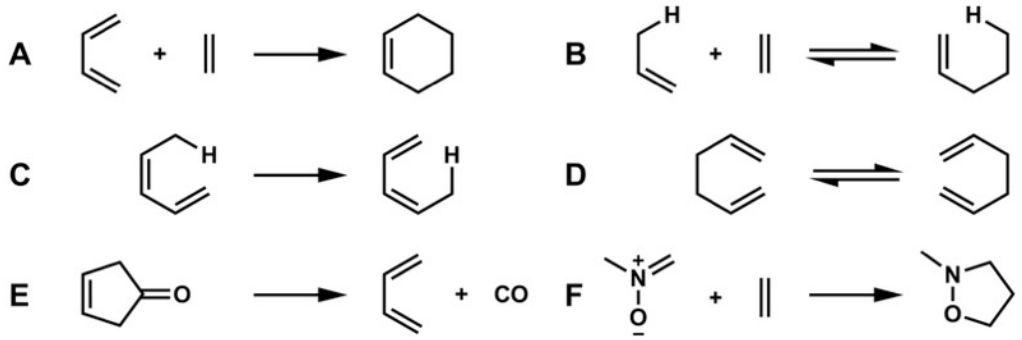

Figure 1
A. Cycloaddition (Diels-Alder reaction). ***B.*** Alder-ene reaction (a Miscellaneozation). ***C.*** 1,5-Sigmatropic hydrogen shift, ***D.*** [3,3]-Sigmatropic shift (Cope rearrangement). ***E.*** Cheletropic reaction. ***F.*** A 1,3-dipolar cycloaddition, a hetero-pericyclic reaction.

The examples in Figure 1 are all of unsubstituted systems with six electrons involved in bonding changes, while the other orbitals have only minor perturbations such as rehybridization. For each reaction, there are numerous examples of substituted cases. These are examples of hydrocarbon reactions, or of a ketone in Figure 1e, and Figure 1f is another example of a vast number of pericyclic reactions involving heteroatoms.

Substitution influences activation barriers and sometimes even the mechanism, but the basic theoretical conclusion that these reactions are “allowed” to be pericyclic does not change. In each case, there are stereochemical restrictions on allowed pericyclic transition states, and the number of electrons is also important. For example, Figure 2 shows allowed and forbidden six-electron and four-electron electrocyclic reactions, and how the stereochemistry changes with the number of electrons involved.

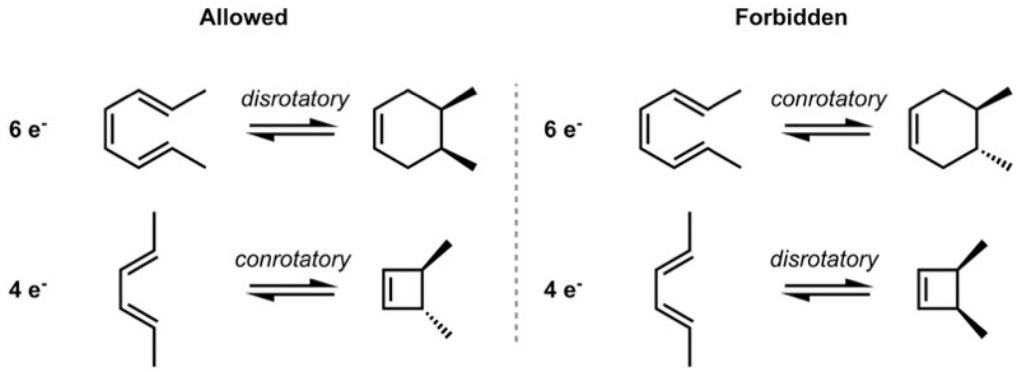

Figure 2
Allowed and forbidden electrocyclic reactions involving 6 and 4 electrons. In each case, only the allowed pathways are observed. Conrotatory, both termini rotate in the same direction; disrotatory, two termini rotate in the opposite direction.

The selection rules were derived in various ways, including consideration of frontier molecular orbital interactions or the use of orbital correlation diagrams showing the behavior of orbitals along a reaction pathway. The simplest approach to understand what causes an allowed reaction to be favored, and forbidden to be disfavored, is to consider the aromaticity or anti-aromaticity of the transition state (Figure 3). The Diels-Alder transition state, like benzene, has a cyclic array of 6 electrons, while the [2+2] concerted transition state has a cyclic array of 4 electrons, like the anti-aromatic cyclobutadiene. Aromatic molecules (and transition states) are highly stabilized, more stable than linear

conjugated systems (or acyclic transition states), while anti-aromatic molecules are destabilized.

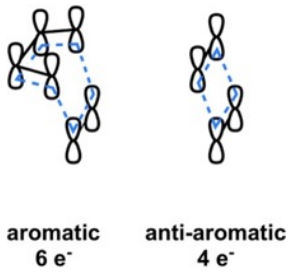

Figure 3
Schematic representation of the aromaticity of the allowed Diels-Alder transition state and anti-aromaticity of the [2+2] cycloaddition transition state.

1.4 Mechanistic Considerations: What is a Pericyclase?

Some reactions that are allowed to be concerted pericyclic processes can occur by other mechanisms. For example, while most Diels-Alder reactions are concerted, there are some that, by virtue of substitution, occur by stepwise mechanisms (Figure 4). The definition of “concerted” has also been the subject of discussion and has evolved. A concerted reaction was originally taken to mean a reaction in which all bonding changes occur in concert in one step, while a stepwise reaction occurs in several steps involving one or more intermediates.

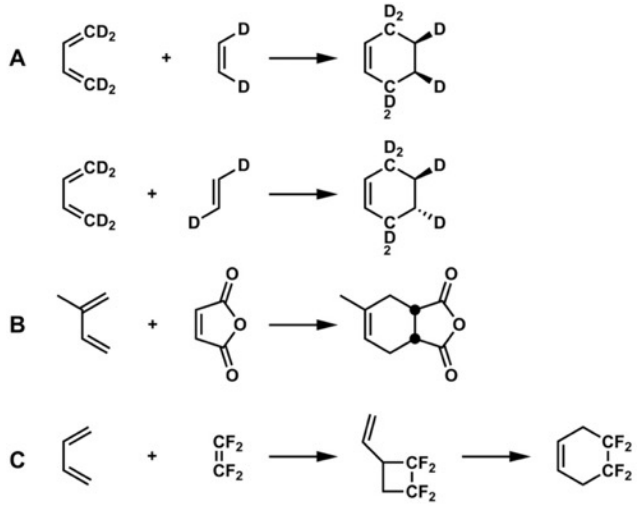

Figure 4
Diels-Alder reactions: Concerted proven by (***A.***) stereospecificity[1] and (***B.***) kinetic isotope effects.[2] Stepwise proven by (***C.***) identification of an intermediate cyclobutane.[3]

When reliable quantum mechanically computed transition geometries became available in the 1990s, it became more apparent that concerted reactions could involve symmetrical (synchronous) or unsymmetrical (asynchronous) bond formation. Baldwin defined "bonding concerted" and "bonding stepwise" based on whether several bonds are formed all at once or sequentially.[17] Our group defined "dynamically concerted" as reactions in which both bonds are formed with a time gap of <60 femtoseconds (fs). This quantity, 60 fs, is the time of passage over a potential energy maximum in Eyring's transition state theory and is a time comparable to the lifetime of a CC vibration (~ 30 fs).[18] Dynamically stepwise reactions are energetically concerted with only one potential energy maximum but with a bonding time gap greater than 60 fs. Such reactions are found on flat potential energy surfaces as found for several Diels-Alderases discussed later. Dynamically concerted and dynamically stepwise reactions can both be pericyclic when the rate-determining TS has partial bonding on a "closed curve".

We define pericyclases as those enzymes that catalyze pericyclic reactions, reactions that have transition states with bonds partially made or broken in a cyclic array. It is this cyclic array of bonding changes in the rate-determining transition state that is special for a pericyclic reaction, rather than the detailed shape of the potential surface. A time gap between formation of the two new bonds of <60 fs is the definition of dynamically concerted, but we consider reactions as pericyclic as long as the reaction is energetically concerted, with a rate-determining TS that has a cyclic array of bonding interactions that eventually lead to products.

1.5 Synthetically Useful Pericyclic Reactions

The Diels-Alder reaction has been applied to many elegant syntheses. Woodward's reserpine synthesis involved a first step where three new stereocenters are formed stereoselectively. A double bond in the product served as the locus of two additional stereocenters. (Figure 5a).[19–21] This synthesis has long been considered a classic of "substrate-controlled" stereoselective synthesis.[22]

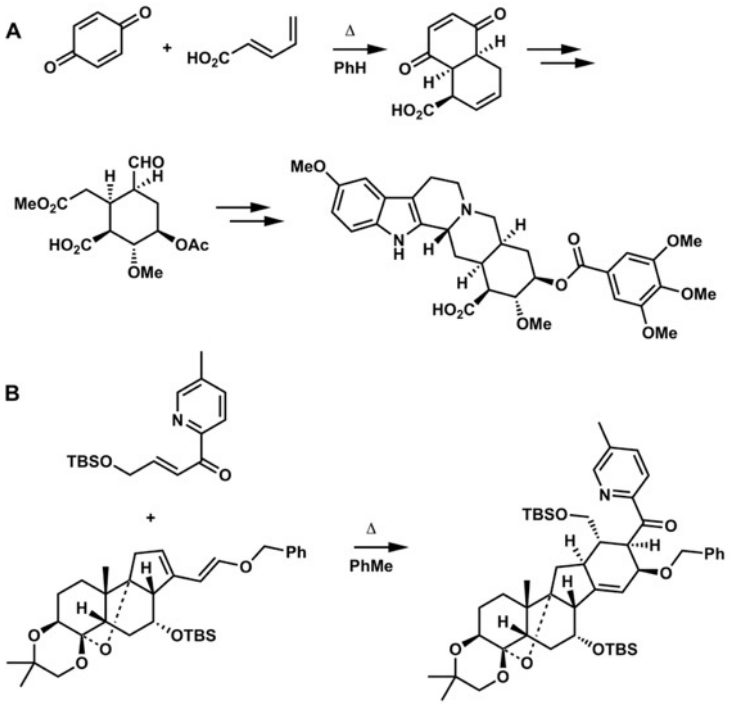

Figure 5
Diels-Alder steps in (***A.***) Woodward's reserpine synthesis (1956) and (***B.***) Stork's approach to the synthesis of 4-methylenegermine (2017).

Many Diels-Alder reactions are included in Nicolaou and Sorensen's "Classics in Total Synthesis".[23] In Gilbert Stork's last paper, published shortly before he died in 2017, a complicated Diels-Alder reaction was used to create a cyclohexene with complete control of stereochemistry, both *exo*/*endo* and facial selectivity (Figure 5b), leading to four new stereocenters, properly fixed with respect to the pre-existing stereocenters in the diene.[24] Other types of pericyclic reaction are also commonly used in synthesis, such as the Ireland-Claisen rearrangement. Figure 6 shows this [3,3]-sigmatropic shift used in Rizzacasa's (+)-zaragozic acid C synthesis from Zakarian's review on the use of these reactions in synthesis[4] and an electrocyclization used in Kwon's approach to the synthesis of reserpine,[5] respectively. The Ang Li group at SIOC has developed a general synthetic route to highly substituted aromatics, involving the electrocyclic reactions of

hexatrienes. His group has used this electrocyclization to good advantage for the synthesis of a number of daphniphyllium alkaloids.[25–27] The Maulide group in Austria has harnessed stereoselective cyclobutene ring-opening reactions for the synthesis of diene units of various macrolides.[28,29] It is fair to single out pericyclic reactions as principle weapons in the arsenal of synthetic strategians to conquer complex stereochemical issues.

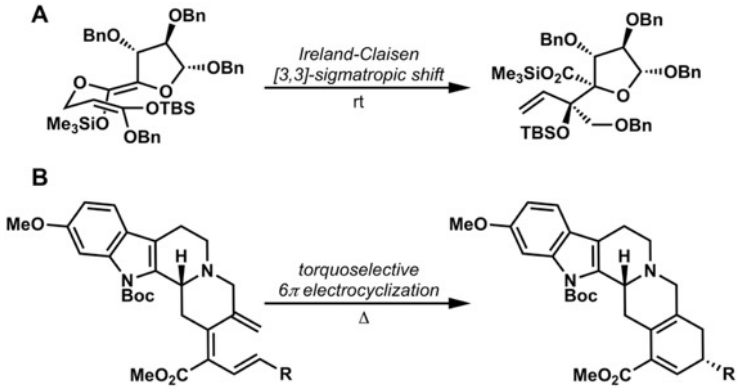

Figure 6
Examples of (***A.***) a [3,3]-sigmatropic shift[4] and (***B.***) an electrocyclization[5] involved in synthesis.

1.6 The Emergence of Diels-Alderases

The first authenticated Diels-Alderases might be considered to be catalytic antibodies and designed enzymes, since these proteins are indeed catalysts of pericyclic reactions. The designed unnatural enzyme by Baker and Houk, which catalyzes the reaction shown in Figure 7, is often highlighted as the first designed enzyme that catalyzes a bimolecular Diels-Alder reaction.[7] However, this reaction had been catalyzed earlier by a catalytic antibody produced in response to inoculation with a transition state analog, by the Lerner and Houk groups.[6] Indeed, a number of groups have developed antibodies that catalyze a variety of Diels-Alder reactions.[30,31]

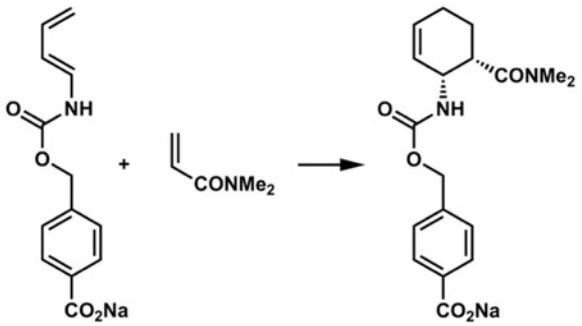

Figure 7
The Diels-Alder reaction catalyzed by a catalytic antibody[6] and later by a computationally designed enzyme.[7]

The groups of Baker and Houk used the computational "inside-out" approach to design the enzyme for the reaction in Figure 7 that is both stereospecific and accelerates the reaction 100-fold with respect to the reaction in water.[7] Fold-It players on Baker's on-line game improved this further by designing a loop that improves substrate binding,[32] while Hilvert improved catalysis even further by directed evolution.[33]

There are many natural products containing cyclohexenes or substituted cyclohexanes, and there has been much speculation that there might be Diels-Alderases in Nature.[34] Three of these Diels-Alderases, macrophomate synthase, lovastatin nonaketide synthase (LovB) and solanapyrone synthase (Sol5) were reported during late 1990s to early 2000s.[8,35–38] LovB and Sol5 catalyze the intramolecular Diels-Alder reactions that form *trans*- and *cis*-decalin scaffolds (Figure 9a), respectively. These enzymes catalyze the formation of the acyclic precursor, as well as the subsequent regioselective and stereoselective Diels-Alder reactions. Since LovB and Sol5 have additional activities other than those of Diels-Alderases, it has been difficult experimentally to prove that these enzymes catalyze the cycloaddition events. For example, although LovB has been shown

to be required to afford the desired decalin stereoisomer in dihydromonacolin L,[37] the exact domain of the megasynthase that catalyzes this reaction has not been identified.

Perhaps the first Diels-Alderase was proposed by Watanabe *et al*. in 2000, who provided evidence for the multistep catalysis by macrophomate synthase, including formation of a Diels-Alder adduct as an intermediate followed by decarboxylation and dehydration to form macrophomate (Figure 8).[8]

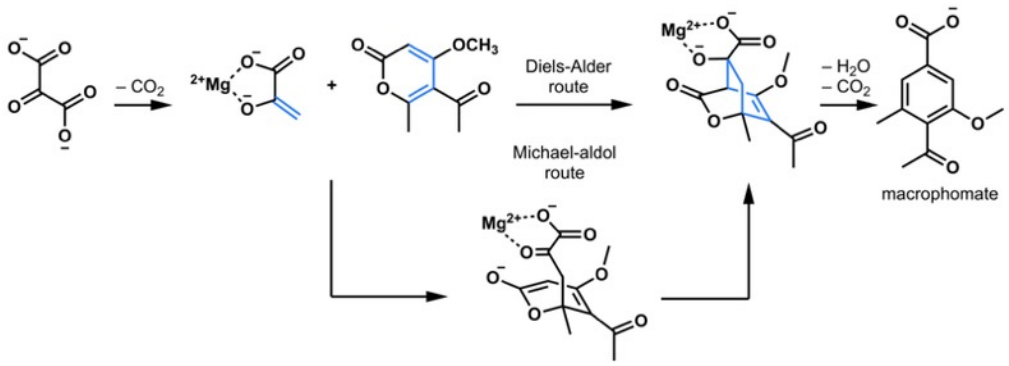

Figure 8
Reaction scheme comparing the concerted and stepwise Diels-Alder route to macrophomate catalyzed by macrophomate synthase.[8]

A crystal structure of the multifunctional macrophomate synthase was obtained by Ose and Watanabe *et al*. in 2003 and 2004,[39,40] which allowed Jorgensen *et al*. to carry out a detailed computational-mechanistic study that showed the Diels-Alder reaction occurs in two distinct steps, Michael addition to give a stable intermediate, and a subsequent aldol reaction to give a less stable intermediate that is then decarboxylated and dehydrated by the enzyme (Figure 8).[41] Because of the stepwise nature of this process, Jorgensen concluded that this was not a Diels-Alderase. This finding received publicity in the chemical press,[42] and is widely quoted. According to our definitions, however,

macrophomate synthase is a Diels-Alderase, since it does catalyze the reaction of a diene and an alkene to form a cyclohexene; overall a Diels-Alder reaction occurs. However, in line with Jorgensen's finding, macrophomate synthase is not a pericyclase, since the mechanism has been clearly established by Jorgensen *et al*. to be a stepwise Michael-aldol reaction, not a pericyclic reaction.

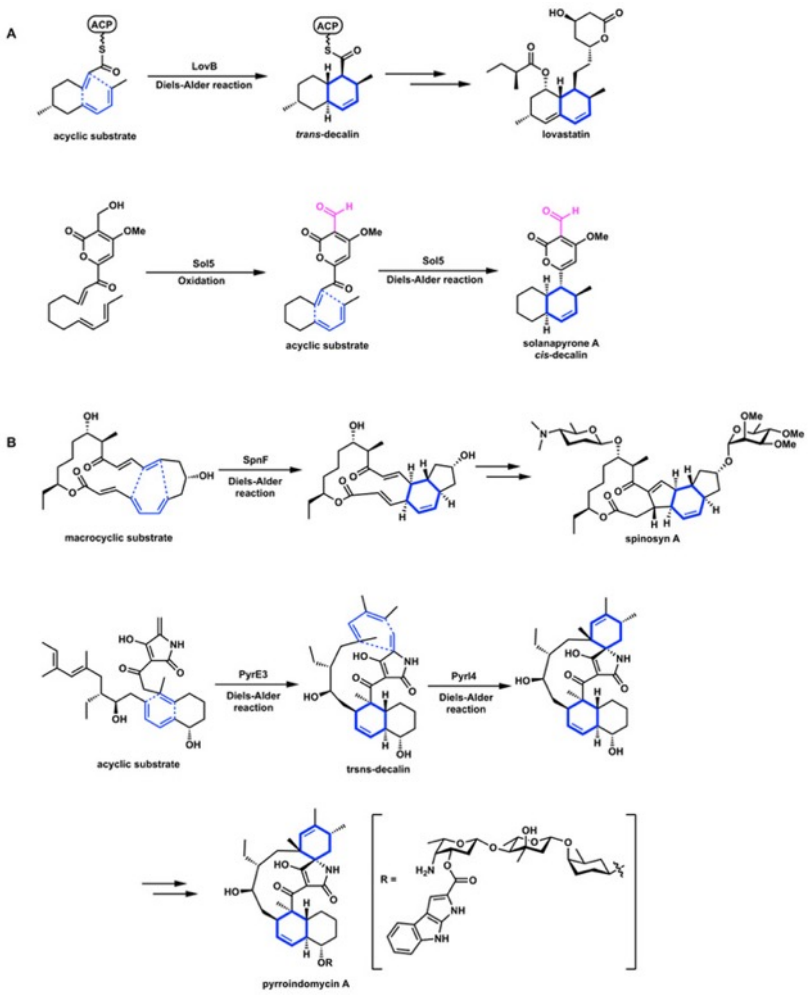

Figure 9
Examples of enzyme-catalyzed Diels-Alder reaction. (***A.***) Multifunctional enzymes that have Diels-Alderases activities, LovB and Sol5. (***B.***) Stand-alone Diels-Alderases, SpnF from spinosyn A biosynthesis, and PyrE3 and Pyl4 from pyrroindomycin A biosynthesis.

In 2011, Liu and co-workers reported the characterization of Diels–Alderase SpnF from insecticide spinosyn A biosynthetic gene cluster.[43] This is widely touted as the first enzyme that catalyzes only the Diels-Alder cycloaddition, rather than synthesis of the precursor and (perhaps) the cycloaddition itself, as often is the case. Although SpnF was originally annotated by primary sequence comparisons to be an apparent S-adenosyl-L-methionine (SAM)-dependent methyltransferase, similar to LepI that is described later, SpnF indeed catalyzes and accelerates the rate of Diels–Alder conversion of an α,β,γ,δ-unsaturated macrolactone precursor to the tricyclic cyclohexene-containing product by approximately 500-fold (Figure 9b).[43]

After the discovery of SpnF, the advancement of genome sequencing and searching tools for secondary metabolite gene clusters has led to the identification of numerous stand-alone Diels-Alderases, especially from bacterial biosynthesis pathways. For example, the pyrroindomycin biosynthetic pathway involves two sequentially unrelated enzymes acting consecutively to perform tandem Diels-Alder reactions, a decalin-forming Diels-Alder reaction by PyrE3 and then a spirotetronate-forming Diels-Alder reaction by Pyrl4 enzyme (Figure 9b).[44] Gene encoding Pyrl4 homologues VstJ,[45] and AbyU[46] are also found in the biosynthetic gene clusters of other spirotetronate-containing natural products.

Recently, an enzymatic aza-Diels-Alder reaction was confirmed in the final step of thiazolyl peptide thiocillin biosynthesis.[47] The single enzyme TclM, originally annotated as a dehydratase, was found to catalyze the formation of the trisubstituted pyridine core of thiocillin, through a Diels-Alder reaction between dihydroalanine residues (Figure 10).

In the last two years, there have been several reviews of the many new Diels-Alderases identified in Nature.[44,48,49]

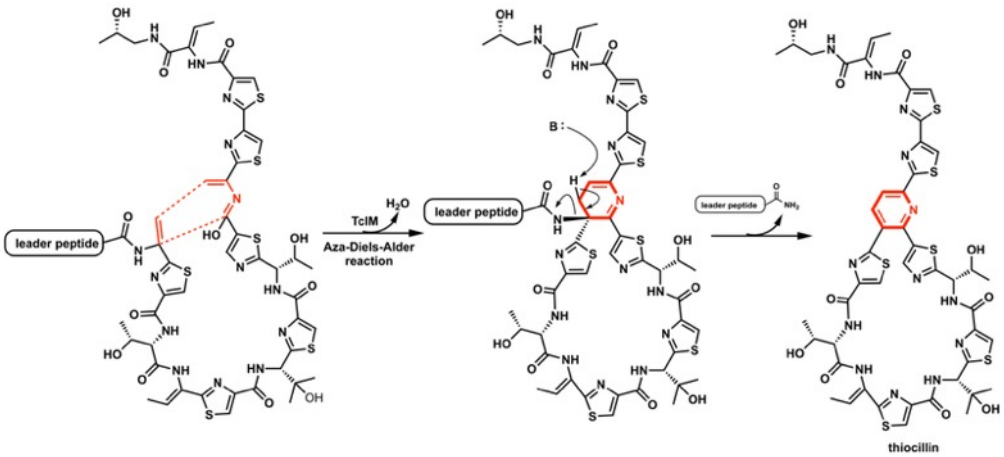

Figure 10
Enzymatic intramolecular hetero Diels–Alder reaction in formation of thiocillin.

1.7 Recently Discovered Diels-Alderases and Ambimodal Pericyclases

There have been a few pericyclases discovered that catalyze pericyclic processes other than the Diels-Alder reaction. Chorismate mutase is now recognized as the first documented "pericyclase"; this enzyme catalyzes the Claisen rearrangement of chorismate to prephenate in primary metabolism (Figure 10a).[50] Tantillo has characterized enzymatic carbocation [1,2]-shifts in natural product biosynthesis.[51–53] Isochorismate-pyruvate lyase,[54,55] precorrin-8x methyl mutase,[56] and dimethylallyltryptophan synthase[57] were later reported and proposed to involve pericyclic reactions (Figure 11b–d). In the past few years, multiple putative pericyclase-catalyzed 1,3-dipolar cycloadditions have been proposed.[58–60]

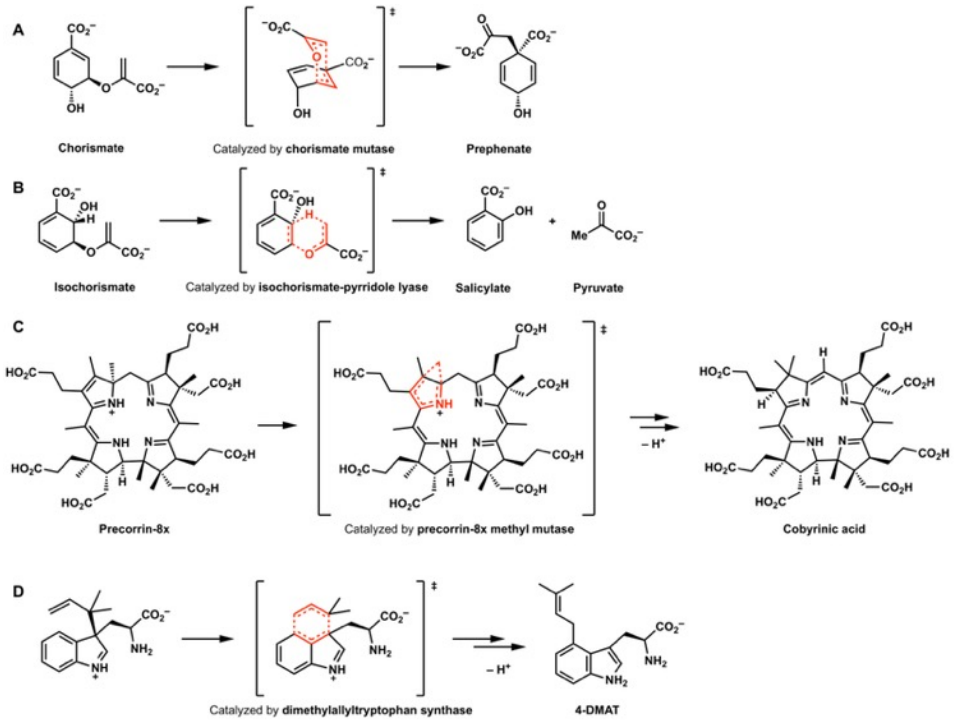

Figure 11
A. The Claisen rearrangement ([3,3]-sigmatropic shift) catalyzed by chorismate mutase; reactions putatively catalyzed by (***B.***) isochorismate-pyrridole lyase, (***C.***) precorrin-8x methyl mutase, and (***D.***) dimethylallyltryptophane synthase.

In this section, we review some of the recently discovered enzymes from our labs and others that catalyze prototypical pericyclic reactions. These involve primarily cycloaddition and [3,3]-sigmatropic rearrangement reactions. We have discovered that some of these enzymes involve “ambimodal” transition states, where a single transition state connects with multiple products via a post-transition state bifurcation.[61,62]

In addition to the Diels-Alderases described above, both pericyclic and stepwise, a number of additional Diels-Alderases have been discovered recently in our labs. These are described here.

1.7.1 MycB; Another Decalin Forming Diels-Alderase

The decalin motif is frequently observed in natural products produced by bacteria and fungi.[63] It has been found to involve an intramolecular Diels-Alder reaction, the simplest example of which is shown in Figure 12. Substituted versions of the decatriene backbone motif are synthesized from polyketide synthases (PKSs), especially bacterial multimodular and fungal iterative PKSs.[64] In organic synthesis, decalins can be synthesized from intramolecular Diels-Alder reactions (IMDA). The parent system, studied both experimentally and theoretically, shows no significant stereoselectivity, but substitution can alter the intrinsic preference.[65]

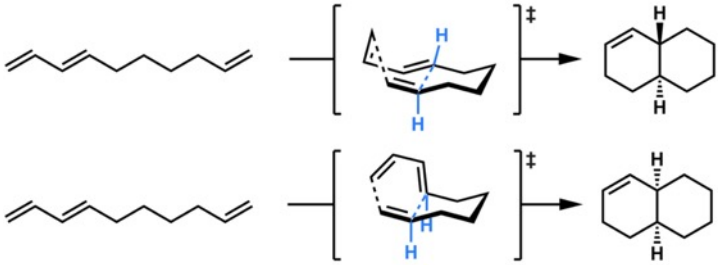

Figure 12
Intramolecular Diels-Alder reactions to form *cis*- and *trans*-octahydrodecalins.

Decalins are often derived in biosynthesis from acyclic polyketide precursors. During PKS-catalyzed synthesis of acyclic precursors, programming rules of the PKSs strategically leave double bonds unreduced in the polyketide chains at precise positions to generate a diene and a dienophile interrupted by four contiguous sp3 carbons; the decatriene units can undergo Diels-Alder cyclizations.[34,6663,67] Indeed, the hypothesis is that Diels-Alder reactions are involved for many, if not all, of the decalins formed in biosynthesis. Bioinformatics analysis and genetic evidence have suggested that a class of lipocalin-like enzymes such as CghA and Fsa2 may be involved in the formation of the

decalin ring systems of Sch210972 and equisetin, respectively.[68] *In vitro* characterization of these enzymes using acyclic substrates was unsuccessful, partly due to the inability to capture these substrates, which are prone to undergo spontaneous uncatalyzed cycloaddition reactions to form a mixture of decalin stereoisomers.[69,70] In late 2016, we serendipitously captured an overly oxidized acyclic substrate for lipocalin-like enzyme MycB from the myceliothermophins biosynthetic gene cluster.[71] Myceliothermophins, including myceliothermophin A and E, are cytotoxic compounds isolated from the thermophilic fungus *Myceliophthora thermophilia*.[72] *In vitro* characterization of MycB using the acyclic substrate showed that MycB is responsible for the formation of the *trans*-decalin scaffold from the substrate (Figure 13a). The uncatalyzed Diels-Alder reaction of the acyclic substrate is predicted to be very slow with $\Delta G_{uncat}^{\ddagger}$ = 25.1 kcal/mol, which would lead to a rate constant of ~ 10^{-5} s^{-1} at room temperature according to transition state theory. In contrast, the spontaneous Diels-Alder reaction in the biosynthesis of Sch210972 is very fast, with $\Delta G_{uncat}^{\ddagger}$ ~ 12 kcal/mol, which accounts for our inability to isolate the acyclic substrate for CghA.[69,71] Quantum mechanical calculations on a model substrate for the MycB reaction predicted that the uncatalyzed reactions will produce a mixture of diastereomers with the unobserved cis-adduct being the major isomer (Figure 13b). This occurs because the *exo*-transition state (*cis*-decalin) barrier is lower than the *endo* (*trans*-decalin). MycB must stabilize the thermodynamically unfavorable *endo* transition state in the active site to facilitate the exclusive formation of the *trans*-decalin structure. Calculations performed with *p*-cresol to mimic the effects of a catalytic tyrosine residue in the enzyme active site, predict the *endo* adduct will be favored. Our calculations

showed that the endo transition state of MycB-catalyzed cyclization is asynchronous but concerted, indicating that MycB is a pericyclase that catalyzes the IMDA reaction.

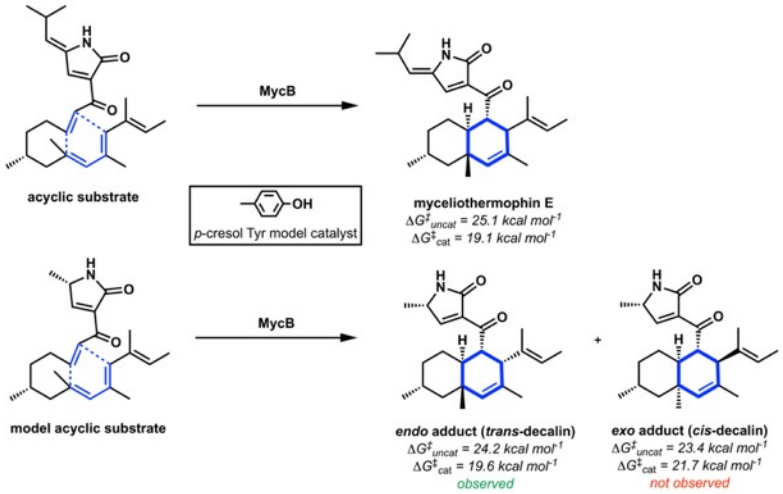

Figure 13
The MycB-catalyzed Diels-Alder reaction with calculated free energy barriers for spontaneous and model-catalyzed reactions.

1.7.2 SpnF; ambimodal [4+2]/[6+4]-cycloaddition and Cope rearrangement

As mentioned previously, SpnF is the first characterized monofunctional Diels-Alderase discovered in Nature.[43] SpnF accelerates a nonenzymatic Diels-Alder cycloaddition reaction of the macrocyclic precursor by 500-fold to form the 5,6-bicyclic system during the biosynthesis of spinosyn A. In Smentek and Hess' theoretical study, the SpnF-catalyzed nonenzymatic cycloaddition was described as highly asynchronous.[73] Liu and coworkers discussed the possibility that the catalytic cycle involves a concerted pericyclic or alternative stepwise cyclization mechanism, but no direct evidence for mechanism was obtained in the original experimental studies.[43]

Recently, extensive quantum mechanical computations and dynamic simulations by our group showed that the transition state for the nonenzymatic reaction is an ambimodal

transition state that leads directly to the observed Diels−Alder and to an unobserved [6+4]-cycloadduct (Figure 14).[12,74] The unobserved [6+4]-adduct has higher free energy than the Diels-Alder adduct and is predicted to readily convert to the Diels-Alder adduct via a Cope rearrangement. We predict that both [4+2] and [6+4] adducts are formed via a *bis*-pericyclic[75] ambimodal transition state, but the [6+4] adduct is rapidly converted to the observed [4+2] Diels-Alder adduct.[12] Dynamics simulations indicate that both dynamically concerted and dynamically stepwise trajectories occur from the single ambimodal transition state.[74] Since the single transition state contains a cyclic array of breaking and forming bonds, these are indeed pericyclic reactions. We have also developed an environment-perturbed transition-state sampling (EPTSS) method based on QM/MM molecular dynamics. The EPTSS method makes it possible to understand the role of solvent or SpnF enzyme structure on control of the reaction pathways.[74] The EPTSS method has also been used for free-energy calculations and kinetic isotope effect calculations in solvents and enzymes. Molecular dynamics (MD) simulations show that trajectories passing through the ambimodal transition state subsequently bifurcate to the [6+4]-adduct and the Diels–Alder adduct with a ratio of 1:1 in the gas phase, 1:1.6 in water, and 1:11 in the enzyme (Figure 14).[74] From gas phase to water, a trend toward [4+2]-adduct was observed, indicating that increase in solvent polarity promotes the formation of the [4+2]-adduct over the [6+4]-adduct. The enzyme SpnF alters the ambimodal transition state geometry and the post-TS bifurcation dynamics in the active site by perturbing the energy surface to favor formation of the [4+2]-adduct. We are still investigating if SpnF catalyzes the Cope rearrangement of the [6+4]-byproduct to [4+2]-

adduct, but this seems likely due to the similarities of the cycloaddition and Cope transition states.

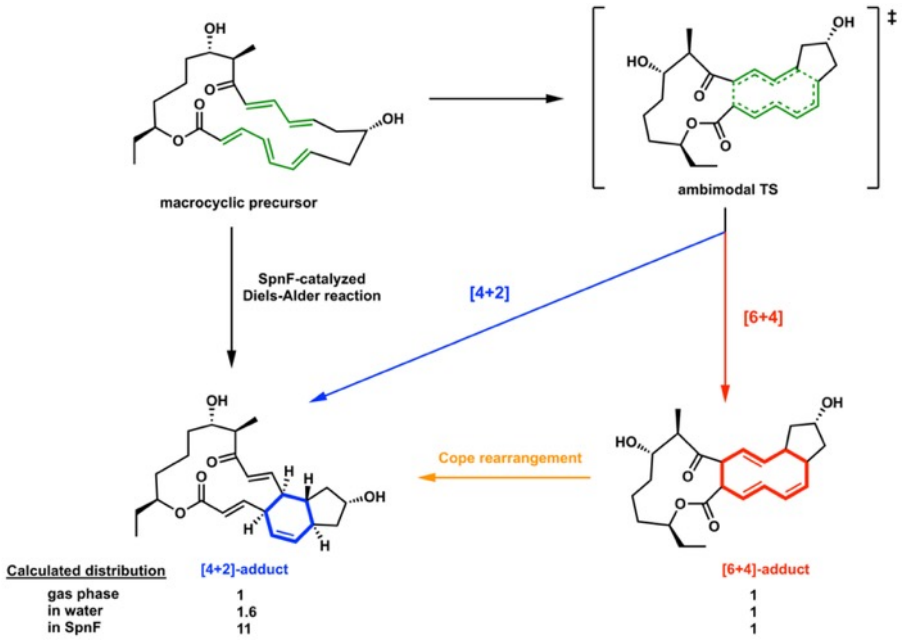

Figure 14
SpnF-catalyzed transannular cycloaddition reactions of the macrocyclic precursor via the single ambimodal transition state to form the [4+2] and [6+4] adducts. Ratios given are from MD simulations, although the rapid Cope rearrangement converts the [6+4] adduct to the more stable Diels-Alder adduct for thermodynamic reasons.

1.7.3 LepI; ambimodal DA/HDA and retro-Claisen rearrangement

The inverse-electron-demand hetero-Diels Alder reaction has been proposed as a key biotransformation to give a dihydropyran, which is a frequent structural feature in natural products including cytotoxic leporin B.[34,76–78] Our groups recently studied the leporin B biosynthetic pathway and discovered a new pericyclase that can catalyze another important pericyclic reaction, the hetero-Diels-Alder (HDA) reaction. The synthesis of the dihydropyran core in leporin without the enzyme involves the *E*/*Z* geometric mixture of the unstable *o*-quinone methide intermediates generated from the dehydration of a 2-pyridone alcohol precursor.[79] The uncatalyzed process gives a mixture of only minor

amounts of the naturally formed HDA adduct leporin C and mostly other regio- and stereoisomeric IMDA and HDA adducts that are not observed in the catalyzed process. Therefore, an enzyme must be encoded in the leporin biosynthetic gene cluster to catalyze the HDA reaction in a stereoselective fashion and to suppress the IMDA reaction to afford the dihydropyran core in leporin.

Although the biosynthetic gene cluster of leporin B was reported by Cary and coworkers, no candidate enzyme encoded in the cluster that could catalyze the HDA reaction was evident in the first pass.[76] Our investigation of dihydropyran core construction led to the discovery of a multifunctional pericyclase LepI that is solely responsible for the pyran formation.[80] This protein was annotated as a SAM-dependent *O*-methyltransferase, but we found that it catalyzes the stereoselective dehydration of the alcohol to (*E*)-quinone methide (QM) and then catalyzes three pericyclic transformations: IMDA and HDA via a single ambimodal transition state, and also a retro-Claisen rearrangement (Figure 15). The HDA reaction catalyzed by LepI to generate the pyran product leporin C is the most direct pathway to go from (*E*)-QM to leporin C. Alternatively, the enzyme-bound (*E*)-QM can also undergo a competing IMDA cyclization to give a spirobicyclic product that can be released from the enzyme. This IMDA reaction and the HDA reactions are in competition, indicated by computational results to occur from a single ambimodal transition state (Figure 15a). Periselectivity is therefore controlled by the post-transition state bifurcation of the ambimodal transition state. In the case of the IMDA route, the spirobicyclic intermediate can then be recaptured by LepI and converted to the final product leporin C by a retro-Claisen rearrangement, the first enzymatic example of this

type of pericyclic reaction. The bifurcating fate of the initially dehydrated quinone methide intermediate thus reveals three pericyclic transformations that take place in the LepI active site.

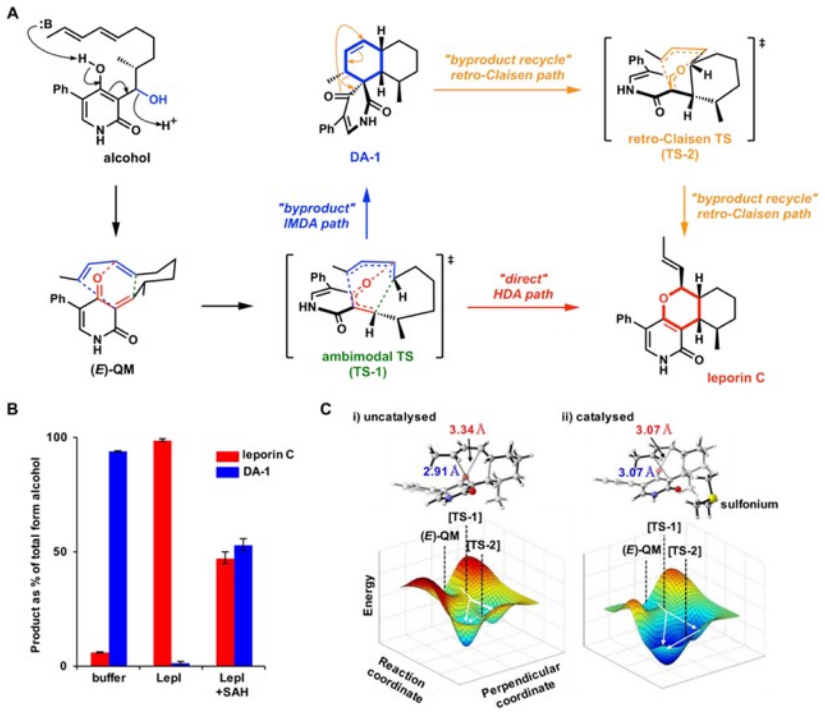

Figure 15
A. Reactions catalyzed by LepI in leporin C biosynthesis. ***B.*** Summary of cascade of LepI-catalyzed reactions. ***C.*** Ambimodal transition state structures and asymmetrical bifurcating PES for the formation of leporin C and DA-1 from (*E*)-QM.

Molecular dynamics simulations were performed on the spontaneous reaction and a simple electrostatic catalysis trimethylsulfonium ion model, to probe possible modes of catalysis by SAM. The sulfonium catalysis model switches reaction periselectivity to favor leporin C formation; switching HDA:IMDA ratios of 0:100 (spontaneous) to 83:17 (catalyzed). Furthermore, the sulfonium model lowers the retro-Claisen barrier by 2.4 kcal mol−1 (100-fold rate acceleration). LepI-catalyzed pericyclic reactions are the first well-documented examples of SAM-catalyzed pericyclic reactions.

1.7.4 Stig cyclase

The Cope rearrangement is another very common [3,3]-sigmatropic rearrangement, frequently used in synthesis.[4,81] Until recently, there has not been mechanistic evidence of an enzymatic Cope rearrangement using a purified enzyme. Both the Sherman and Liu groups reported that an enzymatic Cope rearrangement occurs at an early step in the formation of a set of prenylated cyanobacterial indole monoterpene scaffolds, including hapalindoles, fischerindoles, ambiguines, and welwitindoles.[82–85] Interestingly, the formation of polycyclic scaffolds of the hapalindole family are catalyzed by a related set of calcium dependent dimeric cycloisomerases, namely the Stig cyclases from Stigonentales cyanobacteria. The Stig cyclases are proposed to perform the Cope rearrangement of the 3-geranyl-3-isocyanylvinyl indolenine, followed by aza-Prins cyclization and a proposed three-way partition to product families shown in Figure 16.

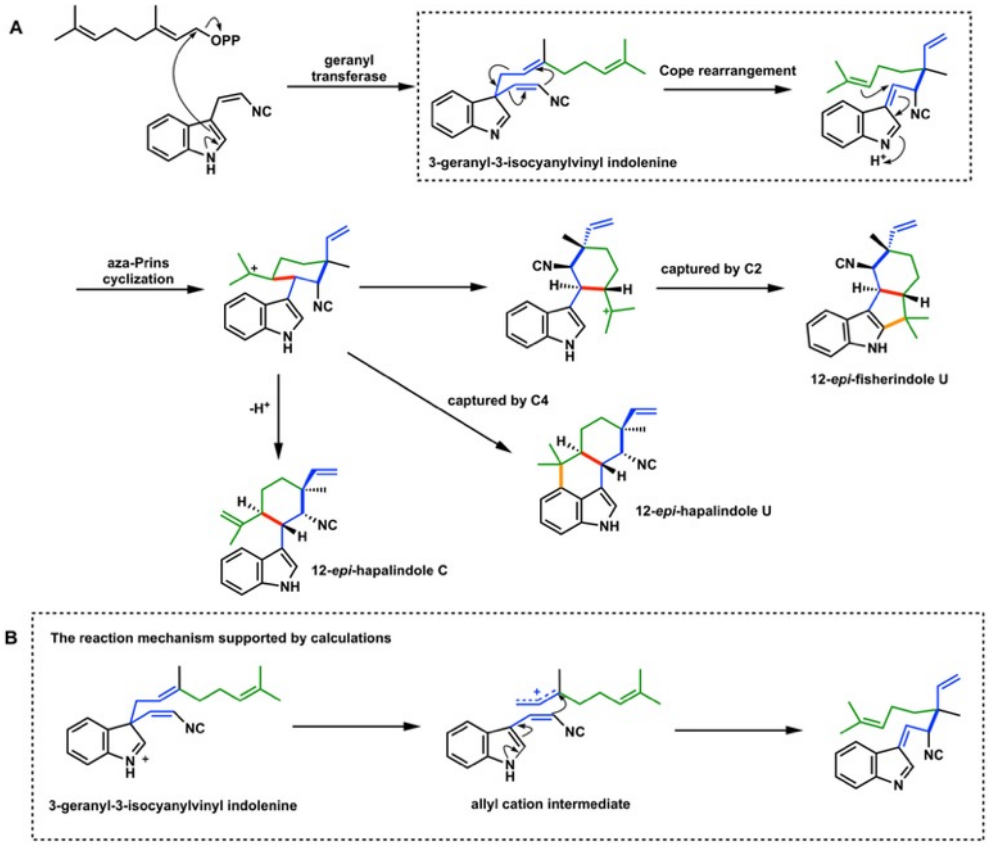

Figure 16
A. The Cope rearrangement involved in hapalindole and fischerindole biosynthesis. ***B.*** The likely acid-catalyzed stepwise (nonpericyclic) mechanism.

Theoretical studies by our group indicate that the pericyclic Cope rearrangement mechanism is accelerated by hydrogen-bonding groups, while full protonation of the indoline will cause the mechanism to change to a stepwise dissociative process involving an allyl cation intermediate (Figure 16b).[85] The mechanism of this reaction has not been established experimentally, so it is not certain if this enzyme is a true pericyclase or catalyzes a dissociation and recombination of a protonated intermediate. This mechanistic detail is surprisingly difficult to experimentally tease out. Similar issues have been raised for prenylation of lysergic acid or enzyme-catalyzed formation of 4-dimethylallyl tryptophan (4-DMAT). These reactions can proceed directly by C4

prenylation or indirectly via prenylation at the more nucleophilic C3-position followed by a Cope rearrangement, deprotonation and rearomatization.[86] This is the putative Cope pathway for catalytic formation of 4-DMAT by 4-DMAT synthase.[86] Therefore, the discovery of a true pericyclase that catalyzes Cope rearrangement remains an attractive topic for discovery.

1.8 Other Pericyclases to be Discovered in Nature

While enzyme catalyzed Diels-Alder reactions have been an attractive target for chemists due to the prominent usefulness in organic synthesis fields, other pericyclic reactions such as inverse electron demand Diels-Alder reaction (IEDDA),[87,88] Alder-ene reaction,[89,90] [3,3]-sigmatropic rearrangement[4,91] and electrocyclic reactions[92] are also widely utilized in synthetic chemistry. Given this and our recent discoveries of enzymatic ambimodal pericyclic reactions and retro-Claisen rearrangement, we expect that more pericyclic biosynthetic enzymatic transformations remain to be discovered in naturally occurring enzymes.

Recently, Erb and coworkers reported the identification of a transient covalent ene intermediate between NADPH and the acyl-CoA thioester during the catalysis of crotonyl-CoA carboxylase/reductase (Ccr, Figure 17a).[93] They proposed that the ene adduct is formed through an intermolecular electrocyclic Alder-ene reaction mechanism; this was supported by structure of a Ccr homolog cocrystallized with NADP+ and its 2-enoyl-CoA substrate. Nay and co-workers proposed that flavin-dependent monooxygenase AuaG catalyzes the tandem retro-[2,3]-Wittig rearrangement/Claisen rearrangement in addition

to the epoxidation during the aurachin B biosynthesis (Figure 17b).[94] Although it still remains unclear whether the reaction mechanisms of Ccr and AuaG are indeed pericyclic mechanisms or alternative stepwise mechanism, these enzymes certainly provide new opportunities for pericyclases in Nature.

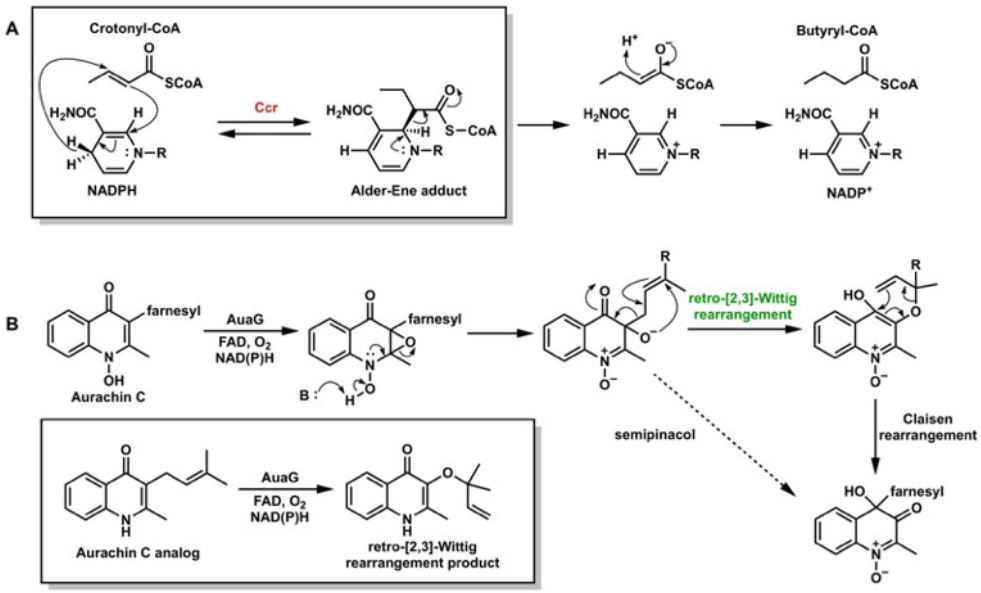

Figure 17
Proposed pericyclic (***A.***) Alder-ene reaction in catalysis of Ccr; (***B.***) retro-[2,3]-Wittig and Claisen rearrangements catalyzed by AuaG.

The discovery of SpnF and LepI encourages us to find other plausible intramolecular ambimodal pericyclic reactions. For example, intramolecular ambimodal pericyclic reactions would occur in substrates bearing two dienolic components as seen in LepI-catalyzed reactions, which can undergo formal Diels-Alder or inverse electron demand Diels-Alder reactions. Intermediates in natural product biosynthetic pathways that have this structural hallmark are likely to contain pericyclases that can catalyze ambimodal pericyclic reactions.

1.9 Conclusions

The number of known enzymes that can catalyze pericyclic reactions rapidly increased in the past five years. There will always be questions about whether the formal pericyclic reaction is truly concerted or not, and this provides a challenging area for experimental and theoretical mechanistic analysis. Regardless of detailed mechanism, an enzyme that catalyzes a Diels-Alder reaction or Cope rearrangement is a “Diels-Alderase” or “Copease.” We have described here that it is correct to consider a reaction in which the rate-determining transition state has a cyclic array of bonding interactions as a pericyclic reaction. This fits the original Woodward-Hoffmann definition and takes into account the possibility of a whole spectrum of asynchronicities, including those that include “entropic intermediates” with lifetimes of hundreds of femtoseconds. Pericyclases catalyze reactions that do not have long-lived observable intermediates. The Woodward-Hoffmann rules govern the possible products of such reactions. Genomic and bioinformatic analysis will continue to be a fruitful approach to the discovery of new pericyclases in cryptic biosynthetic pathways.

Chapter 2. Genome-Mined Diels–Alderase Catalyzes Formation of the cis-Octahydrodecalins of Varicidin A and B

2.1 Contributions

This is an author manuscript from the publication: Tan, D.; Jamieson, C. S.; Ohashi, M.; Tang, M. C.; Houk, K. N.; Tang, Y. Genome-Mined Diels-Alderase Catalyzes Formation of the Cis-Octahydrodecalins of Varicidin A and B. *J. Am. Chem. Soc*. **2019**, *141* (2), 769–773. https://doi.org/10.1021/jacs.8b12010. This project was a collaboration between my advisors' laboratories, Kendall N. Houk and Yi Tang. Postdoctoral fellow Dan Tan and I were co-first authors on this publication. Dan Tan conducted all biochemical experiments and I conducted all computational investigations. Dan Tan was advised and assisted with experiments by Masao Ohashi and Man-Cheng Tang.

2.2 Abstract

Pericyclases are an emerging family of enzymes catalyzing pericyclic reactions. A class of lipocalin-like enzymes recently characterized as Diels-Alderases (DAses) catalyze decalin formation through intramolecular Diels-Alder (IMDA) reactions between electron-rich dienes and electron-deficient dienophiles. Using this class of enzyme as a beacon for genome mining, we discovered a biosynthetic gene cluster from *Penicillium variabile* and identified that it encodes for the biosynthesis of varicidin A (**1**), a new antifungal natural product containing a *cis*-octahydrodecalin core. Biochemical analysis reveals a carboxylative deactivation strategy used in varicidin biosynthesis to suppress the nonenzymatic IMDA reaction of an early acyclic intermediate that favors *trans*-decalin

formation. A P450 oxidizes the reactive intermediate to yield a relatively unreactive combination of an electron-deficient diene and an electron-deficient dienophile. The DAse PvhB catalyzes the final stage IMDA on the carboxylated intermediate to form the *cis*-decalin that is important for the antifungal activity.

2.3 Introduction

Pericyclic reactions such as cycloadditions are often used by synthetic chemists to synthesize complex natural products (NPs). One of the most ubiquitous pericyclic reactions is the Diels-Alder (DA) reaction between a 1,3-diene and a dienophile (alkene) to form an unsaturated six-membered ring with up to four stereocenters in a regioselective and stereoselective manner.[22,80,95] Both normal- and inverse-electron demand DA reactions (NEDDA and IEDDA, respectively) are known, with the former being more common in synthetic chemistry.[96–98] These reactions differ in the frontier molecular orbital (HOMO and LUMO) energy levels of the dienes and dienophiles involved in the reactions.[99–101] Thousands of NPs have been identified to contain fused carbocycles or heterocycles, which led to identification of pericyclases: enzymes that catalyze pericyclic reactions.[102] The most prevalent pericyclases are Diels-Alderases (DAses), such as SpnF, PyrE3, Pyrl4 and AbyU.[43,44,46] One emerging class of fungal DAses have sequence homology to lipocalin-like enzymes, which bind to steroids and other hydrophobic molecules.[69,103] They are usually encoded in biosynthetic gene clusters containing a polyketide synthase-nonribosomal peptide synthetase (PKS-NRPS), and perform an intramolecular DA (IMDA) reaction on the immediate product of the PKS-NRPS.[34,48,104]

To date, reactions catalyzed by this family of enzymes, such as CghA[69], MycB[71]

and Fsa2,[70] are all NEDDA and proceed via the endo transition state to yield trans-decalin products with different facial stereoselectivities (Figure 18).

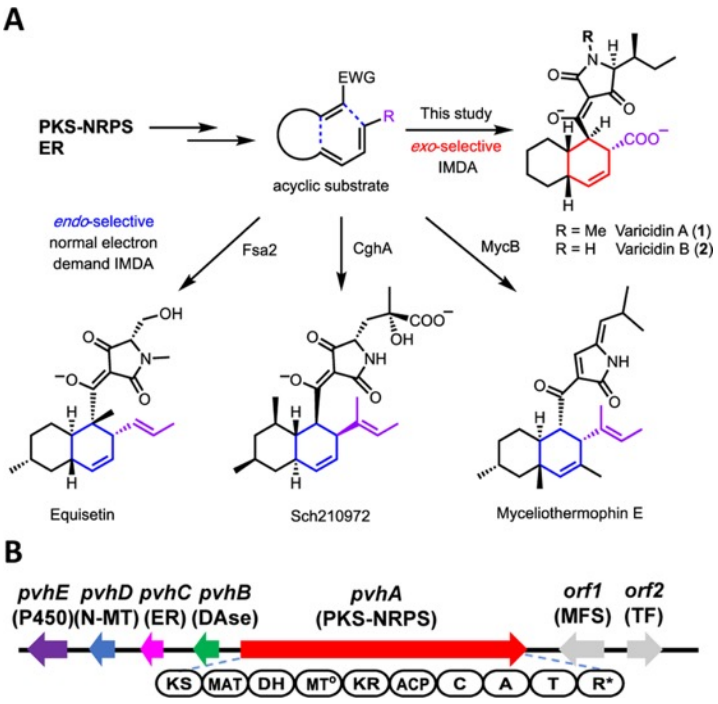

Figure 18
Lipocalin-like DAses catalyzes IMDA reactions in biosynthesis of decalin-containing fungal NPs. (***A.***) Characterized DAses and their decalin containing products; (***B.***) Genome mining of a DAse (PvhB) containing cryptic gene cluster from P. variable. Abbreviations: KS, ketosynthase; MAT, malonyl-CoA transferase; DH, dehydratase; MT, methyltransferase; KR, ketoreductase; ACP, acyl carrier protein; C, condensation; A, adenylation; T, thiolation; R, reductase. MFS: major facilitator superfamily; TF: transcription factor; N-MT: N-methyltransferase; ER: enoylreductase; DAse: Diels-Alderase.

Combinatorial pairing of PKS-NRPS and DAses from different biosynthetic gene clusters has led to new decalin compounds, demonstrating the potential of these enzymes in diversification of NPs structures.[105,106] A large number of cryptic biosynthetic gene clusters can be found in sequenced fungal genomes using the lipocalin DAse such as MycB[71] as the search query. We therefore reasoned that DAses with distinct functions to generate different core structures may be found among these gene clusters. In this work,

we focused on a compact gene cluster found in *Penicillium variabile* that encodes a DAse sharing low sequence homology with the characterized ones (36% and 27% sequence identities to Fsa2 and MycB, respectively). The pvh cluster also encodes a PKS-NRPS (pvhA), a trans-acting enoylreductase (ER) (pvhC), a putative DAse (pvhB), a predicted N-methyltransferase (pvhD), and a cytochrome P450 (pvhE) (Figure 18b). No known decalin-containing NPs have been isolated from *P. variabile*.

2.4 Varicidin Biosynthesis

The five genes (pvhA-E) were introduced into an engineered *Aspergillus nidulans* expression host[69] on three episomal vectors. Compared to the negative control, the extract contained a new metabolite **1** with molecular weight (MW) of 375 (Figure 19a, trace *i*). This compound was isolated and characterized by 1D- and 2D-NMR spectroscopy to be a tetramate-containing decalin. Based on NOESY, the decalin ring of **1** (named varicidin A) is in the cis configuration and is carboxylated at C21 (Figure 19b). The amide nitrogen in the 2,4-pyrrolidinedione ring is methylated and is consistent with the coexpression of a N-methyltransferase PvhD. Expression of pvh gene cluster without pvhD in *A. nidulans* led to the biosynthesis of a new compound **2** (varicidin B), which was shown by NMR to be the N-desmethyl variant of **1** (Figure 19a, trace *ii*). We were able to obtain an X-ray crystal structure of **2** (Figure 19d), which allowed us to confirm the *S*-stereochemistry at C17 and the absolute stereochemistry of **2**. The absolute stereochemistry of **1** was assigned based on that of **2** (Figure 19b). The structure and stereochemistry of the C17 branched chain indicate the incorporation of L-isoleucine by

the NRPS module. Both **1** and **2** exhibited antifungal activities against *Candida albicans*[107] with minimum inhibitory concentrations (MICs) of 8 and 16 μg/mL, respectively.

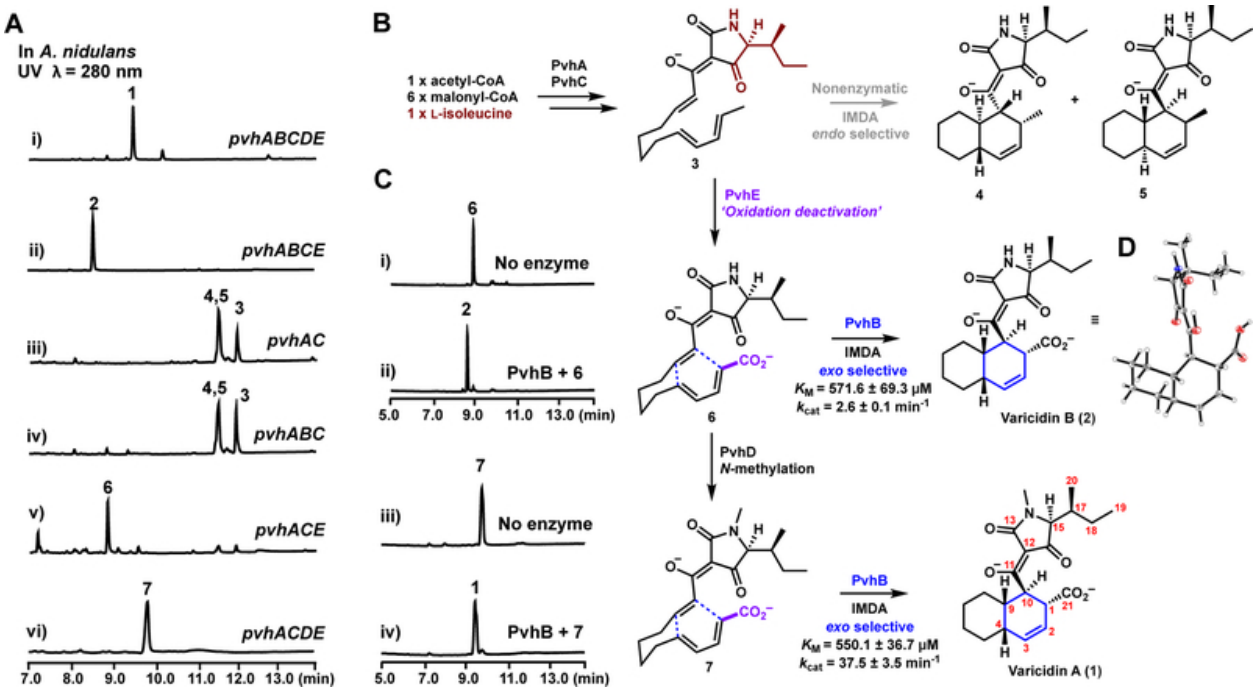

Figure 19

Biosynthesis of varicidin A **1**. (***A.***) Product profiles of *A. nidulans* transformed with combinations of pvh genes; (***B.***) The proposed biosynthetic pathway of **1**; (***C.***) Biochemical characterization of the DAse PvhB *in vitro*. The traces are HPLC with λ = 280 nm. (***D.***) Crystal structure of **2**.

2.5 Computational and Biochemical Characterization of Pericyclase PvhB

Presumably, the *cis*-decalin structures of **1** and **2** would be formed by *exo*-IMDA reactions from acyclic precursors, and PvhB represents the most likely enzyme to catalyze this diastereoselective reaction, as no isomeric cycloadducts can be detected in the extracts. To confirm the function of PvhB, we only expressed the PKS-NRPS PvhA and its partnering ER PvhC in *A. nidulans*. Analysis of the extract showed the accumulation of **3**–**5** with the same MW of 331. **3** is an acyclic tetramate. Based on previous studies on decalin-containing NPs such as equisetin[70] and Sch210972,[69] the biosynthesis of **3** is

expected to follow the similar logic: the PKS domains iteratively synthesize the polyketide portion. Selective enoylreduction by the ER during different cycles furnishes both the diene and the dienophile. The polyketide acyl chain is then condensed with L-isoleucine, followed by a Dieckmann cyclization to afford **3**. Compounds **4** and **5** were purified by chiral HPLC and structurally elucidated to be *trans*-decalin diastereomers, which are expected to be derived from the *endo*-specific IMDA reactions from **3**. When **3** was left in buffer at pH 7.0, nonenzymatic formation of **4** and **5** can be observed, consistent with the heterologous expression results in Figure 19a in which **4** and **5** were co-isolated. A mixture of other products was also detected, but the yields were too low for structural characterization. In agreement with experimental data which showed the rate constant (k_{non}) of the nonenzymatic IMDA reaction of **3** was ~ 4.0×10^{-4} min^{-1} in HEPES buffer at 30 ºC, the density functional theory (DFT) calculations[108–110] at the M06–2X/6–311+G(d,p)/CPCM(H2O)//M06–2X/6–31G(d)/SMD(H2O) level of theory predicted this value $k_{non, calc}$ to be 1.1×10^{-5} min^{-1} (Figure 20a, **TS-1** $\Delta G^{‡}$ = 26.6 kcal·mol^{-1} and **TS-2** $\Delta G^{‡}$ = 26.8 kcal·mol^{-1} for **4** and **5**, respectively). In **TS-1** and **TS-2**, secondary orbital interactions of the diene and tetramate carbonyl favor these *endo*-cyclizations. DFT predicts the product mixture contains one *exo*-cycloadduct in similar yield.

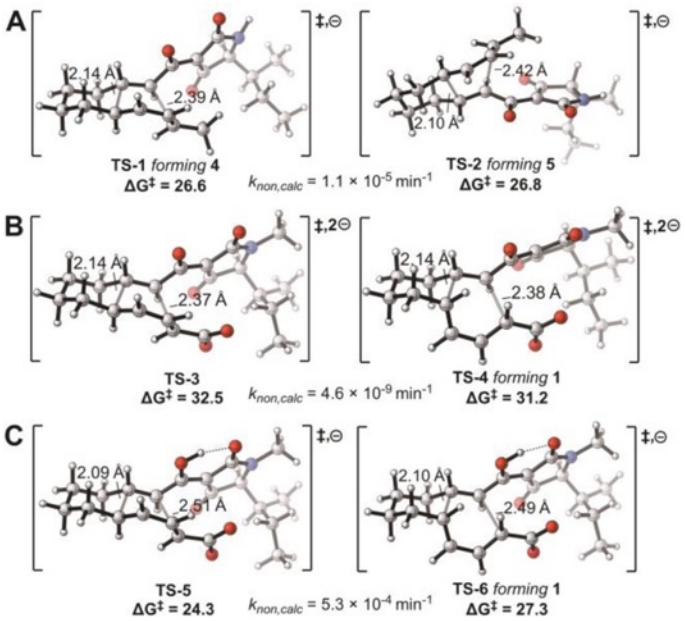

Figure 20
DFT calculated transition states of NEDDA and IEDDA. ***A.*** Transition state structures **TS-1** and **TS-2** with energies shown for nonenzymatic endo-cyclizations of **3** forming **4** and **5**, respectively. ***B.*** *endo* **TS-3** and *exo* **TS-4** of IEDDA reactions in solution as dianions. **TS-4** leads to formation of the *cis*-decalin stereochemistry for varicidin A. ***C.*** *endo* **TS-5** and *exo* **TS-6** of NEDDA reactions when tetramic acid is protonated.

Coexpressing PvhAC with PvhB did not change the metabolite profile, with **3**–**5** remained as the main products (Figure 19a, trace *iv*), indicating **3** is not a substrate of PvhB. PvhB was expressed and purified from *E. coli* following codon optimization. Adding PvhB to **3** further confirmed that no *cis*-decalin products can be formed. To determine the timing and substrate of PvhB, we coexpressed PvhAC together with P450 PvhE in *A. nidulans*, which produced a new metabolite **6** (Figure 19a, trace *v*). NMR analysis showed it to be the carboxylated version of **3**. PvhE was then expressed in *Saccharomyces cerevisiae* RC01,[111] and whole-cell biotransformation was performed by feeding 5 mM of either **3** or a mixture of **4** and **5**. Whereas the acyclic **3** was oxidized to **6** readily, neither the trans-decalin compounds were modified. This confirms the role of PvhE in catalyzing oxidation of the C21 methyl group in **3** to the carboxylate in **6**. An additional heterologous

expression construct was made by coexpressing the *N*-methyltransferase PvhD with PvhACE, yielding a new compound **7** (Figure 2, trace vi), which was structurally determined to be the *N*-methylated version of **6**. Recombinant PvhD purified from *E. coli* was able to completely methylate **6** to **7** in the presence of *S*-adenosylmethionine (SAM), while unable to methylate **2** into **1**. Therefore, the function and timing of PvhD were confirmed to act on **6** to give **7** (Figure 19a).

Notably, replacing the electron-donating methyl in **3** by the electron-withdrawing carboxylate in **6** (and **7**) significantly suppressed nonenzymatic IMDA reactions. Incubation of **6** and **7** in various solvents, even at high temperatures, did not lead to formation of any IMDA products. In solution near neutral pH, oxidized **6** and **7** are expected to exist as dianions.[112] Consequential electrostatic repulsion between the two anions increases the reaction barrier, suppressing the nonenzymatic IMDA reaction. The poor reactivity can also be explained by the pairing of an electron-deficient diene and an electron-deficient dienophile. The dienylcarboxylate and the alkylidenetetramate withdraw electron-density from the diene and dienophile, respectively, increasing the reaction barrier. Furthermore, oxidation alters the electronic nature of the IMDA, switching the reaction type from NEDDA to IEDDA. We believe that both the electrostatic anion repulsion and the electron-deficient nature of diene and dienophile raise the barrier of **7** to the *endo* **TS-3** and the *exo* **TS-4** that leads to **1** to $\Delta G^{\ddagger}$ = 32.5 and $\Delta G^{\ddagger}$ = 31.2 kcal·mol^{-1}, respectively (Figure 20b). This is a 10,000-fold decrease in rate compared to the nonenzymatic cyclizations of **3**. These IEDDA cycloadditions are predicted to be slow ($k_{non,calc}$ = 4.6 × 10^{-9} min^{-1}, Figure 3b) at room temperature, and experimentally no

reaction is observed. We hypothesize that protonation may play an important role in catalysis. To investigate the potential modes of catalysis by the enzyme, we explored the possible influence of protonation of the tetramate. Such a protonation is unusual and unlikely in solution as the pKa of the carboxylate is greater than that of the tetramate.[112] We calculated that *exo* reaction of the dienylcarboxylate with the protonated alkylidene tetramic acid lowers the activation energy to form **1** by 3.9 kcal·mol^{-1} via **TS-6** (Figure 20c). Therefore, depending on the protonation state of the tetramic acid in the enzyme active site, these cyclizations could either be NEDDA or IEDDA in presence of PvhB.

These results indicate the DAse PvhB must lower the high barrier of the IEDDA TS in catalyzing the cycloaddition of **6** or **7** to *cis*-decalin **2** or **1**, respectively (Figure 2a). This was verified by *in vitro* assay of purified PvhB, showing that more than 95% of **7** or **6** was converted to **1** or **2** respectively when incubated with PvhB within 12 hrs (Figure 19c, trace *iv*, *ii*). Kinetic measurements showed PvhB to have a K_M of 571.6 ± 69.3 μM and k_{cat} of 2.6 ± 0.1 min^{-1} toward **6**; and K_M of 550.1 ± 36.7 μM and k_{cat} of 37.5 ± 3.5 min^{-1} toward **7** (Figure 19b). The 15-fold higher specificity (k_{cat}/K_M) of PvhB toward **7** over **6** indicated that **7** is most likely the native substrate of PvhB. This allowed us to propose the overall biosynthetic pathway in which PvhB-catalyzed IMDA reaction is the final step (Figure 19b). We added a strong Lewis acid SnCl4 to **6** in dichloromethane to examine outcomes of the chemical catalysis. However, the Lewis acid gave complex mixtures with compound **2** being a minor product. PvhB is therefore a strong and stereo-selective DAse to catalyze formation of a single *exo*-specific *cis*-decalin product from the acyclic precursors.

2.6 Conclusions

Collectively, we propose a “carboxylative deactivation” strategy used in this biosynthetic pathway to construct the antifungal **1**. Our results show that the activity of redox enzymes can influence the course of biosynthetic pathways that involve IMDA reactions. The acyclic PKS-NRPS product **3** is prone to nonenzymatic IMDA to yield the *trans*-decalin products **4** and **5**. Oxidation of the diene portion of **3** to the dienocarboxylate **6** significantly increases the IMDA barrier and effectively suppresses the nonenzymatic reactions. This can be overcome by the activities of the stereospecific DAse PvhB to arrive at the desired *cis*-decalin product. The discovery of PvhB further illustrates the functional diversity of the lipocalin-like DAses in fungi, and the prospects of using these enzymes as beacons for new natural product discovery.

Chapter 3. Enzyme-catalyzed Inverse-Electron Demand Diels–Alder Reaction in the Biosynthesis of Antifungal Ilicicolin H

3.1 Contributions

This is an author manuscript from the publication: Zhang, Z.; Jamieson, C. S.; Zhao, Y.-L.; Li, D.; Ohashi, M.; Houk, K. N.; Tang, Y. Enzyme-Catalyzed Inverse-Electron Demand Diels–Alder Reaction in the Biosynthesis of Antifungal Ilicicolin H. *J. Am. Chem. Soc.* **2019**, *141* (14), 5659–5663. https://doi.org/10.1021/jacs.9b02204. This project was a collaboration between my advisors laboratories, Kendall N. Houk and Yi Tang. Postdoctoral fellow Zhuan Zhang conducted all biochemical experiments and I conducted all computational investigations. Dan Tan was advised and assisted with experiments by Masao Ohashi and Man-Cheng Tang. Yi-Lei Zhao, Dehai Li, and Masao Ohashi provided advice and assistance with experiments and calculations.

3.2 Abstract

The pericyclases are a growing superfamily of enzymes that catalyze pericyclic reactions. We report a pericyclase IccD catalyzing an inverse-electron demand Diels–Alder (IEDDA) reaction with a rate acceleration of 3×10^5 fold in the biosynthesis of fungal natural product ilicicolin H. We demonstrate IccD is highly periselective towards the IEDDA cycloaddition over a competing normal electron demand Diels-Alder (NEDDA) reaction from an ambimodal transition state. A predicted flavoenzyme IccE was identified to epimerize the IEDDA product 8-epi-ilicicolin H to ilicicolin H, a step that is critical for the observed antifungal activity of ilicicolin H. Our results reveal the ilicicolin H biosynthetic

pathway and add to the collection of pericyclic reactions that are catalyzed by pericyclases.

3.3 Introduction

Diels-Alder (DA) reactions, involving the cycloaddition between a 1,3-diene and a dienophile to form an unsaturated six-membered ring, are among the most powerful synthetic transformations to construct complex natural products.[22] Depending on substituents, the reaction can proceed via the normal- or inverse-electron demand Diels-Alder (NEDDA or IEDDA) pathways that differ in relative frontier molecular orbital (FMO, HOMO–LUMO) energies (Figure 21a). Hundreds of natural products with unsaturated cyclohexenes or octahydrodecalins have been identified.[34] Many of these are products of pericyclic reactions, and it is now known that a variety of pericyclases—enzymes that catalyze pericyclic reactions—exist.[102] PyrE3,[44] CghA[69] and MycB,[71] and others,[105,113] are all decalin-forming pericyclases that catalyze NEDDA reactions (Figure 21a). In contrast, no enzyme-catalyzed IEDDA reaction has been reported to date. Structural examination and biomimetic synthesis of natural products, however, suggest enzyme-catalyzed IEDDA reaction should exist in Nature.[48]

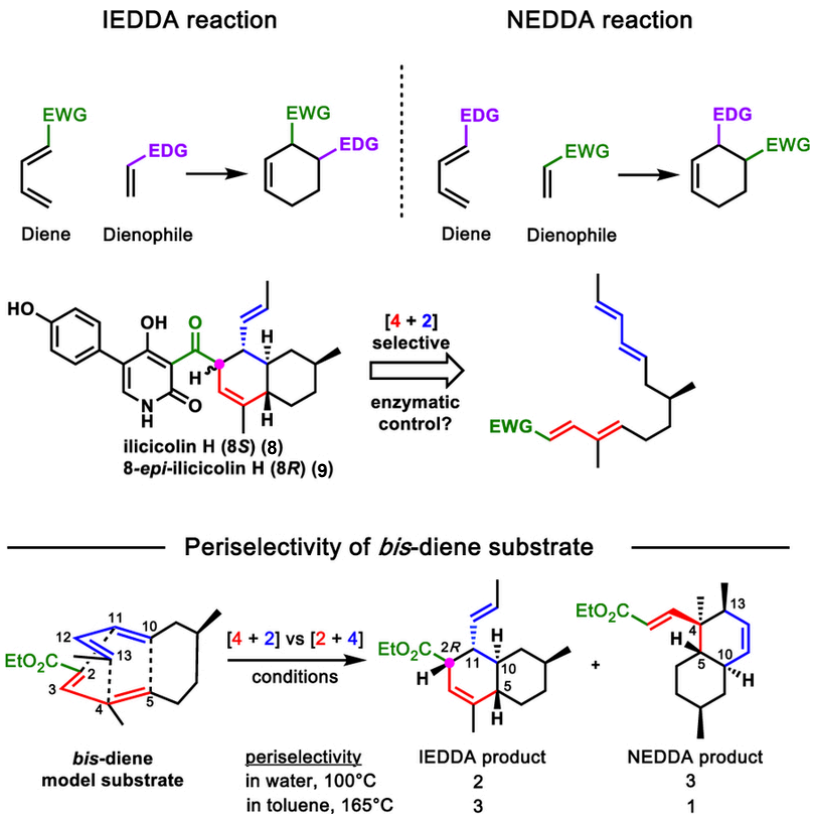

Figure 21
NEDDA and IEDDA reactions. ***A.*** General scheme of both reactions. EWG: electron withdrawing group; EDG: electron donating group; ***B.*** Proposed enzyme-catalyzed IEDDA reaction in ilicicolin H (**8**) biosynthesis, as demonstrated in total synthetic effort towards **8**.

One potential IEDDA pericyclase candidate is in the biosynthetic pathway of ilicicolin H (**8**) (Figure 21b).[114,115] The decalin-containing **8** was isolated from *Cylindrocladium ilicicola* MFC-870 and other fungi.[114–118] **8** is a 4-hydroxy-2-pyridone alkaloid, and has a potent (sub μg/mL) and broad (*Candida*, *Aspergillus* and *Cryptococcus*) antifungal activities by inhibiting the mitochondrial respiration chain.[119,120] While the biosynthesis of **8** has remained unresolved, a biomimetic total synthesis of (±)-**8** was reported by Williams *et al*. using an intramolecular IEDDA step to form the *trans*-octahydrodecalin.[121] A model study using an ethyl ester of the acyclic precursor showed that heating the *bis*-diene compound in boiling water or refluxing toluene afforded opposite selectivity towards

IEDDA or NEDDA reaction (Figure 21b).[122] Pericyclic reaction selectivity can be rationalized by FMOs, and selectivity for a specific pericyclic reaction is referred to as periselectivity.[123] The synthetic results therefore indicated that NEDDA and IEDDA reactions are competitive, and periselectivity depends on solvent polarity (Figure 21b). The synthetic studies were not able to afford only the desired IEDDA product. This led us to hypothesize that an enzyme must control the IEDDA periselectivity in biosynthesis of **8**.

To identify the responsible enzyme, we first searched for candidate genes that are likely to participate in the biosynthesis of **8** in the genome sequence of a producing fungus, *Nectria sp*. B-13.[117] As with other fungal 2-pyridone compounds, we propose biosynthesis of **8** starts with formation of the tetramic acid **10** by a polyketide non-ribosomal peptide synthetase (PKS-NRPS) with a partnering enoylreductase (ER), followed by a P450-catalyzed ring expansion of the tetramate to the acyclic **11**.[124] This led to the identification of one candidate cluster ncc that contains five genes, encoding a PKS-NRPS (nccA), a partnering ER (nccB), a P450 (nccC), a predicted C-methyltransferase (C-MT, nccD), and a predicted old yellow enzyme (OYE, nccE) (Figure 22a). We searched for homologs of this five-gene cassette computationally, which revealed this combination is widely distributed in fungi: 41 different sequenced fungal strains in the NCBI database were found to minimally contain the five-gene pathway. For example, we identified the icc cluster that contains the five genes from the recently sequenced *Penicillium variabile* (Figure 22a).[125] The cDNA library of *P. variabile* was available to us, and the icc cluster

was therefore used to study the functions and products of the conserved five-gene cassette.

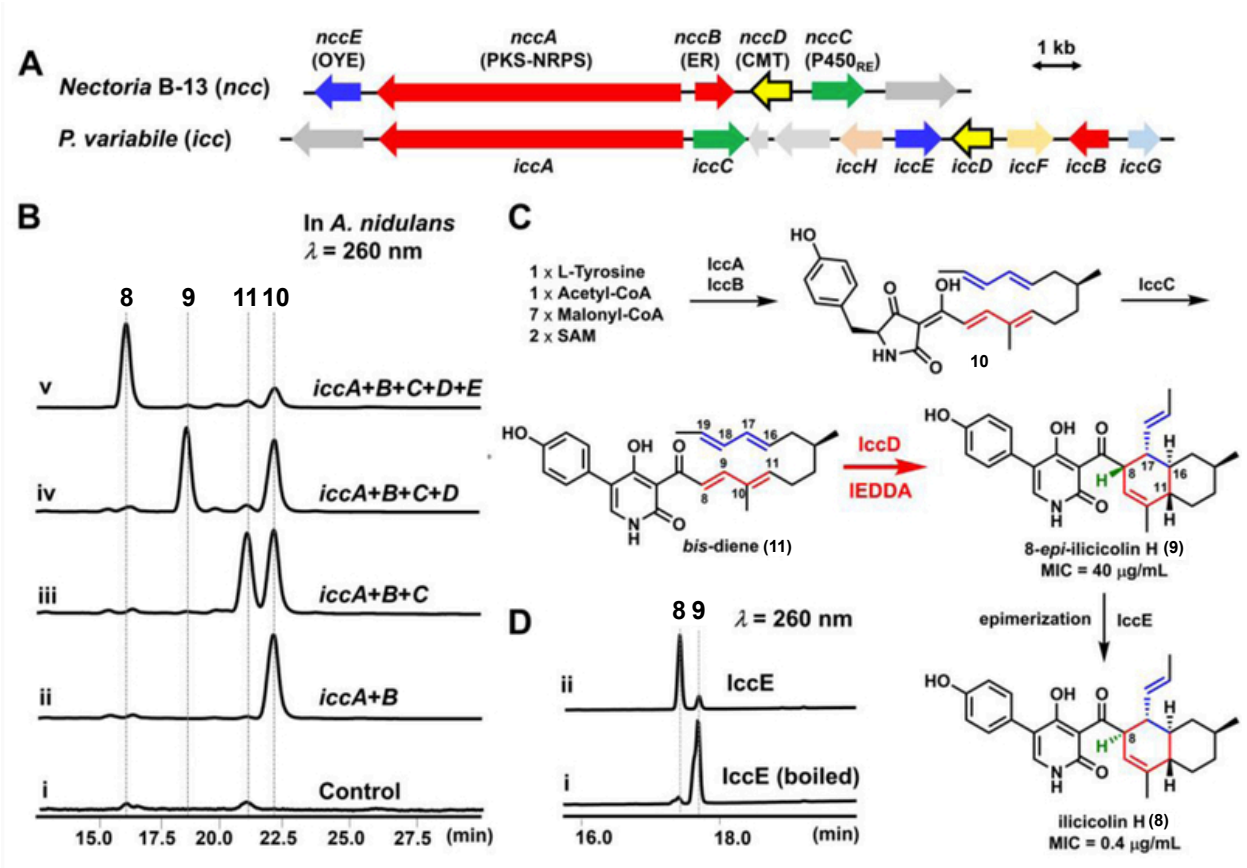

Figure 22

Characterization of ilicicolin H (**8**) biosynthesis. ***A.*** The icc cluster encodes a PKS-NRPS (KS-AT-DH-MT-KR-ERo-ACP-C-A-T-R. KS, ketosynthase; AT, acyltransferase; DH, dehydratase; MT, methyltransferase; KR, ketoreductase; ACP, acyl carrier protein; C, condensation; A, adenylation; PCP, peptidyl carrier protein; R, reductase) IccA, a trans-ER IccB, a ring expansion P450 IccC, a putative C-methyltransferase IccD and a putative old yellow enzyme IccE; ***B.*** Product profiles from heterologous expression of different combinations of icc cluster in *A. nidulans* A1145. Control in trace *i* is *A. nidulans* transformed with empty vectors only; ***C.*** Proposed biosynthetic pathway of **8**; ***D.*** *In vitro* characterization of IccE-catalyzed epimerization. The assays were conducted in 50 mM Tris-HCl at pH 7.0, in the presence of 0.2 mM **9** and 0.1 μM IccE.

3.4 Biochemical Characterization of Ilicicolin Biosynthesis

We heterologously expressed the five icc genes in *Aspergillus nidulans* A1145 followed by metabolite isolation and structural characterization. Co-expression of the PKS-NRPS IccA and ER IccB yielded tetramate **10** (20 mg/L) (Figure 22b, trace *ii*). Further coexpression of ring-expansion P450 IccC led to the production of 2-pyridone **11** that contains the *trans bis*-diene chain (20 mg/L) (Figure 22b, trace *iii*). The two remaining enzymes, C-MT IccD and OYE IccE, were then expressed in *A. nidulans*. Adding IccD to the strain that produced **11** yielded a new prominent product **9** (10 mg/L)(Figure 22b, trace *iv*). Structure characterization by NMR demonstrated **9** as the *endo* IEDDA product 8-*epi*-ilicicolin H. This result confirmed that IccD is responsible for the transformation of *bis*-diene **11** to **9**, thus suggesting IccD acts as a pericyclase for this IEDDA reaction. After identifying **9**, we found trace amounts of **9** can be detected in IccA-C expression strain (Figure 22b, trace *iii*). Finally, adding IccE led to near complete conversion of **9** to the final product **8** (10 mg/L)(Figure 22b, trace *v*). This assigns the role of IccE in the epimerization of **9** to **8**. The gene-by-gene reconstitution in *A. nidulans* therefore confirmed i) the five conserved enzymes IccA-IccE are necessary and sufficient to biosynthesize **8**; ii) the acyclic *bis*-diene is relatively unreactive under culturing conditions, and enzymatic acceleration of the IEDDA reaction is required; and iii) the C-MT homolog, IccD, catalyzes the IEDDA cycloaddition.

We then assayed the activities of IccD using C-His-tagged enzyme heterologously expressed and purified from *E. coli* BL21(DE3). When 0.1 mM **11** was incubated with 1 μM IccD in Tris-HCl (pH 7.0), more than 60% of **11** was converted to **9** within 2 hr (Figure

23a), after which IccD denatured rapidly. The catalytic efficiency of IccD was determined by assaying the initial velocity of the transformation. IccD exhibited K_M of 54 ± 0.5 μM towards **11** and k_{cat} of 54 ± 7.8 min^{-1}. In the absence of IccD, the uncatalyzed reaction was nearly undetectable at room temperature in aqueous solution. We were able to measure the rate of uncatalyzed cycloaddition in toluene, with a $k_{non} = 1.8 \times 10^{-4}$ min^{-1}. Therefore, IccD is able to significantly accelerate the reaction rate by 3×10^5 fold (compared with nonenzymatic reaction measured in toluene). IccD belongs to the C-MT superfamily, with an intact *S*-adenosyl-L-methionine (SAM) binding motif GXGXG.[126] IccD shows 24 % homology to SpnF, also a predicted C-MT that catalyzes the [4+2] NEDDA cycloaddition in the biosynthesis of spinosyn.[43] Unlike the recently characterized SAM-dependent O-MT-like pericyclase LepI,[80] IccD did not copurify with SAM bound in the active site. Addition of exogenous SAM to the reaction of **11** to **9** had no effect on the reaction kinetics or product profile. Therefore, the IccD-catalyzed IEDDA reaction is most likely SAM-independent.

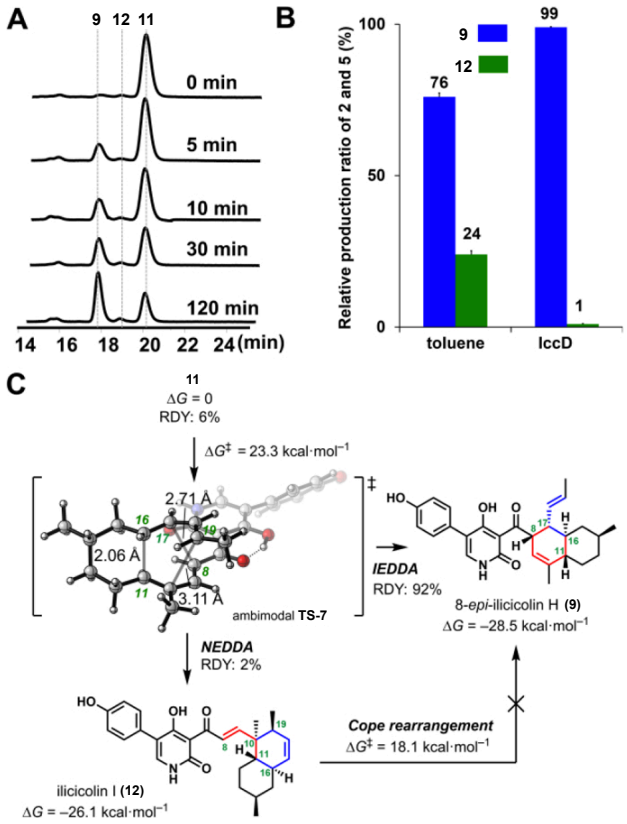

Figure 23
Characterization of IccD-catalyzed pericyclic reaction. ***A.*** HPLC profile of time-course reaction of IccD. The assays were conducted at 28°C from 0 to 120 min; ***B.*** Comparison of relative IEDDA and NEDDA product ratio starting from **11**; ***C.*** Calculated reaction surface energies and dynamics results from **11** converting to **9** and **12**. RDY: reaction dynamics yield from **TS-7**.

3.5 Computational Characterization of Pericyclase IccD Mechanism

To investigate the periselectivity of IccD, we quantified product distribution resulting from IEDDA versus NEDDA reactions with and without IccD. Consistent with synthetic studies with model substrate (Figure 21b), the reaction of **11** in toluene gave **9** and **12** in a ratio of 3:1 (Figure 23b). The minor product **12** was characterized as the NEDDA product ilicicolin I (**12**).[118] The reaction with IccD yielded <1% **12** (Figure 23a,b). **12** can also be detected in trace amounts from *in vivo* reconstitution using extracted ion chromatogram. This raised the possibility that **12** might be an intermediate in the IccD-catalyzed reaction

of **11** to **9**. Since **12** and **9** are derived from the same facial- and *endo*-NEDDA and IEDDA reactions, respectively, conversion of **12** to **9** could be envisioned via a [3,3]-sigmatropic Cope rearrangement (Figure 23c). However, when **12** was directly added to IccD in the reaction buffer, no **9** was formed. Heating **12** in water at 100 ºC also did not form **9**. Therefore, we concluded that **12** is not an intermediate. In turn, our data point to IccD catalyzing a direct IEDDA reaction of **11** to **9** with high periselectivity.

To understand the origin of periselectivity and the potential mode of catalysis for IccD-catalyzed reaction, we performed density functional theory (DFT) calculations at the ωB97X-D/6-311+G(d,p)/CPCM(H2O)//ωB97X-D/6-31G(d)/SMD(H2O) and ωB97X-D/6-311+G(d,p)//ωB97X-D/6-31G(d) levels of theory.[108,110,127,128] We calculated the energy surface from **11** to **9** in the gas phase to model the hydrophobic enzyme pocket (Figure 3c). The lowest energy transition state is the ambimodal **TS-7** ($\Delta G^{\ddagger}$ = 23.3 kcal·mol^{-1}). Ambimodal transition states sequentially connect to a second transition state lower in energy that interconverts two products.[61,62,75] This allows **TS-7** to form both IEDDA-adduct **9** (forming C11–C16 and C8–C17) and NEDDA-adduct **12** (forming C11–C16 and C10–C19, Figure 23c) via post-transition state bifurcation. The possible Cope-rearrangement **TS-8** ($\Delta G^{\ddagger}$ = 18.1 kcal·mol^{-1}) is 5.2 kcal·mol^{-1} lower in energy than **TS-7** (Figure 23c). However, cycloadducts **12** and **9** are much more stable than *bis*-diene **11**. Thus, the barrier to convert **12** to **9** ($\Delta G^{\ddagger}$ = 44.2 kcal·mol^{-1}) is too large for the enzyme to overcome. Hence, the enzyme must control the post-**TS-7** bifurcation dynamics to achieve high IEDDA periselectivity. Since transition state theory cannot determine the kinetic product ratio, quasi-classical reaction dynamics trajectories in gas phase were

initiated from **TS-7** and found to give products **9** and **12** in a ratio of 98:2, respectively (Figure 23c). This ratio of **9** to **12** reproduces experimental enzymatic reactions (Figure 23b). This suggests that IccD-catalyzed reaction takes place in a hydrophobic pocket to direct the near-exclusive formation of **9** by ambimodal **TS-7**.

3.6 Noncanonical Epimerization Reaction Catalyzed by Old Yellow Enzyme IccE

We also characterized the OYE homolog IccE *in vitro* to verify its role in the final epimerization step. The enzyme was expressed and purified as N-His-tagged protein from *E. coli* BL21(DE3). When **9** was incubated with IccE in Tris-HCl (pH 7.0), the epimerization from **9** to **8** occurred readily within 2 h (Figure 22d). Since 8-H of **8** and **9** is relatively acidic, deprotonation of 8-H would lead to epimerization. This was demonstrated by the pH-dependent nonenzymatic epimerization from **9** to **8**, in which the epimerization rate increases as the reaction pH increases. IccE, as with other OYE enzymes, is predicted to be a flavin-dependent enzyme. However, no clear role of the flavin is evident in the proposed epimerization mechanism. This unexpected reactivity of IccE therefore adds to a list of nonredox reactions catalyzed by predicted flavoenzymes.[129]

3.7 Conclusions

The IccE-catalyzed epimerization reaction is critical for the antifungal activities of **8**, as demonstrated in our assay of **8** and **9** against *Candida albicans* SC5314. The antifungal activity of **9** (MIC = 40 μg/mL) is ~100-fold less potent compared to that of **8** (MIC = 0.4 μg/mL). The epimerization reaction catalyzed by IccE can be considered as an activation step in which inversion of one stereocenter in **9** led to drastically enhanced activities. The

icc gene cluster in *P. variabile* encodes additional redox enzymes in addition to the five conserved enzymes that synthesize **8**. In the native host, these additional enzymes could potentially perform modifications on **8** to further enhance its activity. In summary, our efforts uncovered the concise ilicicolin H biosynthetic pathway, featured by the pericyclase IccD that catalyzes a challenging IEDDA reaction of **11** to **9**. Our findings further expand the catalytic repertoire of naturally-occurring pericyclases.

Chapter 4. Enzymatic Intermolecular Hetero-Diels–Alder Reaction in the Biosynthesis of Tropolonic Sesquiterpenes

4.1 Contributions

This is an author manuscript from the publication: Chen, Q.; Gao, J.; Jamieson, C.; Liu, J.; Ohashi, M.; Bai, J.; Yan, D.; Liu, B.; Che, Y.; Wang, Y.; et al. Enzymatic Intermolecular Hetero-Diels-Alder Reaction in the Biosynthesis of Tropolonic Sesquiterpenes. *J. Am. Chem. Soc.* **2019**, *141* (36), 14052–14056. https://doi.org/10.1021/jacs.9b06592. This project was a collaboration between the Kendall N. Houk and Youcai Hu laboratories. I conducted all computational experiments and Qibin Chen and Jie Gao conducted the majority of the experimental work. Qibin Chen and Jie Gao received experimental assistance from Jiawang Liu, Masao Ohashi, Jian Bai, Daojian Yan, Bingyu Liu, Yongsheng Che, and Yanan Wang.

4.2 Abstract

Diels–Alder reactions are among the most powerful synthetic transformations to construct complex natural products. Despite that increasing of enzymatic intramolecular Diels–Alder reactions have been discovered, natural intermolecular Diels–Alderases are rarely described. Here, we report an intermolecular hetero-Diels–Alder reaction in the biosynthesis of tropolonic sesquiterpenes and functionally characterize EupfF as the first fungal intermolecular hetero-Diels–Alderase. We demonstrate that EupfF catalyzed the dehydration of a hydroxymethyl-containing tropolone (**17**) to generate a reactive tropolone *o*-quinone methide (**18**) and might further stereoselectively control the subsequent

intermolecular hetero-Diels–Alder reaction with (1*E*,4*E*,8*Z*)-humulenol (**20**) to produce enantiomerically pure neosetophomone B (**13**). Our results reveal the biosynthetic pathway of **13** and expand the repertoire of activities of Diels–Alder cyclases.

4.3 Introduction

Diels–Alder (DA) reactions, in which a 1,3-diene and a dienophile react to form an unsaturated cyclohexane regio- and stereo-selectively are one of the most powerful synthetic strategies for the synthesis of complex natural products.[77,130] Both intramolecular and intermolecular Diels–Alder cycloadditions are presumed to introduce structure complexity and biological activity in natural compounds. Although increasing numbers of intramolecular Diels–Alderases or [4 + 2]-cyclases[66] such as LepI,[80] SpnF,[43] PyrE3,[44] IccD,[131] PvhB,[113] and others,[14,71,132] have been discovered in Nature, direct biochemical evidence of enzyme-catalyzed intermolecular DA reactions have rarely been described except for macrophomate synthase and riboflavin synthase.[66] Notably, natural products probably biosynthesized via an intermolecular Diels–Alder reaction are frequently reported from bacteria, fungi, and plants.[133–135]

Remarkably, several members of the tropolone-sesquiterpene family of meroterpenoids represented by neosetophomone B (**13**),[136] epolone B (**14**),[137] eupenifeldin (**15**),[138] and pycnidione,[139] isolated as optically pure compounds from a variety of fungi, were proposed to be biosynthesized via one or two tandem hetero Diels–Alder (hDA) reactions (Figure 24).[140] Structurally, these meroterpenoids possess a unique central 11-membered macrocycle flanked by one or two dihydropyrans coupled to tropolones.

Biologically, **13** and **15** were found as very potent antitumor agents with activity at the nanomole level in in vitro tumor cell lines,[136,138] while **14** and pycnidione are stromelysin inhibitors and potential antiarthritic drugs.[139]

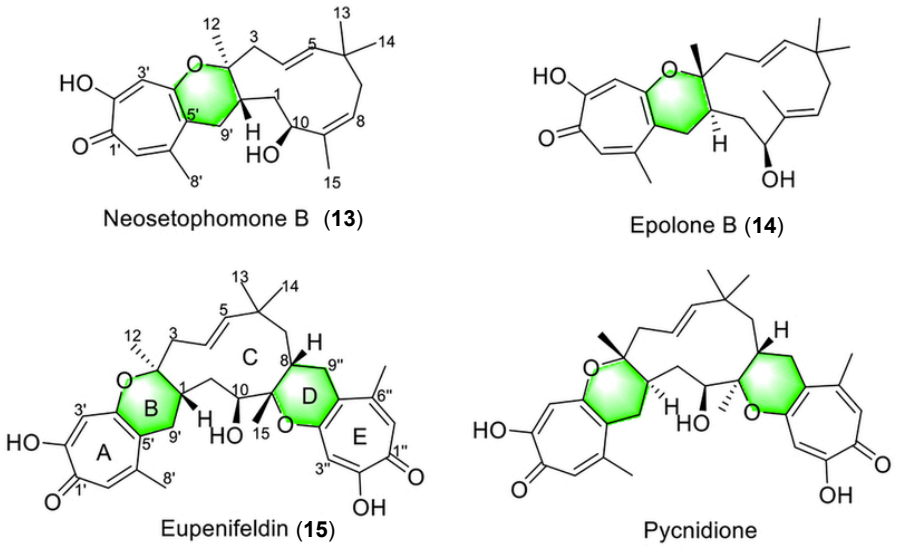

Figure 24
Representative tropolone-sesquiterpenes probably generated from intermolecular Diels–Alder reactions.

Studies toward the biomimetic synthesis of tropolone-sesquiterpenes showed the generation of monotropolone adducts via hDA reaction under thermal conditions achieved success only for unnatural model compounds.[141–143] In fact, the total synthesis of these tropolone-sesquiterpenes has not been completed thus far. It is therefore of interest to identify strategies and enzymes Nature uses to synthesize compounds of this family, especially the structures with observed in **13**.

Biosynthetically, hDA reactions of a tropolone *o*-quinone methide with humulene were proposed for the biosynthesis of **13** and **14**, which further served as an intermediate for the biosynthesis of eupenifeldin and pycnidione, respectively (Figure 25a).[137,144] While

biosynthesis of the tropolone core in stipitatonic acid has been identified (Figure 25a), including a nonreduced polyketide synthase (NR-PKS, TropA), a FAD-dependent monooxygenase (FMO, TropB), and an α-ketoglutarate-dependent dioxygenase (α-KGD, TropC),[145] the enzymatic basis for the DA reaction for **13** biosynthesis has remained unexplored. Here, we report mapping of the cascade of enzymatic steps that furnish the structure of **13**, which include a cytochrome P450 monooxygenase (P450), a short-chain dehydrogenase (SDR), and an intermolecular hetero-Diels–Alderase (hDAase) as key steps. We demonstrate that the hDAase is responsible for the formation of a highly reactive tropolone *o*-quinone methide and may further stereoselectively control the subsequent intermolecular hDA cycloaddition to produce **13**.

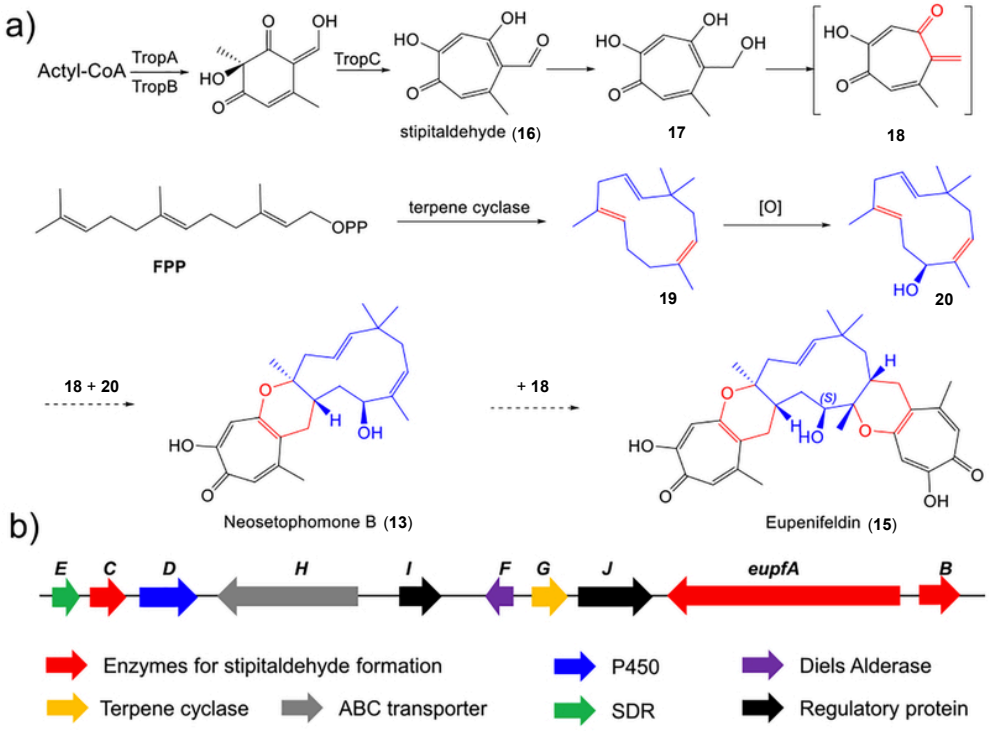

Figure 25
A. Proposed biosynthetic pathways of **13** and **15**. ***B.*** The eupf gene cluster in *P. janthinellum*.

4.4 Isolation of Neosetophomone B and Eupenifeldin

Recently, we coisolated **13** and **15** from the wild-type *Penicillium janthinellum*, a producer of alanditrypinone.[146] Analysis of the crude extract by liquid chromatography mass spectrometry (LC–MS) led to the observation of minor **13** and major **15** with characteristic UV absorption of tropolones and molecular weights of 384 and 548, respectively. Compounds **13** and **15** were fully characterized by NMR and circular dichroism spectra as enantiomerically pure neosetophomone B and eupenifeldin, respectively. To investigate the biosynthetic pathway of **13**, the genome of *P. janthinellum* was queried for the presence of the trop-like gene cluster. Bioinformatics analysis led to the identification of only one trop-like NR-PKS gene cluster (named eupf cluster) in its genome (Figure 25b). In addition to three enzymes (EupfA–C) which are homologues to TropA, TropB, and TropC, respectively, the eupf cluster encodes additionally a cytochrome P450 monooxygenase (EupfD), a short-chain dehydrogenase (EupfE), two hypothetic enzymes (EupfF and EupfG), as well as an ABC transporter and regulators (Figure 25b). EupfF and EupfG show high homology to AsR5 and AsR6 (64% and 62%), respectively, which were recently suggested as putative hetero-Diels–Alderase and humulene synthase, respectively, in the biosynthesis of xenovulene A.[147] A biosynthetic gene cluster eup in *Phoma sp*. has been recently identified by gene deletion for the biosynthesis of eupenifeldin and EupF was also suggested as putative hDAase. However, the function of AsR5 and EupF has not been successfully characterized. It was scrutable that EupfABC were responsible for the formation of stipitaldehyde, and EupfG served as a humulene synthase to form a sesquiterpene, while the only oxygenase EupfD could catalyze the hydroxylation at the terpene moiety at an uncertain stage. The putative hDAase EupfF,

homologous to AsR5 and EupF, was proposed to be involved in the cyclization between diene and dienophile.

4.5 Biochemical Characterization of the eupf Gene Cluster

To verify the eupf gene cluster and elucidate the biosynthetic pathway of **13**, heterologous expression experiments in Aspergillus nidulans were conducted. As expected, expression of eupfABC in *A. nidulans* led to the production of major stipitaldehyde (**16**, Figure 26a), which was suggested as an intermediate for biosynthesis of xenovulene A and other tropolone-sesquiterpenes. To form a diene precursor for the DA reaction, the aldehyde moiety in **16** has to be reduced first. As the only potential reductase in the eupf cluster, Eupf E is highly likely to be involved in this transformation. To verify the function of EupfE, intron-free eupf E was cloned from cDNA, heterologously expressed in *Escherichia coli*, and purified to homogeneity. Compared to control experiments where missing EupfE did not generate new products, incubation of EupfE with **16** and NADPH led to complete conversion to a new product **17** (Figure 26b) with characteristic UV absorption of tropolone and MW of 182, 2 Da more than that of **16**. Although **17** was not stable enough, careful isolation and quick NMR analysis led to the full identification of **17** as we expected (Figure 26d). Dehydration of **17** either spontaneously or enzymatically was proposed to generate the reactive tropolone *o*-quinone methide (**18**).

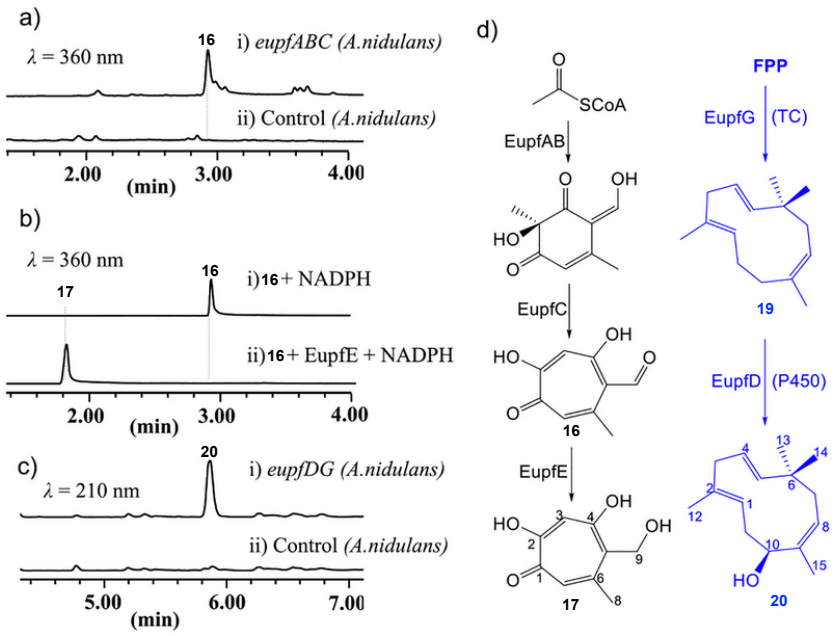

Figure 26
Generation of potential precursors in the biosynthesis of **13**. (***A.,B.,C.***) LCMS traces from heterologous expression of eupfABC/DG in *A. nidulans* or from *in vitro* assay of EupfE. ***D.*** Generation of **17** and **20**.

To identify the dienophile precursor, EupfG, the putative humulene synthase was expressed in *A. nidulans*, which led to the detection of a compound **19** with the same molecular weight (m/z 204) but different retention time from that of α-humulene (**21**) standard indicated by GC–MS analysis, which suggested **19** was an isomer of α-humulene. Isolation of **19** was found to be difficult due to its high volatility. The structure of **19** was suggested by coexpression of eupf G and eupf D in *A. nidulans*, which led to the production of **20** (Figure 26c, trace *i*) with MW of 220, 16 Da more than that of α-humulene. Compound **20** was fully characterized by MS and NMR spectra as a hydroxylated product of **19** (Figure 26d), which also supported that **19** was (1*E*,4*E*,8*Z*)-humulene. Different from α-humulene in which all three olefins are in the *E* form, compounds **19** and **20** possess a *Z* form of the olefinic bond at Δ8,9, which is consistent

with the *Z* form of alkene in **13**. As a result, EupfG was identified as a new sesquiterpene synthase producing (1*E*,4*E*,8*Z*)-humulene other than α-humulene.

We realized that **17** could be O-methylated at C9-OH gradually and partly in methanol. Methylated 5 was isolated and fully characterized by NMR spectra as a tautomer mixture (2:1). The identification of methylated **17** (**18a**) also suggested the spontaneous conversion from **17** to **18** occurred before it underwent 1,4- or 1,6-addition by methanol. Due to the incomplete spontaneous conversion, we believed that enzyme was required to generate **18** from **17**, and EupfF, the putative hetero-Diels–Alderase, was presumed to be involved in this process. However, repeated attempts to obtain soluble EupfF for biochemical assay failed. Fortunately, an enzyme, EupF, highly homologous to EupfF (81% similarity/67% identity), was found in the genome of *Phoma sp.*, which was suggested but not characterized as putative hDAase for the biosynthesis of eupenifeldin.[148] Attempts to obtain soluble EupF (42.0 kDa) from *Escherichia coli* BL21(DE3) were successful. To explore if EupF catalyzed the dehydration of **17**, we performed in vitro EupF assay with **17** as the sole substrate. Since the expected product **18** was extremely instable, we added 1% glycerol in the *in vitro* system to trap **18**. Consequently, 72.5% of **17** converted to two main products, **18b** and **18c**, with molecular weights of 256 and 346, respectively, by EupF after 2 h, while only 21.8% of **17** could be transformed without EupF. On the basis of the MS and UV, **18b** and **18c** were suggested to be 1,4-nucleophilic addition products of **18** with glycerol and **17**, respectively. The results from the *in vitro* assay supported that dehydration of **17** could occur

spontaneously, but EupF remarkably accelerated this process. Hence, the diene precursor **18** could be identified as tropolone *o*-quinone methide.

4.6 Characterization of the Enzymatic Intermolecular Hetero-Diels–Alder Reaction

With **17** and **20** in hand, we were able to examine whether EupF was directly involved in the hDA reaction. We performed an in vitro reaction containing 30 μM EupF, 4.0 mM **17**, and 1.0 mM **20** in 50 mM bicine buffer (pH 8.0). Whereas the control reaction without EupF did not lead to apparent new products, EupF catalyzed the conversion of **17** and **20** into **13** (Figure 27a). Compound **13**'s functionality as an enantiopure compound indicated the hDA reaction was enzymatically controlled since racemic products would be expected from the spontaneous reaction. Interestingly, when the natural substrate **20** was switched to unnatural substrate humulenol (**22**), which was obtained from expression of eupf D in *A. nidulans* by feeding humulene (**21**), in the *in vitro* EupF assay, two products **14** and **23** (1:1 ratio) were detected (Figure 27a, trace *v*). To obtain enough **14** and **23** for structural elucidation, **21** was fed to *A. nidulans* coexpressing eupfABCDEF. Finally, compounds **14** and were fully characterized by NMR and CD as natural epolone B and its isomer, named isoepolone B (Figure 27c), respectively. Trace amounts of **14** and **23** were also detectable (Figure 27a, trace *vi*) in the absence of EupF with low yield compared to the enzymatic reaction. Hence, we suggested (1) the cycloaddition between the reactive tropolone *o*-quinone methide **18** and dienophile (**20** or **22**) could occur spontaneously, (2) EupF directly controlled the stereo-selectivity of hDA reaction in the case of natural substrate **20**, and (3) unnatural substrate **22** was not recognized by EupF but underwent spontaneous cycloaddition with **18**. Thus, EupF was fully characterized as the first

hDAase, which differs from all intramolecular DAases in phylogenetic analysis and has no recognizable cofactor-binding site. A model of EupfF (EupF) computed with SWISS-MODEL and template 2p4o suggest a predicted six-bladed propeller that may provide suitable space for substrates. Although His, Lys, and Arg have been found as potential active sites for dehydration and DA reaction,[149] mutagenesis experiments showed that conserved H37, R51, R92, and R323 were not catalytic residues for EupF, which suggested EupF was different from other DAases.

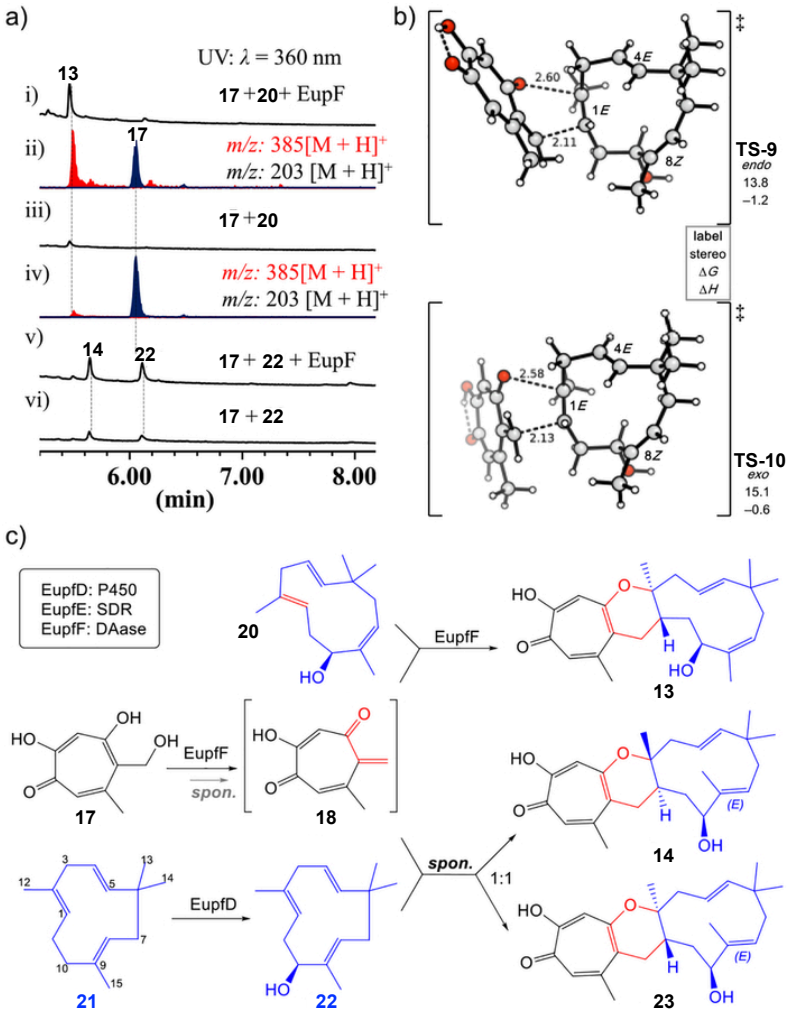

Figure 27
Biosynthesis of **13** and **14**. ***A.*** LCMS traces from *in vitro* assay of EupF. ***B.*** DFT-computed free energies for hDA reaction between **20** and **18**. ***C.*** Biosynthetic pathway of **13**.

To support the proposed pathway, we performed density functional theory (DFT) studies on the Diels–Alder reaction at the PBE0-D3(BJ)/def2-TZVP level of theory.[150–155] These calculations indicate that this cycloaddition is very facile (Figure 27b). Transition states **TS-9** and **TS-10** lead to product **13** and are highly asynchronous with the two forming bonds differing by 0.49 and 0.45 Å, respectively. There is a 0.25 electron charge transfer in the transition state, in **TS-9** the heterodiene has a −0.25 charge, and dienophile has a +0.25 charge. The charges are similar in **TS-10**. It is probable that the rate-determining step is generation of the *o*-quinone methide **18**. After formation of **18**, the reaction barriers of **TS-9** and **TS-10** are purely entropic (**TS-9** $\Delta H^{\ddagger} = -1.2$, $\Delta G^{\ddagger} = +13.8$ kcal·mol^{-1}, **TS-10** $\Delta H^{\ddagger} = -0.6$, $\Delta G^{\ddagger} = +15.1$ kcal·mol^{-1}). These reactions are enthalpically barrierless because the heterodiene is highly electron-deficient and a highly stable aromatic product is formed.

Unexpectedly, neither *in vitro* assay with **17** and **20** as substrates nor feeding experiments led to production of **15** (only **13** was detected), which highly indicated that other or additional enzymes were required for the right side DA reaction in the biosynthesis of **15**. Further investigation on the biosynthesis of bistropolone-sesquiterpenes is in progress.

4.7 Conclusions

In conclusion, we biochemically characterized EupfF (EupF) as the first fungal intermolecular hetero-Diels–Alderase and demonstrated that EupfF catalyzed the generation of a reactive tropolone *o*-quinone methide and further stereoselectively controlled the subsequent intermolecular hetero-Diels–Alder reaction to produce **13**. Our

discovery expands the collection of increasing DAases from fungi and opens a new strategy for mining and combinational biosynthesis of tropolone-sesquiterpenes.

Chapter 5. Structural Basis for Stereoselective Dehydration and Hydrogen-Bonding Catalysis by the SAM-dependent Pericyclase LepI

5.1 Contributions

This is an author manuscript from the publication: Cai, Y.; Hai, Y.; Ohashi, M.; Jamieson, C. S.; Garcia-Borras, M.; Houk, K. N.; Zhou, J.; Tang, Y. Structural Basis for Stereoselective Dehydration and Hydrogen-Bonding Catalysis by the SAM-Dependent Pericyclase LepI. *Nat. Chem.* **2019**, *11* (9), 812–820. https://doi.org/10.1038/s41557-019-0294-x. This project was a collaboration between the Kendall N. Houk, Jiahai Zhou, and Yi Tang laboratories. I conducted all computational experiments. Postdoctoral fellow Marc Garcia-Borras trained me in conducting relevant molecular dynamics simulations. Yujuan Cai completed all crystal structure experiments, Yang Hai and Masao Ohashi conducted biochemical experiments.

5.2 Abstract

LepI is an *S*-adenosylmethionine (SAM)-dependent pericyclase that catalyzes the formation of 2-pyridone natural product leporin C. Biochemical characterization showed LepI can catalyze the stereoselective dehydration to yield a reactive (*E*)-quinone methide that can undergo bifurcating intramolecular Diels-Alder (IMDA) and hetero-Diels-Alder (HDA) cyclizations from an ambimodal transition state, as well as a [3,3]-retro-Claisen rearrangement to recycle the IMDA product into leporin C. Here we solved the X-ray crystal structures of SAM-bound LepI and in complex with a substrate analog, the product leporin C, and a retro-Claisen reaction transition-state analog to understand the structural

basis for the multitude of reactions. Structural and mutational analysis revealed how Nature evolves a classic methyltransferase active site into one that can serve as a dehydratase and a multifunctional pericyclase. Catalysis of both sets of reactions employs H133 and R295, two active site residues that are not found in canonical methyltransferases. An alternative role of SAM, which is not found to be in direct contact with the substrate, is also proposed.

5.3 Introduction

Pericyclic reactions are among the most powerful synthetic reactions for making multiple carbon-carbon and carbon-heteroatom bonds in a regio- and stereo-selective manner.[22] Despite their prevalence in organic synthesis, only a handful of naturally-occurring enzymes have been characterized to catalyze pericyclic reactions and related [4+2] cycloadditions.[102] Structural characterizations of a few of these enzymes, including chorismate mutase (CM), isochorismate lyase, precorrin-8x methyl mutase, SpnF, etc., showed Nature has evolved a variety of protein folds divergently to accelerate pericyclic reactions and control their regio- and stereo-selectivity.[56,156–159]

Recently we discovered a multifunctional *S*-adenosyl-L-methionine (SAM)-dependent *O*-methyltransferase (OMT)-like pericyclase, LepI, that catalyzes a cascade of reactions starting from the 2-pyridone alcohol **25** to form the dihydropyran-containing fungal natural product leporin C (**33**) (Figure 28).[80] In the absence of LepI, the alcohol **25**, which is derived from the ketoreduction of **24**, can undergo dehydration to give either the (*E*)- or (*Z*)-quinone methide **26** or **27**, respectively. The reactive **26** and **27** can undergo

intramolecular Diels-Alder (IMDA) cycloaddition to yield the endo products **32** and **29**, respectively, as well as the exo adducts **31** and **28**, respectively. The inverse-electron demand hetero-Diels Alder (HDA) cycloaddition of **26** and **27**, on the other hand, affords the desired product **33** and the diastereomeric **30**, respectively. Quantum mechanics (QM) calculations revealed that the activation energies for the formation of these six products from either **26** or **27** are comparable, consistent with **33** being only a minor product in the absence of LepI. We showed that in the presence of LepI, **25** is completely converted to **33**.[80] We also demonstrated computationally that the endo IMDA and HDA reactions starting from **26** go through an ambimodal transition state (**TS-11**) and that a post-transition-state bifurcation leads preferentially to the IMDA product in the absence of enzyme catalysis. Therefore, LepI must catalyze the diastereoselective dehydration of **25** to form only **26** and facilitate the subsequent *endo* transition state (**TS-11**) from **26** while suppressing the *exo* transition state (**TS-13**). The active site of LepI can also alter the dynamics of the bifurcating potential energy surface from **TS-11** to favor the HDA product **33** as suggested by computation.[80] Furthermore, we demonstrated that LepI can catalyze the conversion of **32** to **33** via a [3,3]-sigmatropic retro-Claisen rearrangement **TS-12** as a means of kinetically recycling the IMDA shunt **32** to product **33**. While our biochemical and computational studies unveiled these unexpected roles of an enzyme with sequence homology to an OMT, the mechanistic details of catalysis and selectivity achieved by LepI were not known.

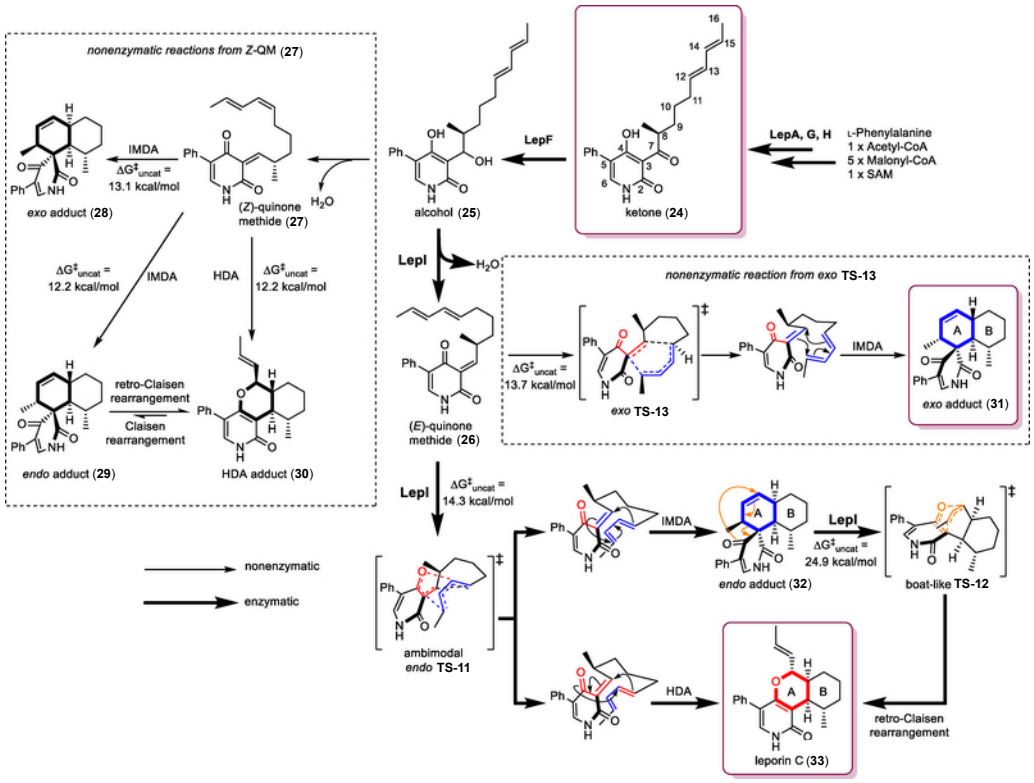

Figure 28
Leporin C biosynthesis pathway highlighting LepI-catalyzed reaction cascade. In the absence of LepI, spontaneous dehydration of alcohol **25** yields a (*E*/*Z*)-mixture of quinone methides (**26**/**27**), which nonenzymatically form Diels-Alder and hetero Diels-Alder adducts. The compounds used in structural study are highlighted by maroon boxes.

Here we report a collection of X-ray crystal structures, which, together with computational studies, uncover the origins of catalysis and stereoselectivity of LepI. We obtained X-ray crystal structures of holo-LepI i) bound with SAM and complexed with ii) the dehydration reaction substrate analogue **24**, iii) product leporin C **33**, and iv) the retro-Claisen reaction substrate analogue **31**. Our structures provide insight into the molecular mechanism of LepI catalysis, including the *E*-stereoselectivity of dehydration, the endo-stereoselectivity of IMDA/HDA reactions, and the rate enhancement of the retro-Claisen reaction. A possible divergent evolutionary relationship with SAM-dependent OMTs and a new role of SAM in catalyzing pericyclic reactions are also proposed.

5.4 Structure of LepI

The structure of LepI was determined by single anomalous diffraction on a selenomethionine (Se-Met) derivative crystal diffracting to 2.58 Å resolution, and the phase was extended to a native crystal with 2.14 Å resolution by molecular replacement. The overall tertiary structure of LepI consists of an N-terminal dimerization domain (residues 1–122) and a C-terminal catalytic domain (residues 123–387) that adopts the typical α/β Rossmann fold observed in all class I SAM-dependent methyltransferases (Figure 29a).[160] In the asymmetric unit, two LepI monomers intertwine through the N-terminal dimerization domains with a dimer interface of ~5,000 $Å^2$ surface area per monomer as calculated by PISA (Figure 29b).[161] Such intimate homodimer architecture is similar to that of many OMTs. Unique to LepI dimer is a domain-swapped four-helix bundle at the N-terminus. This leucine-rich coiled-coil enables LepI dimers to pack against each other and form a dimer of dimers, burying ~1,800 $Å^2$ surface area between the two dimers. In comparison, the oxaline OMT OxaC,[162] the closest homologue to LepI as identified by Dali,[163] also harbors a similar four-helix bundle at the N-terminus, but it is not domain-swapped and does not further dimerize. The tetramer oligomerization of LepI is consistent with sedimentation velocity experiment, which showed that LepI exists in an equilibrium between dimer and tetramer in solution.

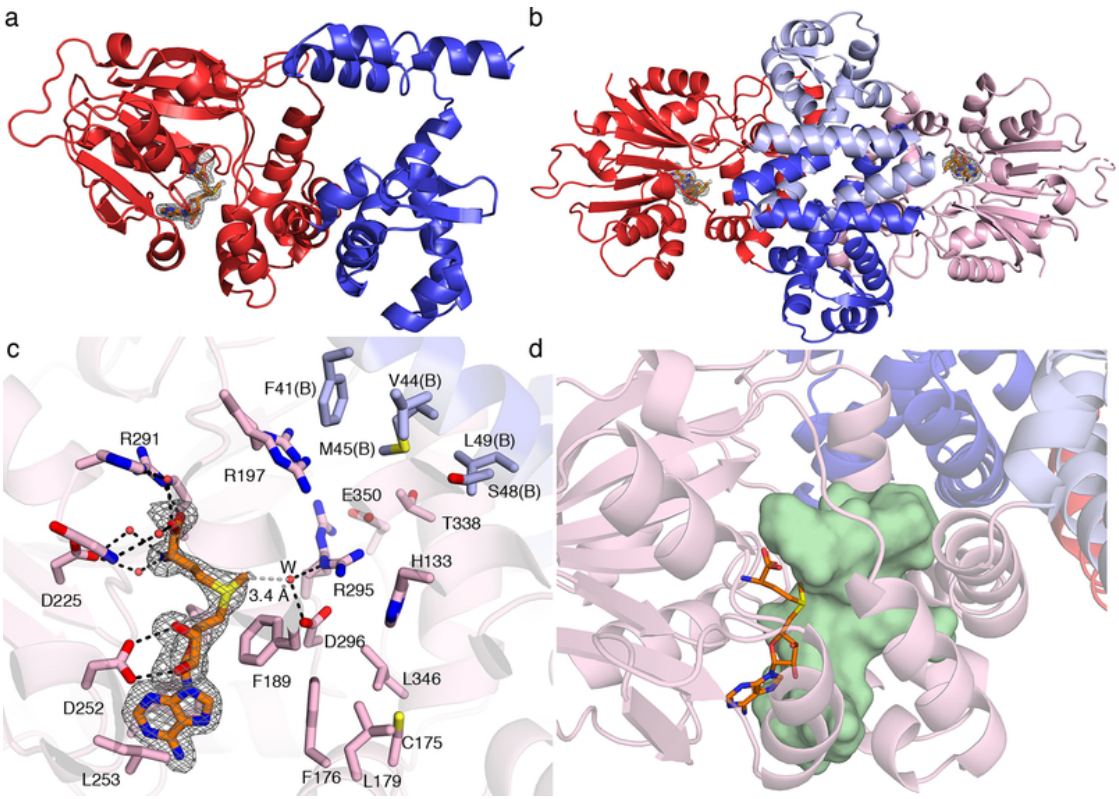

Figure 29
LepI structure and the SAM binding site. (***A.***) The overall tertiary structure of LepI is shown in cartoon model, with the N-terminal dimerization domain and C-terminal catalytic domain colored in blue and red, respectively. Simulated-annealing omit map (grey mesh, contoured at 2.5 σ) indicates binding of SAM at the canonical SAM binding site. (***B.***) Intimate LepI homodimer featured by an intertwined dimer interface. (***C.***) Close-up view of SAM binding site. Hydrogen bond interactions are indicated with black dashes. (***D.***) Next to SAM is a large substrate binding cavity and its entrance tunnel (shown together as green surface). The volume of cavity was calculated using POCASA.[9]

The cofactor SAM is copurified with LepI with >90% occupancy when it is overexpressed in Escherichia coli;[80] no exogenous SAM was supplemented during protein purification and crystallization steps. Electron density unambiguously delineates the binding of SAM in each LepI monomer at the canonical SAM binding site (Figure 29c). LepI makes numerous contacts with SAM that are observed in *bona fide* OMTs: the α-amino and α-carboxylate groups are recognized through direct and water-mediated hydrogen bond networks; the diol group from the ribose ring donates two hydrogen bonds to D252; the

adenine ring is sandwiched between L253 and F276 via van der Waals and π···π interactions. Notably, the sulfonium methyl group makes an unconventional CH···O hydrogen bond with D296, mediated by a water molecule (designated as W, the distance between SAM sulfonium methyl carbon and W is 3.4 Å). Such CH···O hydrogen bonds involving the SAM sulfonium methyl group are prevalent in SAM-dependent methyltransferases and are believed to be important for SAM binding specificity and facilitating the methyl transfer reaction.[164] However, water molecules have rarely been observed as immediate hydrogen bond acceptors for SAM.[165] The water molecule W also makes a hydrogen bond with R295, which resides at the center of a large ~500 $Å^3$ cavity. This putative active site cavity is outlined by both the catalytic domain (monomer A) and the dimerization domain from the other monomer (monomer B) within the homodimer unit (Figure 29d). Adjacent to the adenine ring of SAM is a wide substrate entrance tunnel, whereas on the backside of the cavity at the domain interface, multiple water-filled tunnels are found to connect the cavity to bulk solvent. Such organization implies that the dimerization event is obligatory for LepI function and that each homodimer is a minimal integral functional unit.

5.5 Structure of LepI-substrate analogue ketone complex

To understand how LepI recognizes and orients the substrate alcohol **25** and achieves E-selective dehydration to yield **26**, we cocrystalized LepI with ketone **24**, which serves as an unreactive substrate analogue. The structure of this pseudo enzyme-substrate (Michaelis) complex was determined to 1.70 Å resolution. Electron density clearly reveals the binding of **24** in the proposed substrate binding site adjacent to SAM, as well as an

ethylene glycol molecule serendipitously positioned on top of the pyridone ring (Figure 30a). The atomic resolution of the electron density also allows us to determine the absolute stereochemistry at the chiral C8 of **26** (*S* configuration).

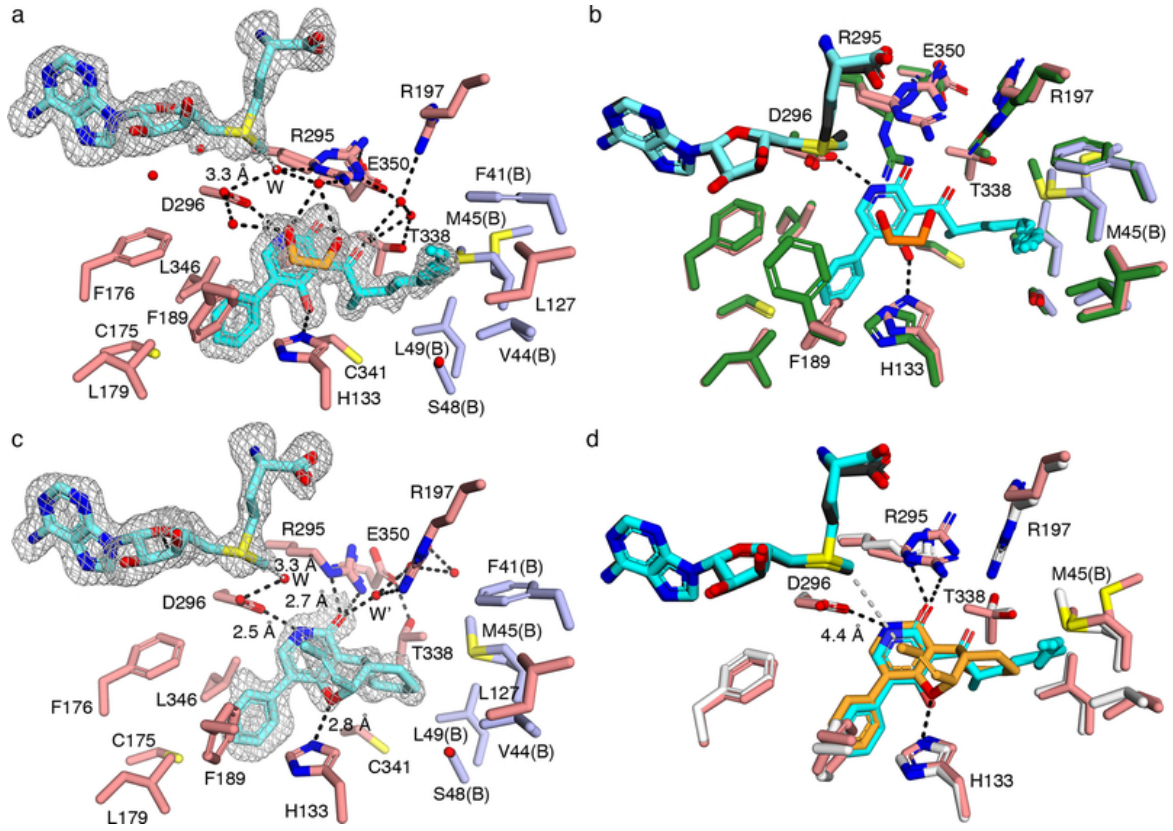

Figure 30

Crystal structure of LepI pseudo enzyme-substrate complex and enzyme-product complex. Simulated-annealing omit maps are shown in black mesh and contoured at 3.0 σ. Hydrogen bond interactions are indicated with black dashed lines. ***A.*** Crystal structure of LepI-SAM-**24** (pseudo enzyme-substrate complex). Note that two rotamers of R295 and M45(B) are observed, and two conformations of diene (*s*-trans and *s*-cis) are modeled according to the electron density. Residues from monomer A are colored in salmon, whereas residues from monomer B are colored in light blue and labeled with B in parenthesis. ***B.*** Superposition of LepI-SAM-**24** complex (colored as in (***A.***)) with unliganded LepI-SAM (residues are colored in dark green while SAM is colored in black). Substantial conformational changes are observed for F189, R295, R197, and M45(B). ***C.*** Crystal structure of LepI-SAM-**33 10**. Residues and ligands are color coded as in (***A.***). ***D.*** Superposition of LepI-SAM-**33 10** (residues are colored in white, SAM is colored in gray, ligand is colored in orange) with LepI-SAM-1 (color coded as in (***A.***), note that ethylene glycol is not shown here for clarity).

The overall LepI-SAM-**24** structure is very similar to the ligand-free structure with an root mean square deviation (r.m.s.d.) of ~ 0.18 Å for 770 Cα atoms. However, local structural changes were triggered upon substrate binding (Figure 30b). The 5-phenyl ring of **24** is locked into a small hydrophobic pocket and participates in favorable π···π interactions with H133 and F189, which cause rotation of F189 side chain. The pyridone ring is recognized via hydrogen bond interactions with H133 and D296 through the 4-OH group and amide nitrogen, respectively.

Unexpectedly, instead of being frozen in the near-attack conformation (NAC) for the cycloaddition step immediately following dehydration, the diene alkyl chain of **24** is captured in an extended conformation projecting into a hydrophobic cleft mainly surrounded by residues from monomer B within the homodimer, and accommodation of this linear alkyl chain caused a ~3 Å shift of M45(B) side chain. Meanwhile, the space left for the diene chain in the NAC is now occupied by the ethylene glycol molecule. The electron density reveals that the diene moiety adopts an alternate conformation (*s*-trans and *s*-cis). In both conformations, the diene could participate in favorable π···π interactions with F41(B) (Figure 30a).

The C7 carbonyl group is oriented in parallel with the amide carbonyl facing towards the aforementioned solvent-filled channel and forms an extensive water hydrogen bond network mediated by residues T338, R197, R295, and E350. Since the C7 carbonyl group closely mimics the alcohol of substrate **25** that leaves in the elimination reaction, such orientation dictates that substrate **25** must undergo anti-elimination exclusively to yield

(*E*)-quinone methide **26**, which explains our previous biochemical characterization that the enzymatic reaction products were derived from (*E*)-quinone methide intermediate.[80] The water hydrogen bond network helps to protonate the leaving alcohol group. The byproduct water may be transiently trapped by the nearby polar residues and eventually exported to bulk solvent through the solvent-releasing channel.

Even though the substrate binding pocket is in proximity to the cofactor SAM, no direct contact was observed between SAM and ketone **24** (the distance between SAM sulfonium methyl carbon and the ketone **24** amide carbonyl oxygen atom is about 6.8 Å). Instead, the water molecule W remains to bridge the SAM sulfonium methyl group with D296 and R295. A structure of LepI-SAH-**24** ternary complex (1.84 Å resolution) was also determined during the course of the study, in which *S*-adenosyl-L-homocysteine (SAH), instead of SAM, was identified in the active site. Even though SAH lacks the sulfonium methyl and a formal positive charge of SAM, the overall structure is essentially identical to the LepI-SAM-**24** complex with an r.m.s.d. of ~ 0.18 Å for 773 Cα atoms., including the active site organization, waters, and substrate binding mode, except that the diene exclusively adopts the *s*-trans conformation; an extra glycerol molecule was also found at the exit of the solvent-releasing channel. The similarity between these two complexes suggests that the contrasting effects of SAM vs. SAH on LepI catalysis previously observed are not attributed to a structural role of SAM or any allosteric effects but rather to the hydrogen bonding and positive charge of SAM that is absent in SAH.

5.6 Structure of LepI enzyme-product complex

To gain more insight into how LepI catalyzes cycloaddition, we next determined the crystal structure of LepI-SAM complexed with leporin C (**33**) to 1.78 Å resolution. As expected, no major conformational change was introduced to LepI upon binding of the product. The crystal structure of enzyme-product complex reveals that **33** is accommodated in a manner similar to **24** in the LepI-SAM-**24** complex (Figure 30c), through hydrophobic and hydrogen bond interactions. Notably, residue R295 now adopts a different conformation to form a bifurcated hydrogen bond with the amide carbonyl of **33**. The amide carbonyl group concurrently accepts a hydrogen bond donated from a water molecule (W'), which likely originates from the leaving alcohol group in the dehydration. This water molecule also participates in the hydrogen bond network at the solvent-releasing channel. The direct hydrogen-bond interaction between the amide carbonyl and guanidinium group of R295 is reminiscent of the electrostatic catalysis predicted previously by our computational study: a sulfonium ion or ammonium ion interacts with the amide carbonyl in the ambimodal **TS-11**.[80] Such electrostatic catalysis was predicted to decrease the C-O bond length and increase the C-C bond length in **TS-11**. This contributes to the observed preference for LepI to catalyze the HDA reaction versus *endo*-mode IMDA in the presence of LepI as compared to nonenzymatic reaction in water. In addition to the amide carbonyl, a lone pair from cyclic ether oxygen of **33** is shown to accept a hydrogen bond from the side chain of H133. Considering that the general base H133 is inevitably protonated after dehydration in the reaction cascade, H133 is most likely present as the imidazolium form, which makes it an ideal hydrogen-bond donor for catalysis in the following pericyclic reactions. The positively-charged

imidazolium ring of H133 maintains hydrogen bonding with the C4-carbonyl of **26** and **TS-11** to enhance the electrophilicity of the pyridone ring. In the [3,3]-sigmatropic retro-Claisen rearrangement, this interaction also stabilizes the developing partial oxyanion in **TS-12**. Together, hydrogen bonds from R295 and H133 to C2 and C4 carbonyl groups activate the quinone methide **27** and the retro-Claisen substrate **32** by stabilizing the polarized transition state.

Superimposing the LepI-SAM-**33** complex onto LepI-SAM-**24** complex reveals that cycloaddition of the diene chain causes the conformational change of M45(B), which swings back to the original position as seen in the unliganded structure (Figure 30d). The previously observed ethylene glycol molecule overlays well with C14-C16 of **33**, which illuminates how the linear portion of quinone methide **26** rearranges to the NAC preceding **TS-11**: the diene alkyl chain of quinone methide **26** is induced by the enzyme binding site to rotate and fold on top of the 2-pyridone ring, leaving the C8-C13 region preorganized into a chair-like conformation with C8 methyl group in the equatorial position and the diene moiety in *s*-cis conformation. Accordingly, we docked the ambimodal *endo* **TS-11** and the [3,3]-sigmatropic retro-Claisen rearrangement **TS-12** into the LepI-SAM-**33** structure omitting ligand **33**. Including the two well-defined water molecules (W and W') and SAM in the structure greatly facilitated docking the ligands in productive poses, thereby supporting the hypothesis that they may play important structural roles in defining the active site binding environment.

The basis for LepI diastereoselectivity (*endo* vs *exo*) in the IMDA/HDA reaction was further supported by modeling the hypothetical LepI-SAM- **TS-13** complex with the assumption that the 5-phenyl group and pyridone ring are bound in a similar fashion as **TS-11** to maintain similar interactions with LepI. To allow for the *exo* **TS-13** to bind, the hydrophobic diene group (C13-C14) is positioned on the hydrophilic side of the active site, which may potentially cause steric clashes with water W' and R295; whereas in the *endo* **TS-11** model, the diene is positioned on the hydrophobic side of the binding site. Thus, the diastereoselectivity likely arises from preference of the diene to avoid the hydrophilic "wall" formed by polar residues (D296, R295, R197, T338) and W'. More insights regarding LepI binding of retro-Claisen reaction substrate **32** were provided by the structure of the LepI-SAM-**31** ternary complex (1.66 Å resolution), where **31** is the unreactive spirocyclic product of nonenzymatic *exo* **TS-13** serving as a mimic of the diastereoisomer spirocyclic **32**.

5.7 Catalytic mechanism of LepI

To verify our interpretations of likely modes of catalysis, we performed site-directed mutagenesis on the implicated residues and examined the enzyme activity in *A. nidulans*. In the presence of upstream enzymes that produce the alcohol **25**, a fully active LepI yields only the product **33**, while a completely inactive LepI (or absence of LepI) leads to a mixture of **28**–**33** (Figure 31a). Consistent with our structural conclusion, removal of the essential general base H133 is detrimental to LepI activity; all four mutations (H133A, H133F, H133Q, H133N) completely abolished enzyme activity (Figure 31a). As observed in the LepI-SAM-**24** structure, R295 may act as a general acid and indirectly protonate

the leaving alcohol. Substitution of R295 with A/Q/F/Y significantly compromised the dehydration activity, but it was effectively rescued by R295H/K/N. Mutation of other residues structurally implicated in the protonation step during dehydration (T338A, T338S, R197A, and R197K) did not affect the activity, suggesting that they are not essential for catalysis. Residue D296 plays a major role in binding and polarizing the substrate in order to lock it in the 2-pyridone form rather than its tautomeric 2-hydroxypyridine form. Substitution of residue D296 with A led to notable increase in shunt products **28**–**32**, and the activity can be restored by D296N and D296E, both of which can accept similar hydrogen bonds from the pyridone NH. Although substantial conformational change was observed on M45 accompanying the cycloaddition of **26**, M45A mutation did not affect LepI function *in vivo*, which strongly suggests that folding of the diene chain of **26** to the NAC preceding **TS-11** occurs spontaneously.

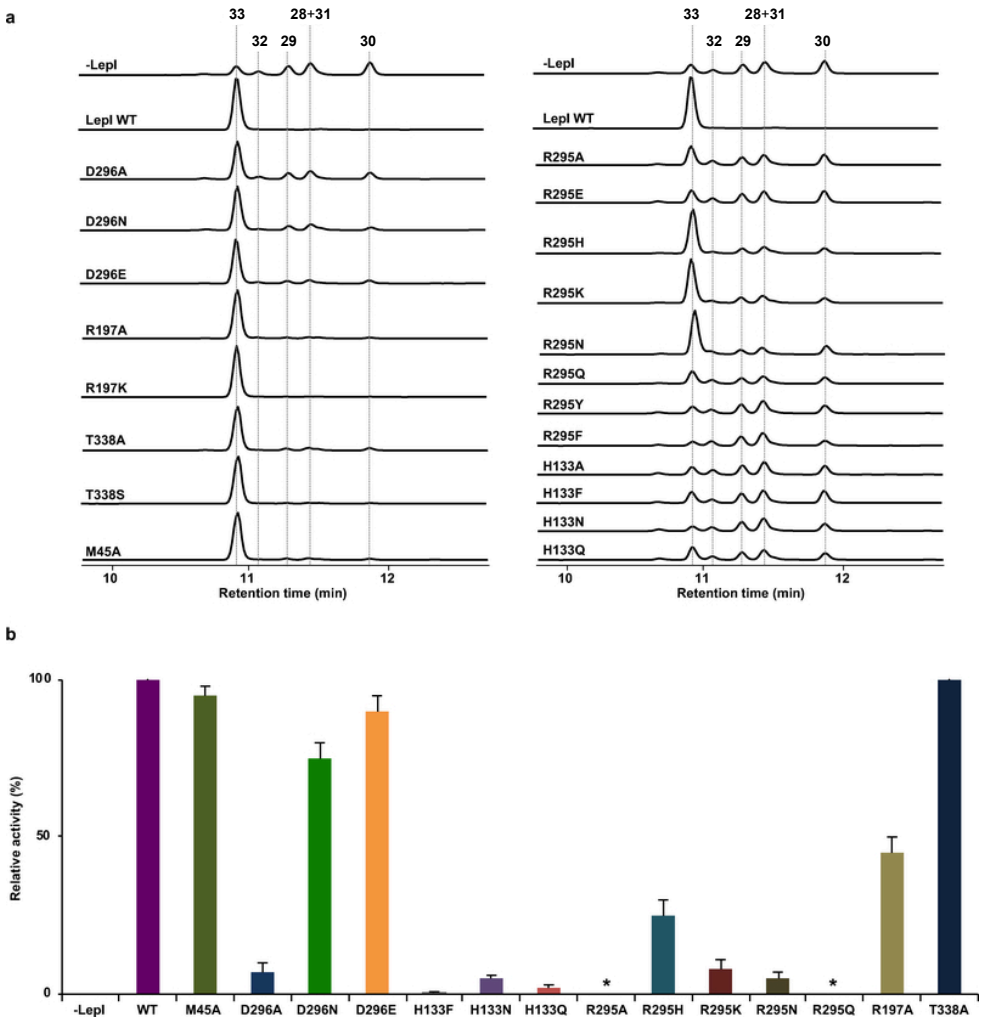

Figure 31
LepI Mutant activity. ***A.*** In vivo activity of LepI or mutants to synthesize leporin C (**33**) starting from the alcohol substrate **25**. **25** is synthesized by upstream biosynthetic enzymes. ***B.*** *In vitro* retro-Claisen rearrangement activity using **32** as the substrate. Asterisks indicate mutants with no measurable activity. Error bars show square deviation (s.d.) of three independent experiments (n = 3).

To examine the contribution of these active site residues to the catalysis of retro-Claisen rearrangement reaction, we assayed the enzymatic activity of the purified mutants using **32** as the substrate *in vitro* (Figure 31b). Consistent with the *in vivo* results, mutation of non-catalytic residues (T338A, M45A) did not affect the pericyclic activity. Alanine substitution for the substrate binding residue D296 caused a 10-fold loss of activity, although the activity was restored to 75% and 90% of the wild-type LepI by replacing

A296 with N and E, respectively. In contrast, mutation of the hydrogen bonding catalyst H133 significantly compromised the pericyclase activity of LepI: H133F decreased the activity by 200-fold, and replacing H133 with other neutral hydrogen-bond donors (e.g. H133Q and H133N) did not restore the activity, which demonstrates that the positively-charged imidazolium group is essential for LepI to catalyze the retro-Claisen rearrangement. Substituting R295 with A or Q also completely abolished the activity, while R295N and R295K mutants were active at 10% level of the wild type. Introducing H at position 295 improved the R295A/Q mutant LepI activity to 30% of the wild type, suggesting that the partial rescue of inactive mutants by R295H may be attributed to the imidazolium ring that can be stabilized by the nearby second-shell residue E350 and donate a favorable hydrogen bond to the amide carbonyl to catalyze the retro-Claisen rearrangement. R197, which makes a water-mediated (W') hydrogen bond to the same amide carbonyl, plays a minor catalytic role in this reaction, as R197A mutant retained 50% activity.

Taken together, this structure-activity relationship study provides mechanistic insights into LepI catalysis (Figure 32). The dehydration step likely proceeds via the E1-cb mechanism: H133 acts as the key general base to deprotonate the 4-OH group and stabilize the corresponding enolate anion intermediate, while the leaving hydroxyl group is ejected anti-periplanar and protonated by water molecules from the water hydrogen bond network, a process that is facilitated by R295. The leaving water molecule (W') could be transiently trapped by these residues and maintain a hydrogen bond with the amide carbonyl. The lack of a dedicated general acid residue to facilitate dehydration

presumably is to prevent the newly-formed highly-reactive (*E*)-quinone methide intermediate **26** from being quenched by W', since a good general acid residue could in principle act as a general base in the reverse reaction. Residue D296 is important for substrate binding and favoring the 2-pyridone tautomer. Overall, the dehydration specificity (1,4-anti-elimination) is accomplished through positioning the general base and acid in trans configurations and trapping the linear alcohol substrate **25** in the corresponding trans-conformer.

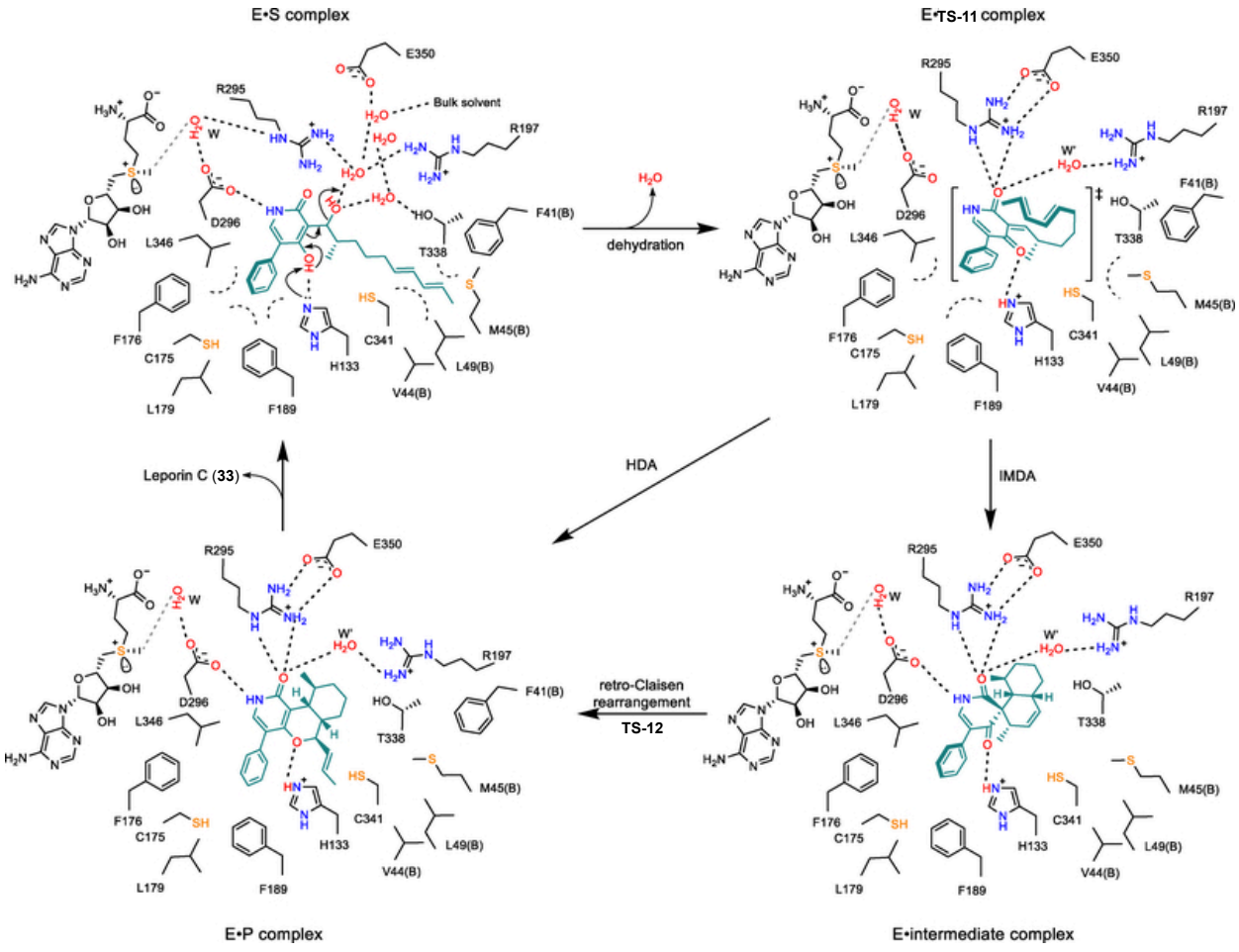

Figure 32
Proposed catalytic mechanism of LepI. Dashed straight lines indicate hydrogen bonds.

In the following cycloaddition reaction, spontaneous bond rotation of diene is driven by filling up the void volume over pyridone ring, and better shape-complementarity in the active site when poised for reaction. The diastereoselectivity was achieved by aligning hydrophilic residues at the *exo* side, which in turn favors the *endo* **TS-11** (hydrophobic effect). Residues H133 and R295 act as hydrogen bond donors to lower the transition-state energy barrier and stabilize both **TS-11** and **TS-12**. In particular, the highly polarized transition state **TS-12** (i.e. the oxyanionic 4-carbonyl oxygen) can be electrostatically stabilized by the positively-charged imidazolium side chain of H133. The cofactor SAM is required for defining the active site shape but not for directly interacting with the substrate. The catalytic role of SAM during the reaction as shown by previous biochemical experiments, and the necessity of a positively-charged analog to effect catalysis is indicative of the electrostatic role of the SAM sulfonium moiety for catalysis, but it is too remote from the substrate for direct hydrogen bonding.

5.8 Conclusions

A common theme found in pericyclases that catalyze [4+2]-additions is that cyclization follows an initial priming/deprotection reaction that activates the substrate to create/unmask the reactive functional groups.[66,102] This priming/deprotection reaction may be catalyzed by a separate enzyme (e.g. tandem reaction catalyzed by SpnM and SpnF) or the cyclase itself (e.g. solanapyrone synthase), which generates the reactive intermediate *in situ*. The second scenario is most often encountered when the liberated intermediate is too reactive and readily forms undesired cyclized products without

enzymatic control. Therefore, by devising such a cascade scheme, the unstable intermediate generated in situ undergoes cyclization immediately inside the cyclase.

LepI also follows this principle, and our studies here provide the structural basis and mechanistic insight into LepI catalysis, such as 1) positioning the general base (H133) and general acid (water facilitated by R295) in the trans-configuration to cause the substrate **25** to undergo stereoselective anti-elimination to yield (*E*)-quinone methide **26**; 2) setting the "amphiphilic" active site to favor the *endo*-conformation during cycloaddition; 3) repurposing the two cationic residues (H133 and R295) as hydrogen bonding catalysts to lower the transition state barrier and to electrostatically stabilize the polarized transition state; 4) repurposing SAM that normally functions as a methyl donor in methyltransferases to play an electrostatic role in non-methyltransfer catalysis.

In both natural and artificial enzymes that catalyze Diels-Alder reactions, it has been found that a strategy for rate enhancement is to donate specific hydrogen bonds to the dienophile in order to lower its LUMO energy[33,48] and to stabilize the polarized transition state. In LepI catalysis, H133 and R295 are vivid examples of hydrogen bond catalysts that simultaneously donate hydrogen bonds to both the amide carbonyl and quinone methide carbonyl groups. Such hydrogen bonding effectively lowers the LUMO energy of quinone methide and stabilizes the transition state that involves charge transfer to this moiety.

While many standalone pericyclases utilize binding energy to preorganize the linear substrate in a restricted NAC to overcome the rotational entropic barrier, LepI apparently does not function as an "entropy trap" to increase reaction rate.[33,46,66,159,166–168] The undehydrated substrate is bound in the extended conformation by LepI in order to minimize the π···π repulsion between the diene and the electron-rich phenolate prior to dehydration. The slight loss in entropy that occurs when the linear substrate rotates from extended conformation to the restricted NAC can be compensated by the gain of enthalpy from interaction between the diene and electron-deficient quinone methide and the enthalpic change that eventually results from the cycloaddition reaction. This may be a general feature of all dehydration-promoted pericyclases.

This feature is also reminiscent of another well-characterized pericyclase, chorismate mutase (CM), which catalyzes the [3,3]-sigmatropic Claisen rearrangement of chorismate to prephenate. Unfavorable decreases in $\Delta S^{\ddagger}$ have been consistently observed for natural CMs and catalytic antibodies, which suggests that CM does not act as an entropy trap.[169] Instead, the strategy for CM catalysis is a combination of both reactant destabilization and transition state stabilization.[169] It has become clear that transition state stabilization is the more important contributor to CM catalysis: donation of favorable hydrogen bond from cationic residue (such as Arg) to the vinyl ether oxygen in chorismate can effectively stabilize the developing partial negative charge on transition state.[170] By replacing this critical arginine with its neutral analogue citrulline, which donates hydrogen bond but is incapable of favorable electrostatic interactions, it has been estimated that this positively-

charged arginine can contribute 5.9 kcal/mol to transition state stabilization versus 0.6 kcal/mol to the binding energy of the ground state.

Strikingly similar to CM, LepI uses cationic residues (H133 and R295) as major contributor for catalyzing [3,3]-sigmatropic retro-Claisen rearrangement of **32** to **33**. Substrate ground-state destabilization does not contribute, since the spirocyclic substrate **32** is essentially being frozen in the NAC like conformation, and no significant bond rotation is required to preorganize this substrate to be shape complementary to the LepI active site. The major contribution to catalysis must come from hydrogen bonding and electrostatic interaction. Substitution of H133 by neutral hydrogen bonding residue Q and N reduces the catalytic activity by 50-fold. This severe loss of catalytic efficiency implies that H133 exists in the positively charged imidazolium form, which underscores the importance of electrostatic complementarity. The importance of positively-charged R295 to this pericyclic reaction has also been demonstrated by both QM studies and our current mutagenesis study. Consistent with this prediction, R295A/Q mutants are devoid of retro-Claisen rearrangement activity (>1,000-fold decrease, undetectable), whereas activity is partially retained with similar cationic mutants such as R295H (30%) (Figure 31b).

Although the precise catalytic role of SAM remains unclear, we have now found that the sulfonium does not contact the amide carbonyl. Nevertheless, the electrostatic effect of the sulfonium or the ammonium analog can stabilize the transition state. Given that the positive charge of SAM is required for optimal activity of LepI, we propose that SAM serves as an electrostatic catalyst that stabilizes the transition state, which has a higher

dipole moment than the reactant. This type of catalysis is well known through the work of Warshel, was demonstrated in solution chemistry by Wilcox, and has gained recent prominence under the name “electric field catalysis” through the work of Boxer, Shaik, Coote, and Head-Gordon.[171–176]

Our structural study of LepI also suggests an interesting evolutionary origin, that a methyltransferase ancestor of LepI has been co-opted to a multifunctional dehydratase and pericyclase. The protein folds and SAM binding pockets of LepI are nearly identical to the methyltransferase OxaC. Comparison of the LepI active site with that of the OMT OxaC, along with structure-based sequence alignment, reveals how key residues have been evolved to catalyze the reactions shown in Figure 28 instead of a S_N2 methyl transfer reaction. In all functional O-MTs, the charge relay system of the His-Glu catalytic dyad is strictly conserved; the histidine acts as the general base that deprotonates the substrate nucleophile (hydroxyl group), and glutamate acts as the second shell residue to elevate the pKa of histidine. In LepI, the glutamate is conserved as E350, whereas the corresponding general base histidine is replaced with arginine. This substitution is beneficial for LepI in two ways. First of all, as discussed above, arginine is a better hydrogen bond donor and electrostatic catalyst in LepI relative to histidine. Secondly, arginine is a poor general base due to its high pKa (12.5) and thus remains protonated in the resting state. Therefore, removing this key general base in LepI may be a strategy to eliminate adventitious methyltransferase activity.

In summary, our structural studies of LepI presented here provide mechanistic insight into enzymatic dehydration-triggered IMDA and HDA reactions, as well as hydrogen bonding and electrostatic catalysis of the retro-Claisen rearrangement. A proper understanding of the molecular mechanism of LepI is important for designing new pericyclases *de novo* and also provides a template for the discovery of novel functions of OMT-like enzymes.

Chapter 6. An Enzymatic Alder-ene Reaction

6.1 Contributions

This is an author manuscript from the publication: Ohashi, M.; Jamieson, C. S.; Cai, Y.; Tan, D.; Kanayama, D.; Tang, M.-C.; Anthony, S. M.; Chari, J. V; Barber, J. S.; Picazo, E.; et al. An Enzymatic Alder-Ene Reaction. *Nature* **2020**, *586* (7827), 64–69. https://doi.org/10.1038/s41586-020-2743-5. This project was a collaboration between the Kendall N. Houk, Jiahai Zhou, and Yi Tang laboratories. Masao Ohashi, myself, and Yujuan Cai were co-first authors on this publication. Myself and Postdoctoral fellow Masao Ohashi developed the project and determined the scope of the study. I assisted Masao Ohashi in genome mining and gene analysis. I conducted all computational experiments. Masao Ohashi conducted all biochemical experiments. Yujuan Cai completed all crystal structure experiments. Dan Tan, Daiki Kanayama, Man-Cheng Tang, Thomas B. Kakule, and Shugeng Cao assisted Masao Ohashi in biochemical experiments. Myself and Masao Ohashi developed synthetic routes to key intermediates which were carried out by Sarah M. Anthony, Jason V. Chari, Joyann S. Barber, and Elias Picazo.

6.2 Abstract

An ongoing challenge in chemical research is to design catalysts that select the outcomes of the reactions of complex molecules. Chemists rely on organo- or transition metal catalysts to control stereo-, regio-, and periselectivity (selectivity among possible pericyclic reactions). Nature achieves these types of selectivity with a variety of enzymes

such as the recently discovered pericyclases – a family of enzymes that catalyze pericyclic reactions.[102] To date, the majority of characterized enzymatic pericyclic reactions are cycloadditions and it has been difficult to rationalize how observed selectivities are achieved.[14,43,44,55,80,131,177–182] We report here the discovery of two homologous groups of pericyclases that catalyze distinct reactions: one group catalyzes an Alder-ene reaction, previously unknown in biology; the second catalyzes a stereoselective hetero-Diels–Alder reaction. Guided by computational studies, we rationalized the observed differences in reactivities and designed mutants that reverse periselectivities from Alder-ene to hetero-Diels–Alder and vice versa. A combination of *in vitro* biochemical characterizations, computational studies, enzyme co-crystal structures, and mutational studies provide a picture of how high regio- and periselectivities are achieved in nearly identical active sites.

6.3 Introduction

Pericyclic reactions are concerted chemical transformations in which all bonding changes occur in a cyclic array of atoms (Figure 33a).[183] Diels–Alder and hetero-Diels–Alder reactions are classics in synthesis, and form cyclohexenes and pyrans, respectively.[22,184] Recently, these pericyclic reactions have been discovered to be catalyzed by enzymes in nature (Figure 33a, b).[80] The Alder-ene reaction (Figure 33a),[185] originally named the 'substituting addition' reaction by Kurt Alder's laboratory in 1943 and subject of his Nobel prize lecture,[186] is an efficient method for carbon-carbon bond formation and has been applied to total syntheses of complex polycyclic natural products.[90,187] While this reaction has been postulated to be involved in several biological processes,[188] there are no

characterized examples of enzyme-catalyzed Alder-ene reactions in biology despite the frequency of substituted pentenes in natural products.[189] To this end, we set out to discover the enzymatic Alder-ene reaction in biosynthesis.

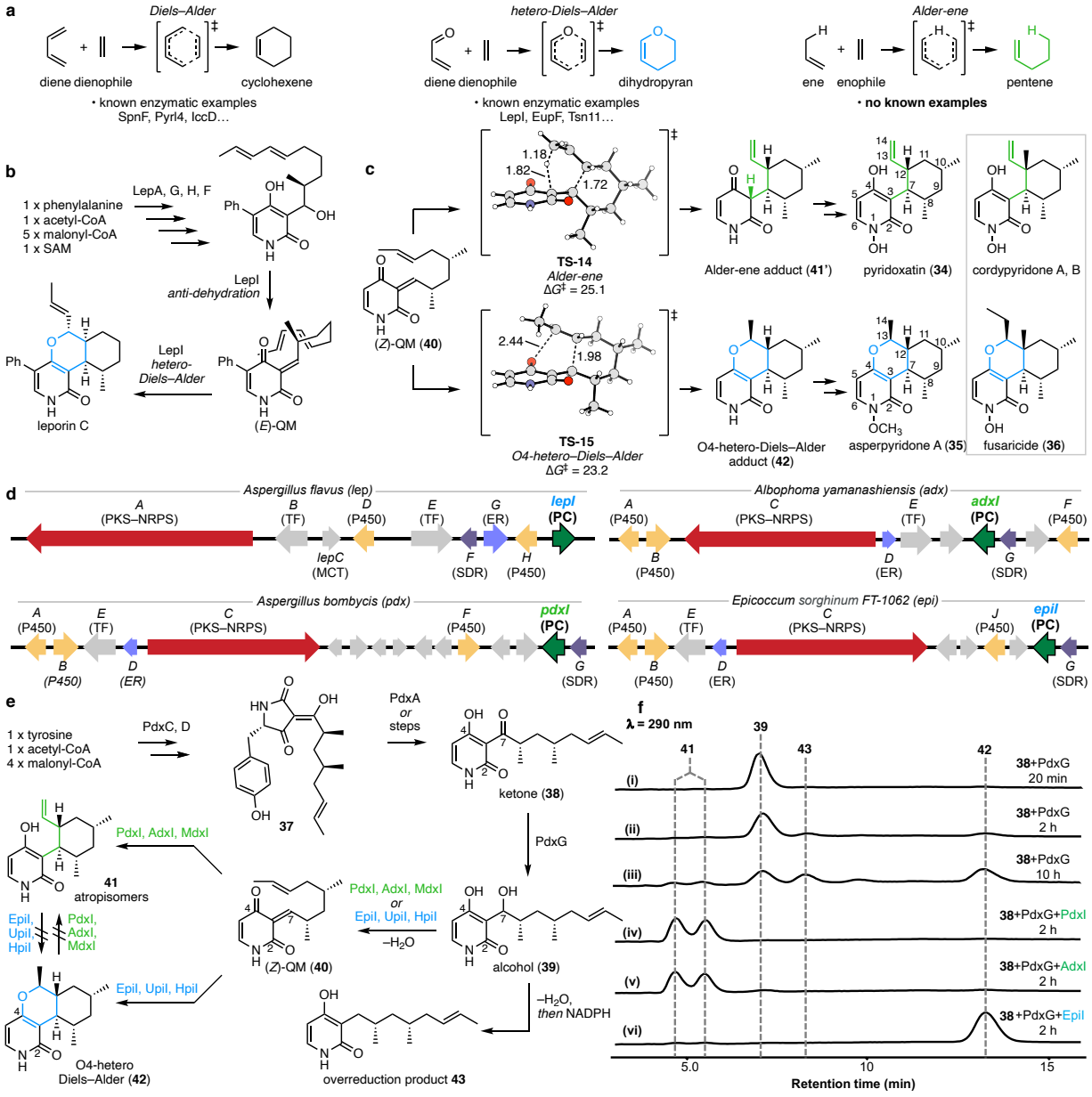

Figure 33

Pericyclic reactions in natural product biosynthesis. ***A.*** Known and unknown enzymatic examples of pericyclic reactions. ***B.*** The biosynthesis of leporin B involves a multifunctional O-methyltransferase-like pericyclase LepI. ***C.*** Theoretical investigations indicate that hetero-Diels–Alder **TS-15** is nonenzymatically favored by 1.9 kcal·mol^{-1} over Alder-ene **TS-14** from a common intermediate **40**. Further transformations lead to natural

products pyridoxatin **34**, cordypyridones, asperpyridone **35** and fusaricide **36**. ***D.*** The biosynthetic gene cluster (lep) of leporin B from Aspergillus flavus, the putative biosynthetic gene cluster (adx) of pyridoxatin from Albophoma yamanashiensis, the putative biosynthetic gene cluster (pdx) of pyridoxatin from Aspergillus bombycis, and the putative biosynthetic gene cluster (epi) of fusaricide from Epicoccum sorghinum FT1062. PKS-NRPS, polyketide synthase-nonribosomal peptide synthetase; TF, transcription factor; MCT, monocarboxylate transporter; P450, cytochrome P450; SDR, short-chain dehydrogenase/reductase; ER, enoylreductase; PC, pericyclase. ***E.*** The proposed biosynthesis of the Alder-ene product (**41**) and the hetero-Diels–Alder product (**42**) from the common intermediate **40**. ***F.*** One-pot *in vitro* tandem assay of **38** with PdxG and in the presence or absence of selected pericyclases.

Chemical syntheses of racemic pyridoxatin (**34**)[190,191] and cordypyridone[192] and our previous work on related leporin 2-pyridone alkaloids[80,149] led us to hypothesize that the vinyl cyclohexane core of **34** could be formed by an Alder-ene reaction of a reactive (*E*)- or (*Z*)-quinone methide (QM) (Figure 33c).[193] The activated QM can also undergo various hetero-Diels–Alder reactions involving either oxygen atom on the pyridone ring. To understand factors controlling the periselectivity, we expanded our study to include related natural products with the identical carbon backbones asperpyridone A (**35**)[194] and fusaricide (**36**)[195,196] that presumably derive from the hetero-Diels–Alder reaction of the same reactive QM. Because Alder-ene reactions are less exothermic (~ −27 kcal·mol^{-1}) than cycloadditions (~ −38 kcal·mol^{-1}), we anticipated that the Alder-ene reaction would be intrinsically more difficult than hetero-Diels–Alder reactions and periselectivity would strongly favor the latter.

6.4 Quantum Mechanical Calculations Guide Genome Mining

To understand the reactivity of the QM in pericyclic reactions, we performed quantum mechanical calculations to determine transition state (TS) geometries and to quantify the barriers of possible pericyclic reactions from (*E*)- and (*Z*)-QM. Calculations indicate that

the Alder-ene reaction has a slight preference (0.4 kcal·mol^{-1}) to occur from the (*Z*)- over the (*E*)-QM. From the (*Z*)-QM **40**, the Alder-ene reaction via **TS-14** is 1.9 kcal·mol^{-1} higher in energy than preferred hetero-Diels–Alder **TS-15** (Figure 33c). This difference in Gibbs free energy corresponds to a nonenzymatic ratio of 1:9 Alder-ene to hetero-Diels–Alder adducts, and indicates that a dedicated pericyclase with strong periselectivity must be involved in each of the biosynthetic pathways for the exclusive formation of either **34** or **35** (and **36**) from the producing strains.

To identify the potential pericyclases, we searched the genomes of 1-producing strain *Albophoma yamanashiensis* and the related pyran-containing, 3-producing strain *Epicoccum sorghinum* FT1062, as the 2-producing strain was unavailable.[196,197] As shown in Figure 33d, the two genomes of *A. yamanashiensis* and *E. sorghinum* FT1062 both encode a homologous biosynthetic gene cluster (adx and epi, respectively) containing a polyketide synthase-nonribosomal peptide synthetase (adxC/epiC), a partnering enoylreductase (adxD/epiD), a ring expansion P450 (adxA/epiA), a putative N-hydroxylation P450 (adxB/epiB), a short-chain dehydrogenase/reductase (SDR) (adxG/epiG) and a putative O-methyltransferase (OMT) (adxI/epiI). We searched the National Center for Biotechnology Information (NCBI) database for other homologous clusters, which are conserved in many sequenced fungal strains such as *Aspergillus bombycis* (pdx), *Monosporascus cannonballus* (modx), *Uncinocarpus reesii* (upi) and *Hymenoscyphus scutula* (hpi) (Figure 33d). Based on the sequence of previously discovered pericyclase LepI in leporin biosynthesis (Figure 33b, d),[80] we hypothesized that the predicted OMT-fold enzymes in these pathways, which are AdxI, EpiI, PdxI,

ModxI, UpiI and HpiI, are potential pericyclases. We proposed that each enzyme catalyzes the stereoselective dehydration of the alcohol (**39**) to **40**; AdxI from the 1-producing strain would then catalyze the subsequent Alder-ene reaction; while EpiI from the 3-producing strain would catalyze the hetero-Diels–Alder reaction (Figure 33e). While there is a high sequence identity between these enzymes (59–83%), they all display very low identity to LepI (~15%).

6.5 In Vitro Biochemical Characterization of Pericyclases

We performed the coupled *in vitro* reactions using enzymatically and chemoenzymatically prepared ketone **38**, the SDR PdxG as the putative ketoreductase, and one of the proposed pericyclases. In the presence of PdxG and cofactor NADPH, **38** is reduced to the alcohol **39** (Figure 33f, trace *i*). In solution, **39** readily underwent nonenzymatic dehydration to generate both (*E*)- and (*Z*)-QM that rehydrate to form **39** and the C7 diastereomer.[198] After 2 h, small amounts of O4-hetero-Diels–Alder product **42** and atropisomeric Alder-ene product **41** were detected in a ratio of 3 to 1 (Figure 33f, trace *ii*) along with three other unidentified minor products. Extended incubation times (10 h) with PdxG generated the overreduced **43**, which is presumably derived from a reduction of the QM (Figure 33f, trace *iii*). When AdxI, PdxI or ModxI was incubated with PdxG, NADPH and **38**, **41** was predominantly formed (>98:2, 8:9) (Figure 33f, traces *iv, v*). On the other hand, when we added EpiI, UpiI or HpiI to the reaction mixtures containing PdxG, NADPH, and **38**, the periselectivity was switched with **42** as the predominant product (<5:95, 8:9) (Figure 33f, trace *vi*). Since **41** and **42** can be chemically interconverted in harsh acidic conditions,[192] we investigated whether these pericyclases could catalyze such a

transformation. However, no enzyme was able to catalyze the interconversion (Figure 33e), which indicates these enzymes catalyze the observed reactions with strong periselectivity. Although these new pericyclases are predicted *S*-adenosyl-L-methionine (SAM)-dependent O-MTs,[80,199] none were copurifed with SAM, nor was SAM or *S*-adenosyl-L-homocysteine (SAH) required for catalysis. Overall, our biochemical data show that the group of AdxI, PdxI and ModxI are the first characterized enzymes to catalyze the Alder-ene reaction forming a *bona fide* Alder-ene adduct. The group of EpiI, UpiI and HpiI were characterized as SAM-independent enzymes that catalyze a hetero-Diels–Alder reaction to form a *trans*-fused hexahydroisochromene, which is in contrast to LepI that forms a *cis*-fused hexahydroisochromene. These discoveries expand the repertoire of reactions catalyzed in Nature.

6.6 Crystal Structures and Molecular Dynamics

To gain mechanistic insight into the enzyme-catalyzed Alder-ene reaction, X-ray crystal structures of apo-PdxI, substrate analogue complex PdxI-**38**, and product complex PdxI-**41** were solved and refined to 2.0 Å, 2.0 Å, and 2.4 Å resolutions, respectively. The apo-PdxI structure adopts a classic α,β-Rossman O-MT fold (Figure 34a)[149] and forms a woven dimer structure by interlocking the N-terminal helices (lime and royal blue, Figure 34b). The PdxI-**38** and PdxI-**41** structures are overall very similar to apo-PdxI (root mean squared deviation (r.m.s.d.) of 0.162 and 0.202 for 831 Cα atoms, respectively). The chain A active site of PdxI-**38** and PdxI-**41** are shown in Figure 34c. The pyridone ring forms hydrogen bonds with the side chains of K337, H161 and Q412, as well as water molecules via T232, D233 and H336 in the active site. The extended alkyl chain of **38** is pointed

towards hydrophobic residue I366 and is not in a near attack conformation for the pericyclic reaction. The C7 ketone of substrate analogue **38** is positioned *syn* to the C4-hydroxyl and is indicative that the alcohol substrate undergoes a syn-dehydration facilitated by K337 to generate (*Z*)-QM **40**. In order to generate an (*E*)-QM the C7 alcohol would need to rotate 180° and be *syn* to the C2-oxygen. The fact that this (*E*)-QM geometry differs greatly from that of the substrate analogue indicates that it is most probable that **40** is generated *in situ*. Substitution of K337 to alanine completely abolished the dehydration activity but can be rescued by mutation to arginine, which supports the role of K337 as a general base for the dehydration step.

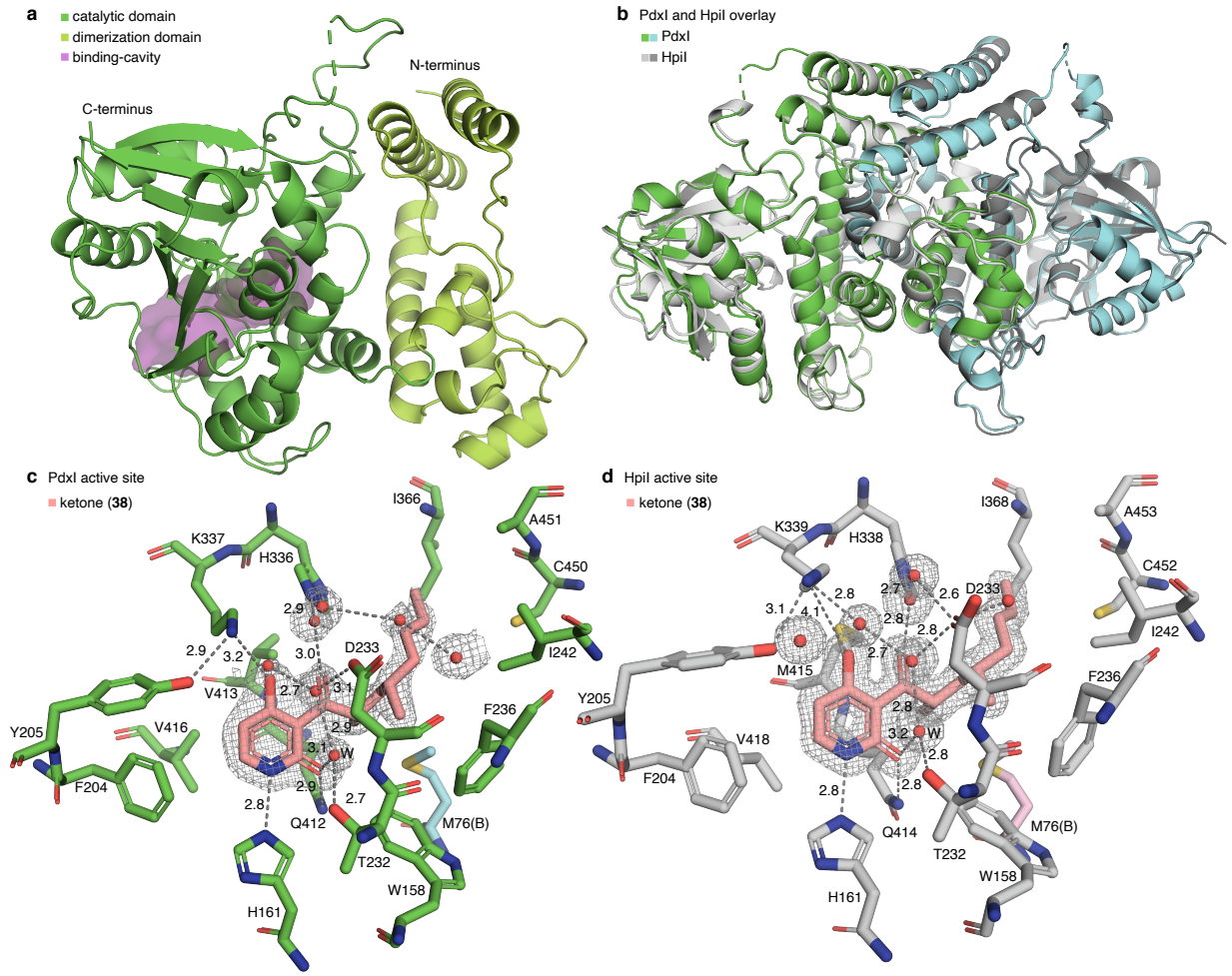

Figure 34
Crystal structures of PdxI and HpiI. Simulated annealing omit map shown in grey mesh and contoured at 1.0 σ. Hydrogen bond interactions are indicated with black dashed lines. ***A.*** Cartoon representation of apo-PdxI tertiary structure and binding-cavity (magenta). The C-terminal catalytic domain is shown in green and the N-terminal dimerization domain in lime. ***B.*** Overlay of interlocking homodimer structures of apo-PdxI and apo-HpiI. ***C.*** Active-site view of co-crystal structure of PdxI with substrate analogue ketone **38**. ***D.*** Active-site view of co-crystal structure of HpiI with substrate analogue ketone **38**. In ***C.*** and ***D.***, M76 from Chain B is indicated in different colors.

To investigate how the active site of PdxI catalyzes the energetically unfavorable Alder-ene reaction and suppresses the hetero-Diels–Alder reaction, we performed multiple 500 ns classical molecular dynamics (MD) simulations of **40** docked into PdxI. Since K337 is expected to be protonated after dehydration of **39** to **40**, we modeled side chain of K337 as an ammonium ion. We analyzed the conformation of the alkyl chain of the reactive **40** throughout the simulations and found that the alkyl chain can reorganize from the extended, unreactive conformation seen in PdxI-**38** into a reactive near attack conformation for 50-100 ns of the 500 ns simulation. In all simulations, H161 and Q412 hydrogen bond to N1 and C2-carbonyl of the pyridone, respectively, whereas K337 and H336 hydrogen bond to the C4-carbonyl. K337 maintains this hydrogen bond to the pyridone C4-carbonyl of 7 for longer durations in the simulation, which implies the protonated K337 may facilitate the Alder-ene reaction by hydrogen bond catalysis.

6.7 Quantum Mechanical 'Theozyme' Models Rationalize Catalysis

Next, we quantified how the K337 and H161 hydrogen bonds affect the reaction rate with a truncated catalytic-residue 'theozyme' model; K337 is modeled as a methyl ammonium and H161 as an imidazole (Figure 35a). The calculations indicate that the energetic barrier for the Alder-ene transition state in the theozyme (**TS-16**) is reduced by 11.7

kcal·mol^{-1}, a rate acceleration of >10^8, when compared to the nonenzymatic reaction (**TS-14**). Protonation of the carbonyl makes C7 highly electrophilic and decreases the nucleophilicity of the carbonyl oxygen. Both of these factors suppress the hetero-Diels–Alder transition state (**TS-17**) and favor **TS-16** by 3.4 kcal·mol^{-1}, a 5.8 kcal·mol^{-1} shift in $\Delta\Delta G^{\ddagger}$ relative to the nonenzymatic reactions (Figure 35a). Mechanistically, calculations indicate that **40** undergoes protonation by K337 and concomitant Alder-ene reaction via **TS-16** with an overall enthalpic barrier of 9.2 kcal·mol^{-1}. Whereas the O4-hetero-Diels–Alder via **TS-17** has a barrier of 12.6 kcal·mol^{-1}. This indicates that the PdxI active site alters the electronics of the reaction, by protonation of O4, to favor the Alder-ene reaction and achieve observed periselectivity.

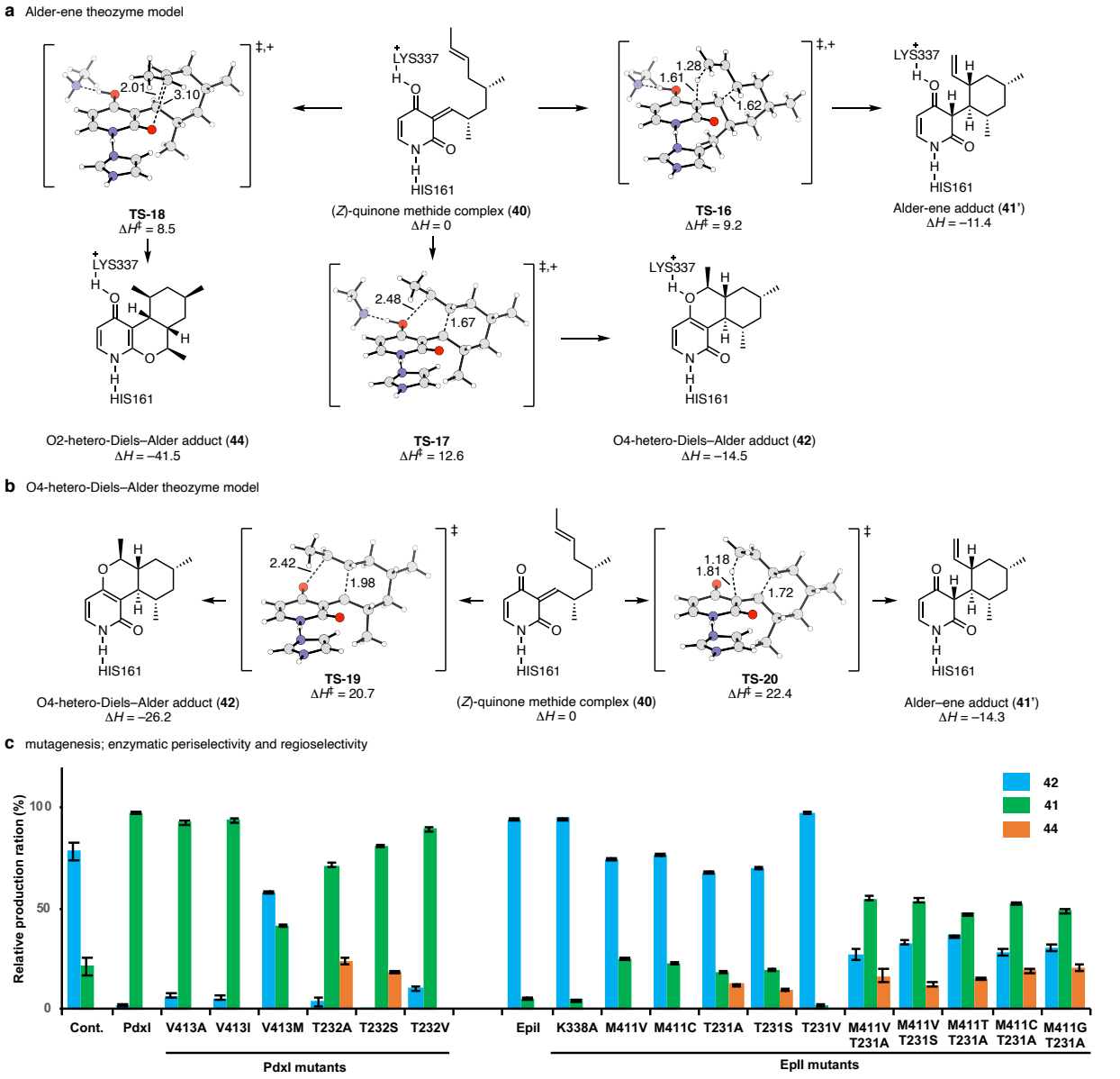

Figure 35

Mechanism of periselective and regioselective pericyclic reactions. ***A.*** Alder-ene theozyme model based on PdxI structure. ***B.*** O4-Hetero-Diels–Alder theozyme model confirmed by HpiI structure. ***C.*** Analysis of the relative production ratio of the O4-hetero-Diels–Alder adduct **42**, Alder-ene adduct **41**, and the O2-hetero-Diels–Alder adduct **44** from *in vitro* reaction of **38** with PdxG, NADPH, and selected pericyclases. To quantify the ratio, the reaction time of control sample without pericyclases (Cont.) was 12 hours, and reaction times with enzyme were 2 hours. Error bars indicate s.d. of three independent replicates. *Putative cyclized products other than **41**, **42**, and **44** were detected in the control reaction.

6.7.1 Regio- and Periselectivity of PdxI

It should be noted that the Alder-ene theozyme model also predicts a distinct, yet favorable hetero-Diels–Alder reaction via **TS-18** to form the *cis*-fused O2-hetero-Diels–Alder 4-pyridone adduct **44** (Figure 35a). However, **44** is not found in the *in vitro* PdxI reaction mixtures (Figure 33f). This implies an additional degree of regio- and periselectivity exerted by PdxI to disfavor formation of **TS-18**. The PdxI structure with a docked **TS-18** indicates that the side chain of T232 and water molecule (W) cause disfavorable interactions with the terminal C14 methyl in **TS-18**. The threonine residue acts as a steric wall to prevent **40** from accessing the **TS-18** conformation. To test this hypothesis, we prepared the PdxI T232A/S/V mutants and performed the coupled *in vitro* reactions. Indeed, the less hindered T232A and T232S mutants generated an appreciable amount of a new compound as compared to the WT PdxI (Figure 35c). Large scale *in vitro* reaction of PdxI T232S mutant led to the isolation and determination of structure as the expected **44**, which is one of the minor, nonenzymatic cyclized product from **40**. Mutation to valine (PdxI T232V), the steric isostere of threonine, did not produce any **44** (Figure 35c) supporting the role of T232 residue in sterically preventing the formation of **TS-18**.

6.7.2 Enzymatic Periselectivity Controlled by Hydrogen Bonding

PdxI crystal structures, molecular dynamics, and the ‘theozyme’ model indicate that the K337 residue acts as a general acid catalyst to favor the Alder-ene reaction over the O4-hetero-Diels–Alder reaction. Then, we calculated the O4-hetero-Diels–Alder ‘theozyme’ model (Figure 35b) by removing the lysine from the PdxI K337 and H161 theozyme model

(Figure 35a), and indeed the O4-hetero-Diels–Alder reaction is preferred by 1.7 kcal·mol^{-1} (**TS-19** vs **TS-20**). This suggests that the group of enzymes (EpiI, HpiI and UpiI) that catalyze the O4-hetero-Diels–Alder reaction, in contrast to PdxI, must avoid proton transfer to the pyridone C4 carbonyl to achieve the opposite periselectivity. Nevertheless, the corresponding lysine is conserved in these three enzymes as well. We solved and refined the crystal structures of apo-HpiI and HpiI-**38** to 1.3 Å and 1.5 Å resolution, respectively (Figure 34d). These structures are highly similar to that of PdxI (r.m.s.d of 0.468 for 415 Cα atoms) (Figure 34b–d). Notably, the binding modes of **38** in PdxI and HpiI are essentially identical (Figure 34c, d) and nearly all amino acid residues in the active site between PdxI and HpiI are conserved except for V413 in PdxI and the corresponding residue M415 in HpiI (Figure 34c, d). This key residue sits below the pyridone binding site and neighbors the aforementioned lysine (K337 in PdxI, K338 in EpiI and K339 in HpiI). The HpiI-**38** complex clearly shows that K339, unlike K337 in PdxI, does not form a hydrogen bond to the 4-hydroxy on the pyridone ring; this distance is stretched out from 3.2 Å in PdxI to 4.1 Å in HpiI (Figure 34c, d). To verify the lysine residue is not catalytic, we prepared the more stable mutant K338A of EpiI. In contrast to PdxI K337A mutant, EpiI K338A mutant retained the majority of the enzymatic activity (~80%) and showed the same periselectivity as WT EpiI (Figure 35c). Thus, the EpiI-catalyzed reactions do not require hydrogen bonding between the C4-oxygen on the pyridone ring and K338. From the crystal structure of HpiI, this loss of a hydrogen bond is caused by the bulkier side chain of M415, which shifts the lysine side chain further away from the substrate (Figure 34d). Consistently, homologous pericyclases such as EpiI, UpiI, and HpiI all catalyze the hetero-Diels–Alder reaction to form **42**, and the methionine residue

is conserved (M411, M413, and M415, respectively). By contrast, pericyclases such as PdxI, AbxI and ModxI catalyze the Alder-ene reaction, and the valine residue (V413) is conserved.

6.7.3 Control of Periselectivity Through Single Point Mutations

We next explored if the periselectivity of PdxI could be switched to favor the hetero-Diels–Alder reaction by replacement of V413 residue with alanine, isoleucine or methionine. Mutating valine to alanine and isoleucine, residues that are smaller than methionine, retained the periselectivity of PdxI for the Alder-ene reaction (Figure 35c). In contrast, the V413M mutant showed reversed periselectivity, switching the major reaction type from Alder-ene to hetero-Diels–Alder, forming **41** and **42** in a ratio of 40:60 compared to the wild-type ratio of >98:2 (Figure 35c). On the other hand, the mutation of M411 in EpiI to the less bulky valine or cysteine altered the product ratio (8:9) from 5:95 to 25:75 (Figure 35c). The mutation of M411 alone in EpiI is not sufficient to reverse the periselectivity, suggesting that other factors such as shape complementarity to restrict the movement of **40** would also contribute to maintaining the observed periselectivity for the hetero-Diels–Alder reaction.

Since the conformational flexibility of **40** is expected to be restricted by both M411 and T231 residues in the EpiI active site based on the HpiI-5 complex (Figure 34d), we mutated the T231 residue to smaller alanine and serine residues. This mutation would increase the conformational flexibility of **40** in the EpiI active site to form the key hydrogen bonding with K338 for the Alder-ene reaction. Indeed, while the hetero-Diels–Alder

product **42** still remains the major product, EpiI T231A and T231S mutants increased the ratio of Alder-ene product **41** along with the O2-hetero-Diels–Alder product **44** as seen in PdxI T232A/S mutants (Figure 35c). Intriguingly, the double mutant M411V/T231A showed the reversed periselectivity with the ratio (**41**:**42**) of 66:33. Other less bulky double mutants such as M411V/T231S, M411T/T231A. M411C/T231A, and M411G/T231A showed similarly reversed periselectivies. Based on these results, we conclude that the replacement of the methionine and threonine with smaller residues enlarges the enzyme active site and allows for greater conformational sampling of **40** and protonation of the C4 carbonyl, thus leading to the opposite periselectivity.

6.8 Conclusions

Our results show that the group of PdxI, AdxI, and ModxI are multifunctional enzymes that catalyze the stereoselective *syn*-dehydration of **39** to **40** and the subsequent Alder-ene reaction of **40** to **41** in a stereo-, regio- and periselective manner. In contrast, the group of EpiI, UpiI, and HpiI catalyze the same stereoselective *syn*-dehydration of **39** to **40** but with orthogonal periselectivity and catalyze the hetero-Diels–Alder reaction of **40** to **42**. Computational studies, comparative analysis of the enzyme-cocrystal structures, and site-directed mutagenesis provided a detailed picture of the catalytic mechanism for PdxI and EpiI. PdxI utilizes K337 as general acid catalyst to facilitate the otherwise energetically unfavorable Alder-ene reaction, while the methionine substitution in EpiI abolishes this interaction to allow only the O4-hetero-Diels–Alder reaction. The steric effect of T232 in PdxI and T231 in EpiI inhibits the formation of the O2-hetero-Diels–Alder product **44** to further control regioselectivity.

In conclusion, we have characterized two homologous groups of enzymes and identified how subtle evolutionary divergence leads to the production of different natural products. The insight gained from our research serves as a basis for developing new biocatalysts that catalyze various natural and unnatural Alder-ene and hetero-Diels–Alder reactions that are valuable synthetic transformations.

Chapter 7. All *Endo*-[6+4] Cycloadditions are Ambimodal

7.1 Contributions

This is an author manuscript from the publication: Jamieson, C. S.; Sengupta, A.; Houk, K. N. Cycloadditions of Cyclopentadiene and Cycloheptatriene with Tropones: All Endo-[6+4] Cycloadditions Are Ambimodal. *J. Am. Chem. Soc.* **2021**, *143* (10), 3918–3926. https://doi.org/10.1021/jacs.0c13401. Myself, and Arkajyoti Sengupta were co-first authors on this publication. I developed this project based on my understanding of higher-order cycloadditions in nature; all published examples of such reactions are ambimodal. I wanted to explore whether this was a general phenomenon. I used this project as a way to train postdoctoral fellow Arkajyoti Sengupta on how to conduct quasi-classical molecular dynamics simulations and how to use ORCA for high-level of theory DLPNO-CCSD(T) calculations.

7.2 Abstract

The cycloadditions of cyclopentadiene and cycloheptatriene with tropone are some of the earliest published examples of [6 + 4] cycloaddition reactions. We report quantum mechanical studies (ωB97X-D and DLPNO-CCSD(T)) of transition structures and products of these reactions, as well as quasi-classical molecular dynamics simulations of reaction trajectories. The study reveals that these cycloadditions involve ambimodal transition states resulting in a web of products by pericyclic interconversion pathways. Combined with these studies, calculations of simple parent systems and a thorough meta-

analysis of literature examples reveal the general concept that all *endo*-[6 + 4] cycloadditions are ambimodal.

7.3 Introduction

In 1965,[200] and in the full description of orbital symmetry selection rules in 1969,[16] Hoffmann and Woodward predicted that trienes and dienes could react in concerted [6 + 4] cycloadditions to give 10-membered-ring products. Later they predicted that this reaction should proceed with *exo*, rather than *endo*, stereochemistry due to repulsive secondary orbital interactions in the *endo* transition state (TS).[201] These predictions were quickly confirmed by independent discoveries by the Cookson and Itô groups,[202–204] both of which studied the reaction of cyclopentadiene and tropone (Figure 36a). The predictions were also verified in the Woodward labs with more heavily substituted reactants (Figure 36b).[205]

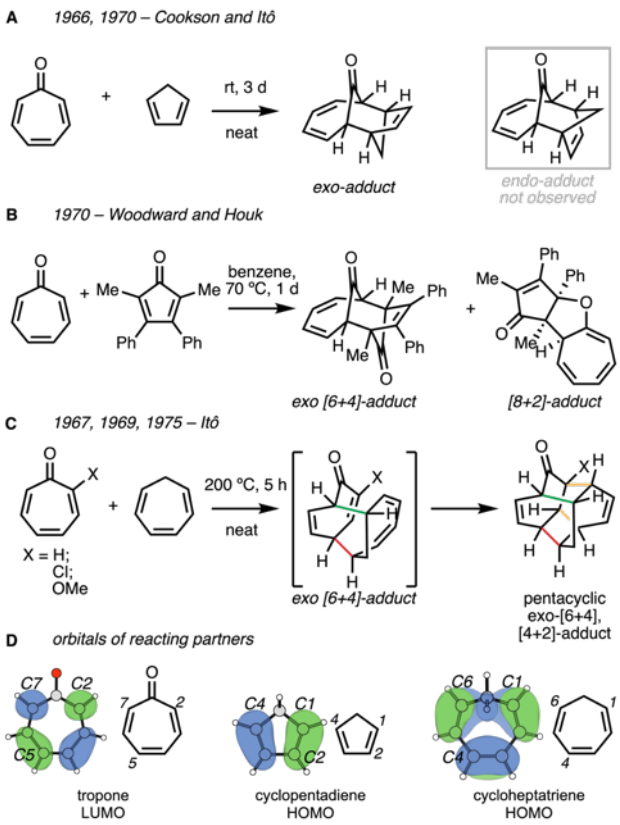

Figure 36
Early examples of higher-order [6 + 4] cycloadditions. ***A.*** Independent studies by Cookson and Itô in 1966 and additionally reported in 1970. ***B.*** Verification of Hoffmann and Woodward predictions by Houk in 1966, published in 1970. ***C.*** Synthesis of pentacyclic molecules involving [6 + 4] cycloadditions by Itô and coworkers in 1967. ***D.*** Shapes of the highest-occupied and the lowest-unoccupied molecular orbitals: LUMO of tropone, and HOMOs of cyclopentadiene and cycloheptatriene.

A variety of [6 + 4] cycloadditions have since been discovered,[206] including some that are catalyzed by enzymes in nature.[12,14,43,102] Among the earliest examples of [6 + 4] cycloadditions were the studies from the Itô group of the reactions of cycloheptatriene with tropone and several substituted tropones (Figure 36c).[207–210] These cycloaddition cascades generate 8 stereogenic centers to form a densely functionalized pentacyclic adduct. We have re-examined these reactions computationally with modern accurate density functional theory (DFT) and molecular dynamics simulations. These studies found a web of hidden processes occurring from ambimodal transition states. Revisiting these

early examples of [6 + 4] cycloadditions revealed a striking and general phenomenon: all *endo*-[6 + 4] cycloadditions are ambimodal.

About 35 years after the first published [6 + 4] cycloaddition, the Caramella group discovered a *bis*pericyclic transition state in the computational investigation of cyclopentadiene dimerization.[75] They showed that one transition state could lead to multiple (in this case 2 identical) pericyclic reaction products due to a post-transition state bifurcation. Such reactions are now generally referred to as ambimodal reactions.[62,211] This phenomenon occurs when a transition state is connected without an intermediate to a second transition state that is perpendicular to the reaction coordinate and interconverts the products. Caramella,[212] Singleton,[213,214] Tantillo,[53,62] and our group[61] have expanded on this concept, discovering transition states that can lead, after multiple bifurcations on the potential surface to three[215] or more pericyclic reaction products. In this context, we hypothesized that the reaction of tropone and either cyclopentadiene or cycloheptatriene could also involve ambimodal transition states.

7.4 Computational Methodologies

We have now explored these reactions with highly accurate DFT and wavefunction methods at the DLPNO-CCSD(T)/cc-pVQZ//ωB97X-D/def2-TZVP level of theory as implemented in ORCA 4.1.1 and Gaussian 16[127,151,153,154,216–219], and describe here the details of calculated reaction energetics of cyclopentadiene with tropone, and of cycloheptatriene with tropone and several substituted tropones. These studies depict the importance of secondary orbital interactions in controlling not only stereoselectivity but

the periselectivity (selectivity between pericyclic reactions) of higher-order cycloadditions and elaborate on the generality of single pericyclic TSs that lead to multiple products.

7.5 Cyclopentadiene and Tropone: Frontier Molecular Orbitals

Cookson and Itô confirmed Hoffmann and Woodward's prediction: tropone and cyclopentadiene react to form an *exo*-tricyclic adduct with π systems *anti* to each other (Figure 36a). Considering the frontier molecular orbitals (Figure 36d), the nucleophilic C1 of cyclopentadiene (highest occupied molecular orbital, HOMO) interacts with the electrophilic C2 of tropone (lowest unoccupied molecular orbital, LUMO) thus also connecting C4 of cyclopentadiene and C7 of tropone. When the π-systems are arranged *syn* – an *endo* orientation – there is an out-of-phase orbital interaction between C2 and C3 of cyclopentadiene and C3 and C6 of tropone that reduces stabilizing orbital interactions. In the *exo* orientation, when the π-systems are *anti*, there are no antibonding interactions. There can be a stabilizing secondary orbital interaction in the *exo* orientation between the tropone oxygen HOMO and C2 and C3 of cyclopentadiene LUMO, although this is the weaker frontier MO interaction and has a small effect at most. Strong secondary orbital interactions can become primary interactions and lead to bond formation; this is manifested in ambimodal reactions, where the transition states have orbital interactions that can lead to several products. Secondly, the related experimental findings by Houk and Woodward showed that substituted cyclopentadienes indeed form the [8 + 2] adduct as a minor product.[205] Given these considerations, we hypothesized that the first report of a [6 + 4] cycloaddition could be ambimodal and have a single transition state that can lead to both the [6 + 4] and [8 + 2] adducts.

7.6 Cyclopentadiene and Tropone: Calculated Reaction

We have calculated the transition states of the reactions of cyclopentadiene with tropone (Figure 37a, b). For the reaction of cyclopentadiene and tropone, the *exo* cycloaddition (**TS-21**) is favored over the *endo* cycloaddition (**TS-22**) by a difference in Gibbs free energy of activation of 3.3 kcal·mol^{-1}. Using transition state theory, this energetic difference ($\Delta\Delta G^{\ddagger}$) corresponds to a predicted product ratio of >99:1 *exo* to *endo* – thus reproducing the experimental result that only the *exo* adduct is observed.

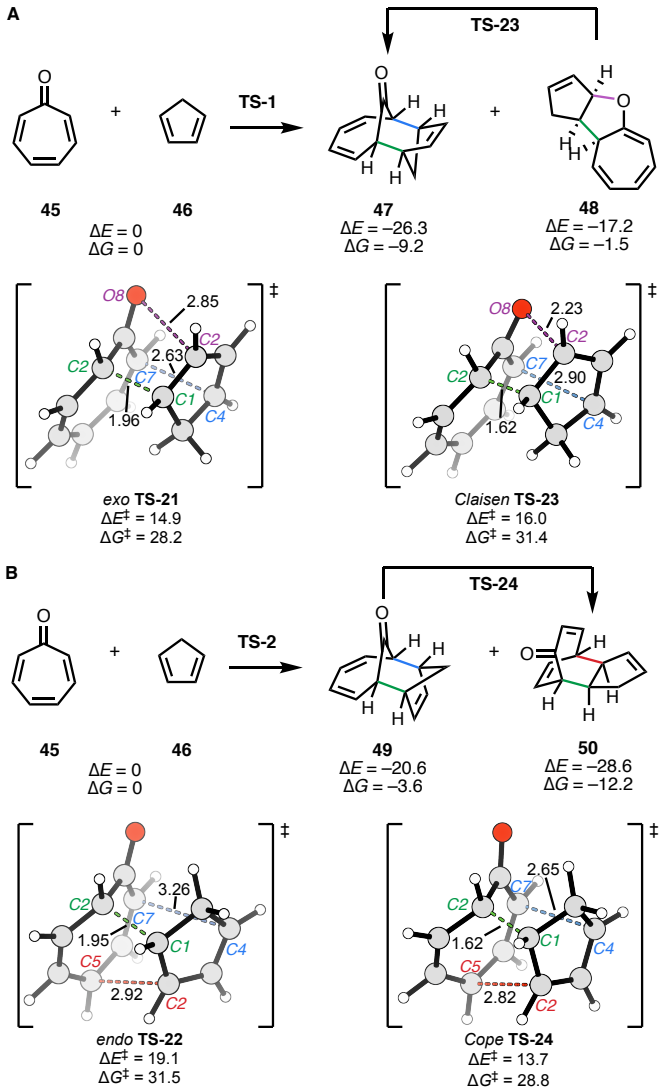

Figure 37
Calculated energy surface for the *exo* (**TS-21**) and *endo* (**TS-22**) reactions of tropone (**45**) and cyclopentadiene (**46**) at the DLPNO-CCSD(T)/cc-pVQZ//ωB97X-D/def2-TZVP level of theory.

TS-21 and **TS-22** feature secondary orbital interactions. In **TS-21**, the exocyclic oxygen (O8) of tropone forms a stabilizing interaction with cyclopentadiene C2 (2.85 Å, purple dashed line, Figure 37a). This interaction destroys the bilateral plane of symmetry in **TS-21** and makes the *exo*-[6 + 4] highly asynchronous. By contrast, we previously showed that cyclopentadiene and cycloheptatriene, which lack this secondary interaction, react via a symmetrical and synchronous [6 + 4] transition state.[220–222] In a typical pericyclic

ambimodal transition state, the common bond among the reactions is significantly formed at ~ 2 Å, and the competing partial bonds are around ~ 3 Å.[10] **TS-21** does exhibit ambimodal character, with bond lengths of 1.96, 2.63 and 2.85 Å. However, the orbital overlap between the exocyclic oxygen of tropone and cyclopentadiene C3 is far from ideal with an angle of 74º. The [8 + 2] product **48** could form, but only as as a minor (~1%) product, and it has not been observed in experiments. The higher energy *endo*-**TS-22** corroborates the lack of experimental observation of any *endo* products . In this TS, to avoid the disfavorable out-of-phase orbital interaction, cyclopentadiene twists nearly 10º to avoid the disfavorable out-of-phase orbital interaction and to form a favorable orbital interaction between tropone C5 and cyclopentadiene C2. This TS merges the *endo*-[6 + 4] transition state with an *exo*-[4 + 2] Diels–Alder TS. This twisting makes the *endo*-[6 + 4] cycloaddition proceed via a single ambimodal *exo*-[4 + 2] / *endo*-[6 + 4] transition state with forming bonds of 1.95, 2.92 and 3.26 Å. This implys that the *endo*-[6 + 4] adduct **49** should be a minor product relative to the *exo*-[4 + 2] adduct **50**. Previously, we reported that the competing bond distances in the TS are related to the product ratio where a difference of 0 Å corresponds to a 50:50 ratio and >0.4 Å corresponds to <1% of the minor product.[10] In **TS-22**, the difference in bond length is 0.3 Å, which correlates to a predicted product ratio of 90:10 **51** : **50**.

In ambimodal reactions, the ambimodal transition state is connected on the potential surface with a second transition state that interconverts the products; in these cases, these TSs are Claisen (**TS-23**) or Cope (**TS-24**) rearrangement transition states (Figure 37a, b). Typically, in ambimodal cycloadditions these interconversion TSs are one or two

kcal·mol^{-1} lower in energy than the preceding ambimodal transition state.[215,223] In this case of the *exo* cycloaddition of **45** and **46**, the interconversion Claisen **TS-23** is higher in energy by 3.2 kcal·mol^{-1}. This indicates that the reverse reaction of **48** is ambimodal and would lead to **45**, **46** and **47**. This is further evidence that in the forward reaction the [8 + 2] adduct **48** should not form in an appreciable amount. Further calculations, dynamics and discussion are in the Supplemental Information.

As shown above, the first [6 + 4] cycloaddition of **45** and **46** is simple experimentally, leading to only a single observable product, but theory reveals the rich complexity of the potential surface that lurks behind the scenes, invisible to experiment. The observed product forms via an ambimodal transition state that can lead to [6 + 4] and [8 + 2] adducts, but forms **47** for dynamic and thermodynamic reasons. The unobserved *endo* **TS-22** is similarly ambimodal and complex. These results lead us to hypothesize that all *endo* [6 + 4] cycloadditions are ambimodal.

7.7 Cycloheptatriene and Tropone: Experiment

About the time of the dawn of pericyclic reactions, the Itô group explored the reactions of the homologous systems, cycloheptatriene and several tropones. (Figure 36c, Scheme 1). They found that pentacyclic adducts are formed by [6 + 4] cycloadditions of the cycloheptatriene as a 6π addend and tropone as a 4π, followed by an intramolecular [4 + 2] cycloaddition. The reactions of **45** and 2-chlorotropone (**45a**) with **51** formed a single pentacyclic adduct (**55** and **55a**), whereas 2-methoxytropone (**45b**) formed a mixture of regioisomers proposed to be **55b** and **55b'**.

Scheme 1
Itô's proposed structures for products of cycloaddition reactions of tropone derivatives (**45**, **45a**, **45b**) with cycloheptatriene (**51**).

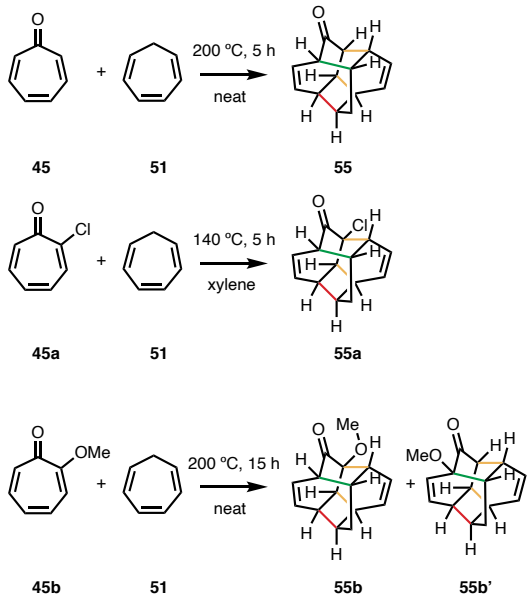

7.8 Cycloheptatriene and Tropone: Frontier Molecular Orbitals

Frontier molecular orbitals indicate that cycloheptatriene, **51**, should act, like **46**, as a nucleophile, with the HOMO at C1 forming a strong interaction at C2 of tropone, **45**, which is the most electrophilic site of tropone as indicated by the LUMO coefficient (Figure 36d). This indicates that C6 of **51** interacts with C5 of **45** as well as C4 of **51** with C7 of **45**. Arranging **45** and **51** in this geometry allows for two [6 + 4] cycloadditions to occur where either molecule can be a 4π or 6π partner. Furthermore, considering the HOMO of **45**, we can envision a third, similar interaction as occurs with cyclopentadiene, where C2 of **7** interacts with the exocyclic oxygen (O8) of **45**. In total, frontier molecular orbitals predict there should be 4 partially formed bonds in the *exo* TS, and these could in theory form two [6 + 4] adducts and an [8 + 2] adduct. This means that this reaction could lead to three products from a single *tri*pericyclic ambimodal TS, a surmise that we have explored

computationally. Because of our longstanding interests to understand periselectivity, we also studied Itô's cycloadditions of the halogenated and methoxylated tropones (Figure 36c, Scheme 1).

7.9 Cycloheptatriene and Tropone: Calculated Reaction

The computed potential surfaces for the reactions of substituted tropones reacting with cycloheptatriene **51** are shown in Figure 38c. The cycloaddition of **45** and **51** favors the *exo* **TS-25** by 2.8 kcal·mol^{-1}. Focusing on **TS-25**, we note as predicted by frontier molecular orbital interactions that there are four partially formed bonds in the TS with distances of 1.92, 2.84, 3.02, and 3.11 Å. **TS-25** has ambimodal character and could lead to three cycloaddition products – two [6 + 4] adducts and an [8 + 2] adduct. This would be the second example of a *tri*pericyclic reaction.[23] All the potential products, have similar energies (ΔG = –1.5 – +1.0) when compared to separated reactants, **45** and **51**. This indicates that the forward and reverse reactions could occur. Next, we performed an intrinsic reaction coordinate calculation and found that **TS-25** leads directly to the [3 , 3]-sigmatropic Cope rearrangement **TS-26** and then proceeds to product **53** (Figure 38b). **TS-26** interconverts the two [6 + 4] adducts **52** and **53**. We extensively searched for [3 , 3] and [5 , 5]-sigmatropic Claisen TSs that would interconvert either [6 + 4] adduct **52** or **53** with the [8 + 2] adduct **54**. After many efforts, we located the [3 , 3]-sigmatropic Claisen rearrangement **TS-27** that interconverts **54** and **53**. This structure is a very late TS with the O8–C2 bond distance nearly formed at 2.19 Å, and is very high in energy ($\Delta G^{\ddagger}$ = 37.3), nearly 5 kcal·mol^{-1} higher in energy than the preceding tripericyclic **TS-25**. Traversing such a barrier would be an extremely rare event and indicates that a very

minor percentage (~ 1%) of **54** could form momentarily before reverting back to either separated reactants or **53**.

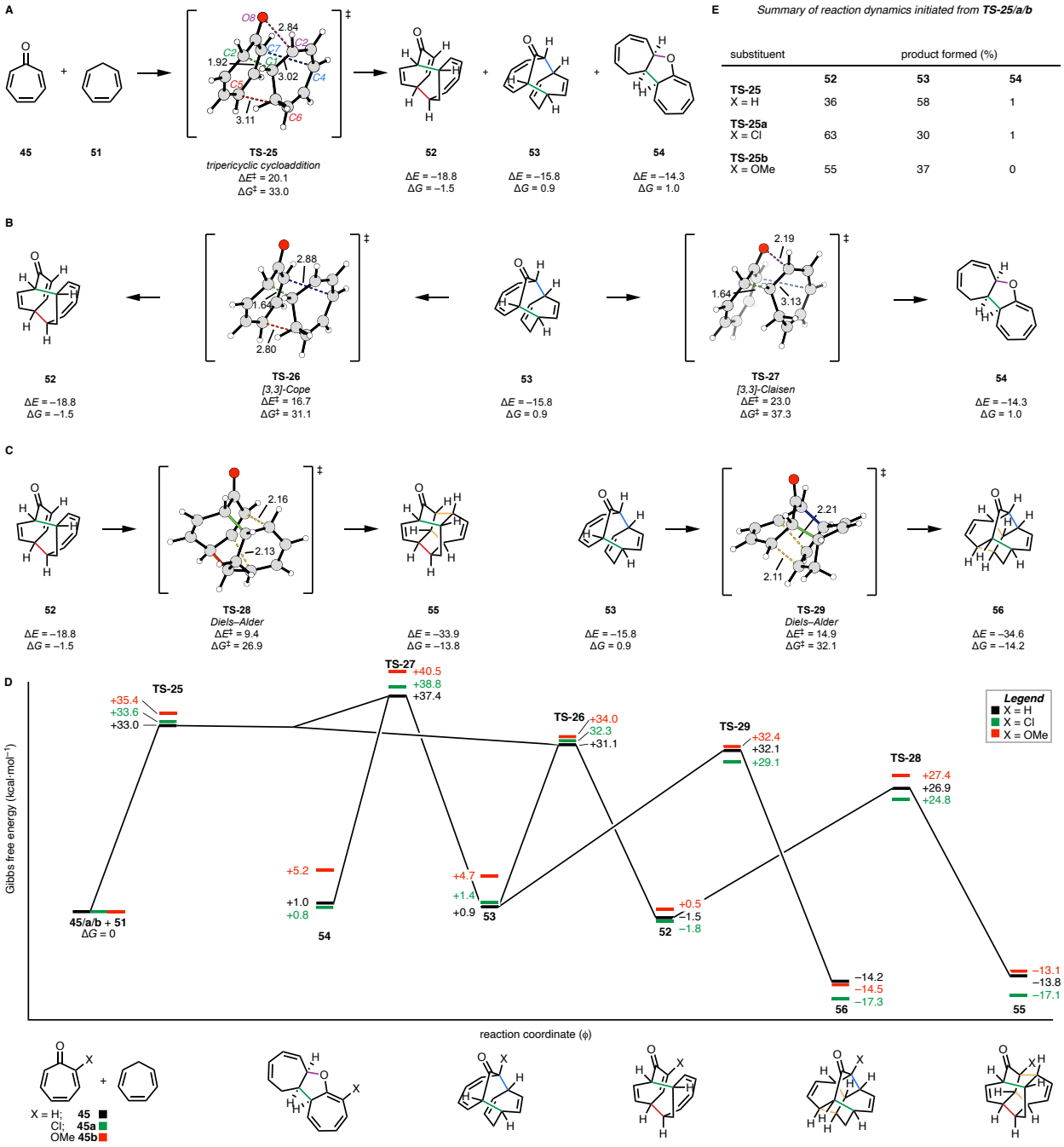

Figure 38

Calculated energy surfaces for tropones reacting with cycloheptatriene (**51**). ***A.*** Calculated reaction energetics of tropone **45** and cycloheptatriene **51**. ***B.*** Interconversion Cope (**TS-26**) and Claisen (**TS-27**) pathways of tropone and cycloheptatriene adducts. ***C.*** Diels–Alder TSs (**TS-28** and **TS-29**) leading to pentacyclic adducts. ***D.*** Free energy

diagram for tropone (black),chloro tropone (**a**, green), and methoxy tropone (**b**, red) reacting with cycloheptatriene. ***E.*** Summary of quasi-classical reaction dynamics trajectory results indicating ratios of **52**, **53**, and **54** formed from **TS-25**, **TS-25a**, and **TS-25b**. Calculations at the DLPNO-CCSD(T)/cc-pVQZ//ωB97X-D/def2-TZVP level of theory. Dynamics at the optimization level of theory. Energies are quasi-harmonic corrected and reported at 1 M and 25 ºC.

This first cycloaddition step via **TS-25** builds a reactive diene in **52** and **53** that is predistorted and ready to undergo a subsequent [4 + 2] Diels–Alder reaction (**TS-28** and **TS-29**). However, **54** does not have such a possibility and is less stable than reactants, and so it presumably undergoes a retro-[8 + 2] to re-form **45** and **51**. The barrier for these Diels–Alder TSs, **TS-28** and **TS-29** are quite different. We hypothesize that this is due to the relative reactivity of the dienophile: the dienophile of **53** is unactivated, whereas the dienophile of **52** is an α,β-unsaturated ketone. We believe that this electronic difference could cause the 5.2 kcal·mol^{-1} difference in $\Delta G^{\ddagger}$ as the structures are similarly strained with related scaffolds. This electronic difference of the dienophiles in **52** and **53** brings the barrier for **TS-28** below that of the interconversion Cope **TS-26** and indicates that **53** will convert via **TS-26** into **52** and then exclusively form the pentacyclic adduct **55**.

Overall, the calculations predict that this reaction undergoes a tripericyclic cycloaddition (**TS-25**) to form **52**, **53**, and **54** that then undergo a concomitant Diels–Alder (**TS-28** and **TS-29**) to form the experimentally observed pentacyclic adduct 11 that feature 4-, 5-, 6-, and 7-membered rings. These results reproduce the Itô group's 1967 report. However, our studies indicate that a second adduct (**56**) could form as a minor product. Interestingly, 28 years later in 1995, Singh published similar findings at a lower temperature (140 ºC versus 200 ºC).[224] In that paper, they report the sole formation of our predicted minor

product **56**. By lowering the temperature, we do not expect the reaction to then 'switch' to proceed through the higher-energy **TS-29**. This reaction warrants further experimental investigation.

We also calculated the chloro (**a**) and methoxy (**b**) substituted tropones that the Itô group studied, in order to understand how substituents influence the tripericyclic reaction product ratios. We calculated the energy surfaces with the substituted tropones (Figure 38c). In general, we found that in the first step, compared to **TS-25** the methoxy raises the reaction barriers (**TS-25b** , +2.4 kcal·mol^{-1}) and the chloro has a small effect (**TS-25a**, +0.6 kcal·mol^{-1}) on the reaction barriers as seen in **TS-25b** and **TS-25a** , respectively. In the second step, the chloro decreases the Diels–Alder barriers substantially (**TS-28a**, **TS-29a**, –2.1 – –3.0 kcal·mol^{-1}) whereas the methoxy has a small effect (**TS-28b**, **TS-29b**, +0.3 – +0.5 kcal·mol^{-1}). Of note, the competing Diels–Alder TSs, with either chloro or methoxy substituents, are more facile than the Cope rearrangement **TS-26a** and **TS-26b**. This indicates that in these substituted systems, a second pentacyclic adduct (**56a** and **56b**) should also be observed. Indeed, Itô did observe a second adduct in the reaction of **45b** with **51**. However, this adduct was assigned as the regioisomer **55b'**, while our calculations predict that **56b** should be formed. (Figure 38).

Substitution alters the geometry of **TS-25**, but does not change the mechanism (Figure 38d, 39). Using the Yang *et al.* bond length model,[10] the subtle changes in forming bond lengths in the TS correspond to unique product distributions of **52**, **53**, and **54**. The Yang *et al.* bond length model from our group is a simple method to predict product ratios of

ambimodal cycloaddition reactions based on the bond lengths in the transition state. Recently, the Goodman group (Lee *et al.*) published a more general method that can be applied to all reaction types.[11] Upon rounding the predicted ratios, both methods make similar predictions for each reaction (Figure 40). Interestingly, the bond distance between the exocyclic oxygen of **45**/**a**/**b** and C3 of **51** is the same, and similar to the distance in the aforementioned reaction with **46**. We hypothesize that this weak secondary orbital interaction is a geometric requirement due to the proximity to the forming carbon-carbon bonds. Such interactions have been noted in dipolar cycloadditions.[225,226]

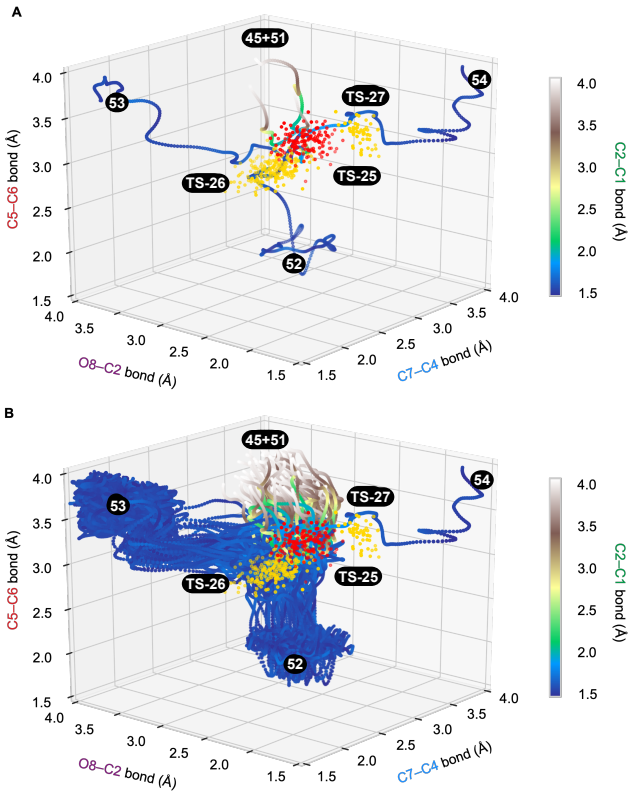

Figure 40
Four-dimensional bond length plots of reaction dynamics trajectories. The color bar maps the common bond (C2–C1, green) among products: separated is grey (4 Å) and formed is blue (1.5 Å). TS ensemble geometries for **TS-25** (red), **TS-26** (gold) and **TS-27** (gold) are overlaid in contrasting colors for clarity. ***A.*** Randomly selected trajectories propagated from **TS-25** leading to each product. ***B.*** Plot of all 135 trajectories propagated from **TS-25**. Calculations are at the ωB97X-D/def2-TZVP level of theory.

In order to test our predicted product ratios from the tripericyclic transition states **TS-25**, **TS-25a** and **TS-25b**, we turned to quasi-classical reaction dynamics simulations. The calculations were performed in the gas phase at the ωB97X-D/def2-TZVP level of theory. Trajectories were initiated from transition state ensembles generated with ProgDyn and propagated using classical equations of motion with forces calculated quantum mechanically on the fly.[227,228] Transition state ensembles were generated by performing a Boltzmann sampling of geometries using normal mode sampling and adding the zero-point energy for each real normal mode and thermal energy at 298 K to the structures.

Reaction trajectories initiated from **TS-25** indicate that the reactants **45** and **51** yield products **52**, **53**, and **54**. This is indeed a tripericyclic reaction, where a single transition state leads to three unique products (Figure 39e, 41). Out of 135 trajectories, 46 (36%) form **52**, 82 (58%) form **53**, and 1 (1%) form **54**. The remaining 6 (5%) trajectories recross (defined as traversing the transition state region but then recrossing to the product on the other side of the TS).[36,37] Substitutions of C2 with chloro (**a**) or methoxy (**b**) groups alter the product ratios. The 2-chloro substituent inverts the product ratio, where the major product is now **52a** (63%). This can be rationalized by considering the steric effect of substituting the reacting center and can be noted in the **TS-25a** structure where the forming bond length is stretched out upon chloro substitution when compared to the unsubstituted **TS-25a** (Figure 39e, 40). The methoxy tropone gives similar product ratios (60% **53**, 40% **52**) to the unsubstituted case despite having different forming bond lengths in the TS. It is interesting how stretching out the C2–C5 bond by >0.1 Å in **TS-25b** does

not alter the product ratio like we saw with a similar distortion in **TS-25a**. Lastly, the methoxytropone dynamics did not yield **54b**. This is likely due to the small number of trajectories propagated as the energetics for **TS-27a** and **TS-27b** are similarly ~5 kcal·mol^{-1} greater than the preceding **TS-25a/b** .

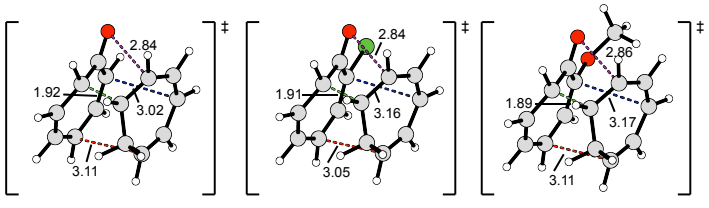

TS-25
$\Delta E^{\ddagger}$ = 20.1
$\Delta G^{\ddagger}$ = 33.0

TS-25a
$\Delta E^{\ddagger}$ = 20.4
$\Delta G^{\ddagger}$ = 33.6

TS-25b
$\Delta E^{\ddagger}$ = 22.2
$\Delta G^{\ddagger}$ = 35.4

predicted product ratios of **52** and **53** (Yang *et al.*)

52	43	64	57
53	57	36	43

predicted product ratios of **52** and **53** (Lee *et al.*)

52	39	52	51
53	61	48	49

Figure 39
Comparison of tripericyclic TS geometries, energies, and predicted product ratios of **52** and **53** by Yang *et al.*[10] and Lee *et al.*[11] with reaction dynamics yields.

Overall, quantum mechanical calculations revealed the ambimodal nature of the first reported [6 + 4] cycloaddition of tropone and cyclopentadiene as well as those more complex examples reported shortly thereafter of substituted tropones and cycloheptatriene. Such results led us to hypothesize on the generality or even requirement for such reactions to be ambimodal.

7.10 Meta-analysis Reveals All Endo-[6 + 4] Cycloadditions are Ambimodal

Here, we postulate that all *endo*-[6 + 4] cycloadditions are ambimodal. In the aid of clarity, we first define *exo* and *endo* for [6 + 4] cycloadditions. Previously the definition for Diels-Alder reactions was based upon whether the dienophile substituent is near (proximal,

endo) or away from (distal, *exo*) the C2 and C3 of the diene, but for [6 + 4] cycloadditions only the all cis and *s*-cis diene and triene were considered. For [6 + 4] cycloadditions, several isomers of the triene are possible, and the diene may react from the *s-trans* conformation. Thus, we define *endo* in the [6 + 4] cycloaddition as the TS or product in which the central unit (Δ3,4, highlighted) of the triene reaction partner is distal (*exo*) or proximal (*endo)* to the diene reaction partner, respectively (Figure 41a). As the triene and diene reaction partners are comprised of smaller π-units, a competing Diels–Alder cycloaddition is always possible. Therefore, in the *endo* orientation, both reactions will occur based solely on spatial orientation. In this case, both reactions share the same favorable frontier molecular orbital interactions. This means that the two reactions will occur through a single ambimodal transition state.

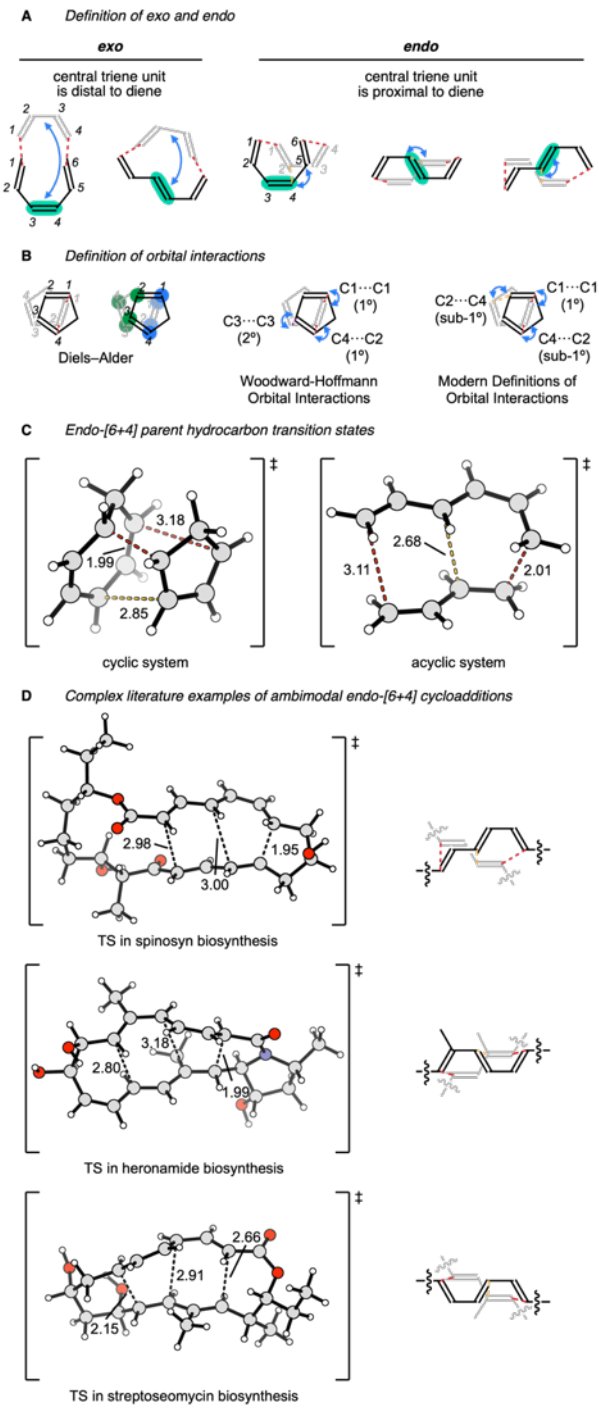

Figure 41

Definition of (***A.***) *exo* and *endo* with regards to [6 + 4] cycloadditions, (***B.***) orbital interactions, and (***C***.) parent hydrocarbon transition states of cyclic and acyclic systems. ***D.*** Meta-analysis of complex published examples of *endo*-[6 + 4] transition states.[12–14]

Our definitions emphasize the difference between Hoffmann and Woodward's definition of secondary orbital interactions and what we define as subordinate primary interactions (sub-1º in Figure 41b), ~ 3 Å bond lengths in ambimodal transition states. Hoffmann and Woodward defined secondary orbital interactions as those that stabilize or destabilize a transition state. This would, for example, be the interaction of C3 of a diene with C3 of a dienophile in a Diels-Alder reaction of two dienes (Figure 41b). Such interactions cannot lead to a stable product. By contrast, subordinate primary interactions lead to a product, as in the interaction of C2 of a diene with C4 of the dienophile (Figure 41b). We propose to call these interactions subordinate primary interactions as they can compete for bond formation; either subordinate primary interaction can lead to one of the products of the reaction.

To investigate the generality of this concept, we calculated the *endo*-[6 + 4] TSs for the parent hydrocarbon cyclic and acyclic systems (Figure 41c). These TSs feature strong secondary orbital interactions (subordinate primary interactions) with competing bond lengths of ~ 2.8 and 3.1 Å. In fact, the Diels–Alder is favored in both systems by having a shorter forming bond length in the TS. Earlier in this paper, we described the transition states and orbital interactions for tropones reacting with cyclopentadiene and cycloheptatriene (i.e. **TS-21**, **TS-22**, **TS-23**). In the Itô group's 1970 publication on the cycloadditions of tropone and cyclopentadiene, a minor (4%) *exo*-Diels–Alder adduct is reported, which suggests that our calculated ambimodal *exo*-[4 + 2]/*endo*-[6 + 4] transition state (**TS-22**) could also be at play.[204] Those systems agree well with our proposal, but we sought to explore other examples of such *endo*-[6 + 4] cycloadditions to determine the

generality of their ambimodal nature and present three examples in Figure 41d. The examples are calculated TSs in spinosyn, heronamide, and streptoseomycin biosynthesis that feature transannular ambimodal cycloadditions.[12–14] Here, we also note that the central triene unit is *endo* with respect to the diene reaction partner in all three examples. These reactions have been characterized in the original publications to be ambimodal. Therefore, all known examples are indeed ambimodal. We conclude based upon this empirical evidence that *endo*-[6 + 4] cycloadditions will always involve ambimodal transition state because of the enforced proximity of atoms that interact and lead to alternative products.

7.11 Conclusion

We report a computational study that highlights the ambimodal nature of higher order cycloadditions of tropone (**45**) with cyclopentadiene (**46**) and cycloheptatriene (**51**). The cycloaddition of tropone and cycloheptatriene involves a tripericyclic transition state that leads to the formation of [8 + 2] and two [6 + 4] cycloadducts. The strength of the subordinate primary orbital interactions control the formation of different cycloadducts. Quasi-classical reaction dynamic simulations resulted in three different products with one of the [6 + 4] adducts as the major product in accordance to the TS geometry. Such simulations revealed the dynamic nature of secondary-orbital interactions morphing into primary bond-forming interactions. We have clarified this situation by defining subordinate primary interactions that may or may not lead to a product, depending on the trajectory. In the reactions of cycloheptatriene with various tropones, subsequent intramolecular [4 + 2] Diels-Alder reactions form the experimentally observed pentacyclic adducts **55** and

56. All of these results point to the overarching concept that all *endo*-[6 + 4] reactions are ambimodal. To verify our hypothesis we analyzed the parent hydrocarbon systems, the reactions of **45**, **46** and **51**, and the known complex examples found in biosynthesis. This empirical evidence confirms our postulate that all *endo*-[6 + 4] reactions are ambimodal.

References

(1) Houk, K. N.; Lin, Y. T.; Brown, F. K. Evidence for the Concerted Mechanism of the Diels-Alder Reaction of Butadiene with Ethylene. *J. Am. Chem. Soc.* **1986**, *108* (3), 554–556. https://doi.org/10.1021/ja00263a059.

(2) Beno, B. R.; Houk, K. N.; Singleton, D. A. Synchronous or Asynchronous? An "Experimental" Transition State from a Direct Comparison of Experimental and Theoretical Kinetic Isotope Effects for a Diels−Alder Reaction. *J. Am. Chem. Soc.* **1996**, *118* (41), 9984–9985. https://doi.org/10.1021/ja9615278.

(3) Getty, S. J.; Borden, W. T. Why Does Tetrafluoroethylene Not Undergo Diels-Alder Reaction with 1,3-Butadiene? An Ab Initio Investigation. *J. Am. Chem. Soc.* **1991**, *113* (11), 4334–4335. https://doi.org/10.1021/ja00011a048.

(4) Ilardi, E. A.; Stivala, C. E.; Zakarian, A. [3,3]-Sigmatropic Rearrangements: Recent Applications in the Total Synthesis of Natural Products. *Chem. Soc. Rev.* **2009**, *38* (11), 3133–3148. https://doi.org/10.1039/b901177n.

(5) Barcan, G. A.; Patel, A.; Houk, K. N.; Kwon, O. A Torquoselective 6π Electrocyclization Approach to Reserpine Alkaloids. *Org. Lett.* **2012**, *14* (21), 5388–5391. https://doi.org/10.1021/ol302265z.

(6) E., G. V.; N., H. K.; Beatriz, de P.-T.; Brett, B.; D., J. K.; A., L. R. Control of the Exo and Endo Pathways of the Diels-Alder Reaction by Antibody Catalysis . *Science (80-.).* **1993**, *262* (5131), 204–208. https://doi.org/10.1126/science.8211138.

(7) Siegel, J. B.; Zanghellini, A.; Lovick, H. M.; Kiss, G.; Lambert, A. R.; St.Clair, J. L.; Gallaher, J. L.; Hilvert, D.; Gelb, M. H.; Stoddard, B. L.; et al. Computational Design of an Enzyme Catalyst for a Stereoselective Bimolecular Diels-Alder Reaction. *Science (80-.).* **2010**, *329* (5989), 309–313. https://doi.org/10.1126/science.1190239.

(8) Watanabe, K.; Mie, T.; Ichihara, A.; Oikawa, H.; Honma, M. Detailed Reaction Mechanism of Macrophomate Synthase: Extraordinary Enzyme Catalyzing Five-Step Transformation from 2-Pyrones to Benzoates. *J. Biol. Chem.* **2000**, *275* (49), 38393–38401. https://doi.org/10.1074/jbc.M003119200.

(9) Yu, J.; Zhou, Y.; Tanaka, I.; Yao, M. Roll: A New Algorithm for the Detection of Protein Pockets and Cavities with a Rolling Probe Sphere. *Bioinformatics* **2010**, *26* (1), 46–52. https://doi.org/10.1093/bioinformatics/btp599.

(10) Yang, Z.; Dong, X.; Yu, Y.; Yu, P.; Li, Y.; Jamieson, C.; Houk, K. N. N. Relationships between Product Ratios in Ambimodal Pericyclic Reactions and Bond Lengths in Transition Structures. *J. Am. Chem. Soc.* **2018**, *140* (8), 3061–3067. https://doi.org/10.1021/jacs.7b13562.

(11) Lee, S.; Goodman, J. M. Rapid Route-Finding for Bifurcating Organic Reactions. *J. Am. Chem. Soc.* **2020**, *142* (20), 9210–9219. https://doi.org/10.1021/jacs.9b13449.

(12) Patel, A.; Chen, Z.; Yang, Z.; Gutiérrez, O.; Liu, H.; Houk, K. N.; Singleton, D. A. Dynamically Complex [6+4] and [4+2] Cycloadditions in the Biosynthesis of Spinosyn A. *J. Am. Chem. Soc.* **2016**, *138* (11), 3631–3634. https://doi.org/10.1021/jacs.6b00017.

(13) Yu, P.; Patel, A.; Houk, K. N. Transannular [6 + 4] and Ambimodal Cycloaddition in the Biosynthesis of Heronamide A. *J. Am. Chem. Soc.* **2015**, *137* (42), 13518–13523. https://doi.org/10.1021/jacs.5b06656.

(14) Zhang, B.; Wang, K. B.; Wang, W.; Wang, X.; Liu, F.; Zhu, J.; Shi, J.; Li, L. Y.; Han, H.; Xu, K.; et al. Enzyme-Catalysed [6+4] Cycloadditions in the Biosynthesis of Natural Products. *Nature* **2019**, *568* (7750), 122–126. https://doi.org/10.1038/s41586-019-1021-x.

(15) Hoffmann, R.; Woodward, R. B. Conservation of Orbital Symmetry. *Acc. Chem. Res.* **1968**, *1* (1), 17–22. https://doi.org/10.1021/ar50001a003.

(16) Woodward, R. B.; Hoffmann, R. The Conservation of Orbital Symmetry. *Angew. Chemie Int. Ed. English* **1969**, *8* (11), 781–853. https://doi.org/10.1002/anie.196907811.

(17) Baldwin, J. E.; Fleming, R. H. Allene-Olefin and Allene-Allene Cycloadditions Methylenecyclobutane and 1,2-Dimethylenecyclobutane Degenerate Rearrangements BT - Dynamic Stereochemistry; Springer Berlin Heidelberg: Berlin, Heidelberg, 1970; pp 281–310.
(18) Black, K.; Liu, P.; Xu, L.; Doubleday, C.; Houk, K. N. Dynamics, Transition States, and Timing of Bond Formation in Diels-Alder Reactions. *Proc. Natl. Acad. Sci. U. S. A.* **2012**, *109* (32), 12860–12865. https://doi.org/10.1073/pnas.1209316109.
(19) Woodward, R. B.; Bader, F. E.; Bickel, H.; Frey, A. J.; Kierstead, R. W. The Total Synthesis of Reserpine. *J. Am. Chem. Soc.* **1956**, *78* (9), 2023–2025. https://doi.org/10.1021/ja01590a079.
(20) Woodward, R. B.; Bader, F. E.; Bickel, H.; Frey, A. J.; Kierstead, R. W. A Simplified Route to a Key Intermediate in the Total Synthesis of Reserpine. *J. Am. Chem. Soc.* **1956**, *78* (11), 2657. https://doi.org/10.1021/ja01592a102.
(21) Woodward, R. B.; Bader, F. E.; Bickel, H.; Frey, A. J.; Kierstead, R. W. The Total Synthesis of Reserpine. *Tetrahedron* **1958**, *2* (1–2), 1–57. https://doi.org/10.1016/0040-4020(58)88022-9.
(22) Nicolaou, K. C.; Snyder, S. A.; Montagnon, T.; Vassilikogiannakis, G. The Diels-Alder Reaction in Total Synthesis. *Angew. Chemie - Int. Ed.* **2002**, *41* (10), 1668–1698. https://doi.org/10.1002/1521-3773(20020517)41:10<1668::AID-ANIE1668>3.0.CO;2-Z.
(23) Nicolau, K. C.; Sorensen, E. J. *Classics in Total Synthesis*; John Wiley & Sons, 1996.
(24) Zirpel, B.; Degenhardt, F.; Martin, C.; Kayser, O.; Stehle, F. Engineering Yeasts as Platform Organisms for Cannabinoid Biosynthesis. *J. Biotechnol.* **2017**, *259*, 204–212. https://doi.org/10.1016/j.jbiotec.2017.07.008.
(25) Lu, Z.; Li, Y.; Deng, J.; Li, A. Total Synthesis of the Daphniphyllum Alkaloid Daphenylline. *Nat. Chem.* **2013**, *5* (8), 679–684. https://doi.org/10.1038/nchem.1694.
(26) Chen, Y.; Zhang, W.; Ren, L.; Li, J.; Li, A. Total Syntheses of Daphenylline, Daphnipaxianine A, and Himalenine D. *Angew. Chemie - Int. Ed.* **2018**, *57* (4), 952–956. https://doi.org/10.1002/anie.201711482.
(27) Zhang, W.; Ding, M.; Li, J.; Guo, Z.; Lu, M.; Chen, Y.; Liu, L.; Shen, Y. H.; Li, A. Total Synthesis of Hybridaphniphylline B. *J. Am. Chem. Soc.* **2018**, *140* (12), 4227–4231. https://doi.org/10.1021/jacs.8b01681.
(28) Souris, C.; Misale, A.; Chen, Y.; Luparia, M.; Maulide, N. From Stereodefined Cyclobutenes to Dienes: Total Syntheses of Ieodomycin D and the Southern Fragment of Macrolactin A. *Org. Lett.* **2015**, *17* (18), 4486–4489. https://doi.org/10.1021/acs.orglett.5b02149.
(29) Misale, A.; Niyomchon, S.; Maulide, N. Cyclobutenes: At a Crossroad between Diastereoselective Syntheses of Dienes and Unique Palladium-Catalyzed Asymmetric Allylic Substitutions. *Acc. Chem. Res.* **2016**, *49* (11), 2444–2458. https://doi.org/10.1021/acs.accounts.6b00375.
(30) Chen, J.; Deng, Q.; Wang, R.; Houk, K. N.; Hilvert, D. Shape Complementarity, Binding-Site Dynamics, and Transition State Stabilization: A Theoretical Study of Diels–Alder Catalysis by Antibody 1E9. *ChemBioChem* **2000**, *1* (4), 255–261. https://doi.org/https://doi.org/10.1002/1439-7633(20001117)1:4<255::AID-CBIC255>3.0.CO;2-S.
(31) Kim, S. P.; Leach, A. G.; Houk, K. N. The Origins of Noncovalent Catalysis of Intermolecular Diels-Alder Reactions by Cyclodextrins, Self-Assembling Capsules, Antibodies, and RNAses. *J. Org. Chem.* **2002**, *67* (12), 4250–4260. https://doi.org/10.1021/jo011180d.
(32) Eiben, C. B.; Siegel, J. B.; Bale, J. B.; Cooper, S.; Khatib, F.; Shen, B. W.; Players, F.; Stoddard, B. L.; Popovic, Z.; Baker, D. Increased Diels-Alderase Activity through Backbone Remodeling Guided by Foldit Players. *Nat. Biotechnol.* **2012**, *30* (2), 190–192. https://doi.org/10.1038/nbt.2109.

(33) Preiswerk, N.; Beck, T.; Schulz, J. D.; Milovník, P.; Mayer, C.; Siegel, J. B.; Baker, D.; Hilvert, D. Impact of Scaffold Rigidity on the Design and Evolution of an Artificial Diels-Alderase. *Proc. Natl. Acad. Sci. U. S. A.* **2014**, *111* (22), 8013–8018. https://doi.org/10.1073/pnas.1401073111.
(34) Oikawa, H.; Tokiwano, T. Enzymatic Catalysis of the Diels-Alder Reaction in the Biosynthesis of Natural Products. *Nat. Prod. Rep.* **2004**, *21* (3), 321–352. https://doi.org/10.1039/b305068h.
(35) Auclair, K.; Sutherland, A.; Kennedy, J.; Witter, D. J.; Van den Heever, J. P.; Hutchinson, C. R.; Vederas, J. C. Lovastatin Nonaketide Synthase Catalyzes an Intramolecular Diels - Alder Reaction of a Substrate Analogue [7]. *J. Am. Chem. Soc.* **2000**, *122* (46), 11519–11520. https://doi.org/10.1021/ja003216+.
(36) Oikawa, H.; Katayama, K.; Suzuki, Y.; Ichihara, A. Enzymatic Activity Catalysing Exo-Selective Diels-Alder Reaction in Solanapyrone Biosynthesis. *J. Chem. Soc. Chem. Commun.* **1995**, No. 13, 1321–1322. https://doi.org/10.1039/C39950001321.
(37) Xu, W.; Chooi, Y. H.; Choi, J. W.; Li, S.; Vederas, J. C.; Da Silva, N. A.; Tang, Y. LovG: The Thioesterase Required for Dihydromonacolin L Release and Lovastatin Nonaketide Synthase Turnover in Lovastatin Biosynthesis. *Angew. Chemie - Int. Ed.* **2013**, *52* (25), 6472–6475. https://doi.org/10.1002/anie.201302406.
(38) Katayama, K.; Kobayashi, T.; Oikawa, H.; Honma, M.; Ichihara, A. Enzymatic Activity and Partial Purification of Solanapyrone Synthase: First Enzyme Catalyzing Diels-Alder Reaction. *Biochim. Biophys. Acta - Protein Struct. Mol. Enzymol.* **1998**, *1384* (2), 387–395. https://doi.org/10.1016/S0167-4838(98)00040-5.
(39) Ose, T.; Watanabe, K.; Mie, T.; Honma, M.; Watanabe, H.; Yao, M.; Oikawa, H.; Tanaka, I. Insight into a Natural Diels-Alder Reaction from the Structure of Macrophomate Synthase. *Nature* **2003**, *422* (6928), 185–189. https://doi.org/10.1038/nature01454.
(40) Ose, T.; Watanabe, K.; Yao, M.; Honma, M.; Oikawa, H.; Tanaka, I. Structure of Macrophomate Synthase. *Acta Crystallogr. Sect. D Biol. Crystallogr.* **2004**, *60* (7), 1187–1197. https://doi.org/10.1107/S0907444904008881.
(41) Guimarães, C. R. W.; Udier-Blagović, M.; Jorgensen, W. L. Macrophomate Synthase: QM/MM Simulations Address the Diels-Alder versus Michael-Aldol Reaction Mechanism. *J. Am. Chem. Soc.* **2005**, *127* (10), 3577–3588. https://doi.org/10.1021/ja043905b.
(42) Wilson, E. K. Is the Case for a Diels-Alderase Dead? *Chem. Eng. News* **2005**, *83* (19), 38.
(43) Kim, H. J.; Ruszczycky, M. W.; Choi, S.; Liu, Y.; Liu, H. Enzyme-Catalysed [4+2] Cycloaddition Is a Key Step in the Biosynthesis of Spinosyn A. *Nature* **2011**, *473*, 109.
(44) Tian, Z.; Sun, P.; Yan, Y.; Wu, Z.; Zheng, Q.; Zhou, S.; Zhang, H.; Yu, F.; Jia, X.; Chen, D.; et al. An Enzymatic [4+2] Cyclization Cascade Creates the Pentacyclic Core of Pyrroindomycins. *Nat. Chem. Biol.* **2015**, *11* (4), 259–265. https://doi.org/10.1038/nchembio.1769.
(45) Hashimoto, T.; Hashimoto, J.; Teruya, K.; Hirano, T.; Shin-Ya, K.; Ikeda, H.; Liu, H. W.; Nishiyama, M.; Kuzuyama, T. Biosynthesis of Versipelostatin: Identification of an Enzyme-Catalyzed [4+2]-Cycloaddition Required for Macrocyclization of Spirotetronate-Containing Polyketides. *J. Am. Chem. Soc.* **2015**, *137* (2), 572–575. https://doi.org/10.1021/ja510711x.
(46) Byrne, M. J.; Lees, N. R.; Han, L.-C.; van der Kamp, M. W.; Mulholland, A. J.; Stach, J. E. M.; Willis, C. L.; Race, P. R. The Catalytic Mechanism of a Natural Diels–Alderase Revealed in Molecular Detail. *J. Am. Chem. Soc.* **2016**, *138* (19), 6095–6098. https://doi.org/10.1021/jacs.6b00232.
(47) Walsh, C. T.; Acker, M. G.; Bowers, A. A. Thiazolyl Peptide Antibiotic Biosynthesis: A Cascade of Post-Translational Modifications on Ribosomal Nascent Proteins. *J. Biol. Chem.* **2010**, *285* (36), 27525–27531. https://doi.org/10.1074/jbc.R110.135970.
(48) Minami, A.; Oikawa, H. Recent Advances of Diels-Alderases Involved in Natural Product

Biosynthesis. *J. Antibiot. (Tokyo).* **2016**, *69* (7), 500–506. https://doi.org/10.1038/ja.2016.67.
(49) Zheng, Q.; Tian, Z.; Liu, W. Recent Advances in Understanding the Enzymatic Reactions of [4+2] Cycloaddition and Spiroketalization. *Curr. Opin. Chem. Biol.* **2016**, *31*, 95–102. https://doi.org/10.1016/j.cbpa.2016.01.020.
(50) Andrews, P. R.; Smith, G. D.; Young, I. G. Transition-State Stabilization and Enzymic Catalysis. Kinetic and Molecular Orbital Studies of the Rearrangement of Chorismate to Prephenate. *Biochemistry* **1973**, *12* (18), 3492–3498. https://doi.org/10.1021/bi00742a022.
(51) Hong, Y. J.; Tantillo, D. J. Consequences of Conformational Preorganization in Sesquiterpene Biosynthesis: Theoretical Studies on the Formation of the Bisabolene, Curcumene, Acoradiene, Zizaene, Cedrene, Duprezianene, and Sesquithuriferol Sesquiterpenes. *J. Am. Chem. Soc.* **2009**, *131* (23), 7999–8015. https://doi.org/10.1021/ja9005332.
(52) Hong, Y. J.; Tantillo, D. J. Quantum Chemical Dissection of the Classic Terpinyl/Pinyl/Bornyl/Camphyl Cation Conundrum - The Role of Pyrophosphate in Manipulating Pathways to Monoterpenes. *Org. Biomol. Chem.* **2010**, *8* (20), 4589–4600. https://doi.org/10.1039/c0ob00167h.
(53) Hong, Y. J.; Tantillo, D. J. Biosynthetic Consequences of Multiple Sequential Post-Transition-State Bifurcations. *Nat. Chem.* **2014**, *6* (2), 104–111. https://doi.org/10.1038/nchem.1843.
(54) Lamb, A. L. Pericyclic Reactions Catalyzed by Chorismate-Utilizing Enzymes. *Biochemistry* **2011**, *50* (35), 7476–7483. https://doi.org/10.1021/bi2009739.
(55) DeClue, M. S.; Baldridge, K. K.; Künzler, D. E.; Kast, P.; Hilvert, D. Isochorismate Pyruvate Lyase: A Pericyclic Reaction Mechanism? *J. Am. Chem. Soc.* **2005**, *127* (43), 15002–15003. https://doi.org/10.1021/ja055871t.
(56) Shipman, L. W.; Li, D.; Roessner, C. A.; Scott, A. I.; Sacchettini, J. C. Crystal Structure of Precorrin-8x Methyl Mutase. *Structure* **2001**, *9* (7), 587–596. https://doi.org/10.1016/s0969-2126(01)00618-9.
(57) Luk, L. Y. P.; Qian, Q.; Tanner, M. E. A Cope Rearrangement in the Reaction Catalyzed by Dimethylallyltryptophan Synthase? *J. Am. Chem. Soc.* **2011**, *133* (32), 12342–12345. https://doi.org/10.1021/ja2034969.
(58) Payne, K. A. P.; White, M. D.; Fisher, K.; Khara, B.; Bailey, S. S.; Parker, D.; Rattray, N. J. W.; Trivedi, D. K.; Goodacre, R.; Beveridge, R.; et al. New Cofactor Supports α,β-Unsaturated Acid Decarboxylation via 1,3-Dipolar Cycloaddition. *Nature* **2015**, *522* (7557), 497–501. https://doi.org/10.1038/nature14560.
(59) Ferguson, K. L.; Eschweiler, J. D.; Ruotolo, B. T.; Marsh, E. N. G. Evidence for a 1,3-Dipolar Cyclo-Addition Mechanism in the Decarboxylation of Phenylacrylic Acids Catalyzed by Ferulic Acid Decarboxylase. *J. Am. Chem. Soc.* **2017**, *139* (32), 10972–10975. https://doi.org/10.1021/jacs.7b05060.
(60) Krenske, E. H.; Patel, A.; Houk, K. N. Does Nature Click? Theoretical Prediction of an Enzyme-Catalyzed Transannular 1,3-Dipolar Cycloaddition in the Biosynthesis of Lycojaponicumins A and B. *J. Am. Chem. Soc.* **2013**, *135* (46), 17638–17642. https://doi.org/10.1021/ja409928z.
(61) Ess, D. H.; Wheeler, S. E.; Iafe, R. G.; Xu, L.; Çelebi-Ölçüm, N.; Houk, K. N. Bifurcations on Potential Energy Surfaces of Organic Reactions. *Angew. Chemie - Int. Ed.* **2008**, *47* (40), 7592–7601. https://doi.org/10.1002/anie.200800918.
(62) Hare, S. R.; Tantillo, D. J. Post-Transition State Bifurcations Gain Momentum-Current State of the Field. *Pure Appl. Chem.* **2017**, *89* (6), 679–698. https://doi.org/10.1515/pac-2017-0104.
(63) Li, G.; Kusari, S.; Spiteller, M. Natural Products Containing “decalin” Motif in

Microorganisms. *Nat. Prod. Rep.* **2014**, *31* (9), 1175–1201. https://doi.org/10.1039/c4np00031e.
(64) Fischbach, M. A.; Walsh, C. T. Assembly-Line Enzymology for Polyketide and Nonribosomal Peptide Antibiotics: Logic Machinery, and Mechanisms. *Chem. Rev.* **2006**, *106* (8), 3468–3496. https://doi.org/10.1021/cr0503097.
(65) Diedrich, M. K.; Klärner, F. G.; Beno, B. R.; Houk, K. N.; Senderowitz, H.; Still, W. C. Experimental Determination of the Activation Parameters and Stereoselectivities of the Intramolecular Diels-Alder Reactions of 1,3,8-Nonatriene, 1,3,9-Decatriene, and 1,3,10-Undecatriene and Transition State Modeling with the Monte Carlo-Jumping between W. *J. Am. Chem. Soc.* **1997**, *119* (43), 10255–10259. https://doi.org/10.1021/ja9643331.
(66) Jeon, B. S.; Wang, S. A.; Ruszczycky, M. W.; Liu, H. W. Natural [4 + 2]-Cyclases. *Chem. Rev.* **2017**, *117* (8), 5367–5388. https://doi.org/10.1021/acs.chemrev.6b00578.
(67) Klas, K.; Tsukamoto, S.; Sherman, D. H.; Williams, R. M. Natural Diels–Alderases: Elusive and Irresistable. *J. Org. Chem.* **2015**, *80* (23), 11672–11685. https://doi.org/10.1021/acs.joc.5b01951.
(68) Healy, A. R.; Westwood, N. J. Synthetic Studies on the Bioactive Tetramic Acid JBIR-22 Using a Late Stage Diels-Alder Reaction. *Org. Biomol. Chem.* **2015**, *13* (42), 10527–10531. https://doi.org/10.1039/c5ob01771h.
(69) Sato, M.; Yagishita, F.; Mino, T.; Uchiyama, N.; Patel, A.; Chooi, Y. H.; Goda, Y.; Xu, W.; Noguchi, H.; Yamamoto, T.; et al. Involvement of Lipocalin-like CghA in Decalin-Forming Stereoselective Intramolecular [4+2] Cycloaddition. *ChemBioChem* **2015**, *16* (16), 2294–2298. https://doi.org/10.1002/cbic.201500386.
(70) Kato, N.; Nogawa, T.; Hirota, H.; Jang, J. H.; Takahashi, S.; Ahn, J. S.; Osada, H. A New Enzyme Involved in the Control of the Stereochemistry in the Decalin Formation during Equisetin Biosynthesis. *Biochem. Biophys. Res. Commun.* **2015**, *460* (2), 210–215. https://doi.org/10.1016/j.bbrc.2015.03.011.
(71) Li, L.; Yu, P.; Tang, M. C.; Zou, Y.; Gao, S. S.; Hung, Y. S.; Zhao, M.; Watanabe, K.; Houk, K. N.; Tang, Y. Biochemical Characterization of a Eukaryotic Decalin-Forming Diels-Alderase. *J. Am. Chem. Soc.* **2016**, *138* (49), 15837–15840. https://doi.org/10.1021/jacs.6b10452.
(72) Yang, Y. L.; Lu, C. P.; Chen, M. Y.; Chen, K. Y.; Wu, Y. C.; Wu, S. H. Cytotoxic Polyketides Containing Tetramic Acid Moieties Isolated from the Fungus Myceliophthora Thermophila: Elucidation of the Relationship between Cytotoxicity and Stereoconfiguration. *Chem. - A Eur. J.* **2007**, *13* (24), 6985–6991. https://doi.org/10.1002/chem.200700038.
(73) Hess, B. A.; Smentek, L. Concerted{,} Highly Asynchronous{,} Enzyme-Catalyzed [4 + 2] Cycloaddition in the Biosynthesis of Spinosyn A; Computational Evidence. *Org. Biomol. Chem.* **2012**, *10* (37), 7503–7509. https://doi.org/10.1039/C2OB25827G.
(74) Yang, Z.; Yang, S.; Yu, P.; Li, Y.; Doubleday, C.; Park, J.; Patel, A.; Jeon, B.; Russell, W. K.; Liu, H.; et al. Influence of Water and Enzyme SpnF on the Dynamics and Energetics of the Ambimodal [6+4]/[4+2] Cycloaddition. *Proc. Natl. Acad. Sci.* **2018**, *115* (5), E848 LP-E855. https://doi.org/10.1073/pnas.1719368115.
(75) Caramella, P.; Quadrelli, P.; Toma, L. An Unexpected Bispericyclic Transition Structure Leading to 4+2 and 2+4 Cycloadducts in the Endo Dimerization of Cyclopentadiene. *J. Am. Chem. Soc.* **2002**, *124* (7), 1130–1131. https://doi.org/10.1021/ja016622h.
(76) Cary, J. W.; Uka, V.; Han, Z.; Buyst, D.; Harris-Coward, P. Y.; Ehrlich, K. C.; Wei, Q.; Bhatnagar, D.; Dowd, P. F.; Martens, S. L.; et al. An Aspergillus Flavus Secondary Metabolic Gene Cluster Containing a Hybrid PKS-NRPS Is Necessary for Synthesis of the 2-Pyridones, Leporins. *Fungal Genet. Biol.* **2015**, *81*, 88–97. https://doi.org/10.1016/j.fgb.2015.05.010.
(77) Stocking, E. M.; Williams, R. M. Chemistry and Biology of Biosynthetic Diels-Alder Reactions. *Angew. Chemie - Int. Ed.* **2003**, *42* (27), 3078–3115.

https://doi.org/10.1002/anie.200200534.
(78) Jessen, H. J.; Gademann, K. 4-Hydroxy-2-Pyridone Alkaloids: Structures and Synthetic Approaches. *Nat. Prod. Rep.* **2010**, *27* (8), 1168–1185. https://doi.org/10.1039/B911516C.
(79) Snider, B. B.; Lu, Q. Total Synthesis of (±)-Leporin A. *J. Org. Chem.* **1996**, *61* (8), 2839–2844. https://doi.org/10.1021/jo952053i.
(80) Ohashi, M.; Liu, F.; Hai, Y.; Chen, M.; Tang, M.; Yang, Z.; Sato, M.; Watanabe, K.; Houk, K. N.; Tang, Y. SAM-Dependent Enzyme-Catalysed Pericyclic Reactions in Natural Product Biosynthesis. *Nature* **2017**, *549*, 502.
(81) Cope, A. C.; Hardy, E. M. The Introduction of Substituted Vinyl Groups. V. A Rearrangement Involving the Migration of an Allyl Group in a Three-Carbon System. *J. Am. Chem. Soc.* **1940**, *62* (2), 441–444. https://doi.org/10.1021/ja01859a055.
(82) Li, S.; Lowell, A. N.; Yu, F.; Raveh, A.; Newmister, S. A.; Bair, N.; Schaub, J. M.; Williams, R. M.; Sherman, D. H. Hapalindole/Ambiguine Biogenesis Is Mediated by a Cope Rearrangement, C-C Bond-Forming Cascade. *J. Am. Chem. Soc.* **2015**, *137* (49), 15366–15369. https://doi.org/10.1021/jacs.5b10136.
(83) Li, S.; Lowell, A. N.; Newmister, S. A.; Yu, F.; Williams, R. M.; Sherman, D. H. Decoding Cyclase-Dependent Assembly of Hapalindole and Fischerindole Alkaloids. *Nat. Chem. Biol.* **2017**, *13* (5), 467–469. https://doi.org/10.1038/nchembio.2327.
(84) Zhu, Q.; Liu, X. Discovery of a Calcium-Dependent Enzymatic Cascade for the Selective Assembly of Hapalindole-Type Alkaloids: On the Biosynthetic Origin of Hapalindole U. *Angew. Chemie - Int. Ed.* **2017**, *56* (31), 9062–9066. https://doi.org/10.1002/anie.201703932.
(85) Newmister, S. A.; Li, S.; Garcia-Borràs, M.; Sanders, J. N.; Yang, S.; Lowell, A. N.; Yu, F.; Smith, J. L.; Williams, R. M.; Houk, K. N.; et al. Structural Basis of the Cope Rearrangement and Cyclization in Hapalindole Biogenesis. *Nat. Chem. Biol.* **2018**, *14* (4), 345–351. https://doi.org/10.1038/s41589-018-0003-x.
(86) Walsh, C. T.; Tang, Y. Recent Advances in Enzymatic Complexity Generation: Cyclization Reactions. *Biochemistry* **2018**, *57* (22), 3087–3104. https://doi.org/10.1021/acs.biochem.7b01161.
(87) Png, Z. M.; Zeng, H.; Ye, Q.; Xu, J. Inverse-Electron-Demand Diels–Alder Reactions: Principles and Applications. *Chem. - An Asian J.* **2017**, *12* (17), 2142–2159. https://doi.org/10.1002/asia.201700442.
(88) Jiang, X.; Wang, R. Recent Developments in Catalytic Asymmetric Inverse-Electron-Demand Diels-Alder Reaction. *Chem. Rev.* **2013**, *113* (7), 5515–5546. https://doi.org/10.1021/cr300436a.
(89) Snider, B. B.; Ron, E. The Mechanism of Lewis Acid Catalyzed Ene Reactions. *J. Am. Chem. Soc.* **1985**, *107* (26), 8160–8164. https://doi.org/10.1021/ja00312a058.
(90) Mikami, K.; Shimizu, M. Asymmetric Ene Reactions in Organic Synthesis. *Chem. Rev.* **1992**, *92* (5), 1021–1050. https://doi.org/10.1021/cr00013a014.
(91) Nubbemeyer, U. Recent Advances in Asymmetric [3,3]-Sigmatropic Rearrangements. *Synthesis (Stuttg).* **2003**, *2003* (7), 961–1008. https://doi.org/10.1055/s-2003-39171.
(92) Bian, M.; Li, L.; Ding, H. Recent Advances on the Application of Electrocyclic Reactions in Complex Natural Product Synthesis. *Synth.* **2017**, *49* (19), 4383–4413. https://doi.org/10.1055/s-0036-1590870.
(93) Rosenthal, R. G.; Ebert, M. O.; Kiefer, P.; Peter, D. M.; Vorholt, J. A.; Erb, T. J. Direct Evidence for a Covalent Ene Adduct Intermediate in NAD(P)H-Dependent Enzymes. *Nat. Chem. Biol.* **2014**, *10* (1), 50–55. https://doi.org/10.1038/nchembio.1385.
(94) Katsuyama, Y.; Li, X. W.; Müller, R.; Nay, B. Chemically Unprecedented Biocatalytic (AuaG) Retro-[2,3]-Wittig Rearrangement: A New Insight into Aurachin B Biosynthesis. *ChemBioChem* **2014**, *15* (16), 2349–2352. https://doi.org/10.1002/cbic.201402373.
(95) Funel, J. A.; Abele, S. Industrial Applications of the Diels-Alder Reaction. *Angew. Chemie*

- *Int. Ed.* **2013**, *52* (14), 3822–3863. https://doi.org/10.1002/anie.201201636.
(96) Patel, P. R.; Boger, D. L. Intramolecular Diels-Alder Reactions of Cyclopropenone Ketals. *Org. Lett.* **2010**, *12* (15), 3540–3543. https://doi.org/10.1021/ol101375a.
(97) Bodwell, G. J.; Pi, Z. Electron Deficient Dienes I. Normal and Inverse Electron Demand Diels-Alder Reactions of the Same Carbon Skeleton. *Tetrahedron Lett.* **1997**, *38* (3), 309–312. https://doi.org/10.1016/S0040-4039(96)02340-4.
(98) Saha, S.; Roy, R. K.; Pal, S. CDASE - A Reliable Scheme to Explain the Reactivity Sequence between Diels-Alder Pairs. *Phys. Chem. Chem. Phys.* **2010**, *12* (32), 9328–9338. https://doi.org/10.1039/b925441b.
(99) Spino, C.; Rezaei, H.; Dory, Y. L. Characteristics of the Two Frontier Orbital Interactions in the Diels-Alder Cycloaddition. *J. Org. Chem.* **2004**, *69* (3), 757–764. https://doi.org/10.1021/jo0353740.
(100) Levandowski, B. J.; Hamlin, T. A.; Bickelhaupt, F. M.; Houk, K. N. Role of Orbital Interactions and Activation Strain (Distortion Energies) on Reactivities in the Normal and Inverse Electron-Demand Cycloadditions of Strained and Unstrained Cycloalkenes. *J. Org. Chem.* **2017**, *82* (16), 8668–8675. https://doi.org/10.1021/acs.joc.7b01673.
(101) Oliveira, B. L.; Guo, Z.; Bernardes, G. J. L. Inverse Electron Demand Diels-Alder Reactions in Chemical Biology. *Chem. Soc. Rev.* **2017**, *46* (16), 4895–4950. https://doi.org/10.1039/c7cs00184c.
(102) Jamieson, C. S.; Ohashi, M.; Liu, F.; Tang, Y.; Houk, K. N. The Expanding World of Biosynthetic Pericyclases: Cooperation of Experiment and Theory for Discovery. *Nat. Prod. Rep.* **2019**, *36* (5), 698–713. https://doi.org/10.1039/c8np00075a.
(103) Flower, D. R.; North, A. C. T.; Sansom, C. E. The Lipocalin Protein Family: Structural and Sequence Overview. *Biochim. Biophys. Acta - Protein Struct. Mol. Enzymol.* **2000**, *1482* (1–2), 9–24. https://doi.org/10.1016/S0167-4838(00)00148-5.
(104) Qiao, K.; Chooi, Y. H.; Tang, Y. Identification and Engineering of the Cytochalasin Gene Cluster from Aspergillus Clavatus NRRL 1. *Metab. Eng.* **2011**, *13* (6), 723–732. https://doi.org/10.1016/j.ymben.2011.09.008.
(105) Kato, N.; Nogawa, T.; Takita, R.; Kinugasa, K.; Kanai, M.; Uchiyama, M.; Osada, H.; Takahashi, S. Control of the Stereochemical Course of [4+2] Cycloaddition during Trans-Decalin Formation by Fsa2-Family Enzymes. *Angew. Chemie Int. Ed.* **2018**, *57* (31), 9754–9758. https://doi.org/https://doi.org/10.1002/anie.201805050.
(106) Kakule, T. B.; Lin, Z.; Schmidt, E. W. Combinatorialization of Fungal Polyketide Synthase-Peptide Synthetase Hybrid Proteins. *J. Am. Chem. Soc.* **2014**, *136* (51), 17882–17890. https://doi.org/10.1021/ja511087p.
(107) National Committee for Clinical Laboratory Standards. *Approved Standard M31-A2*; National Committee for Clinical Laboratory Standards, 2002; Vol. 2nd.
(108) Frisch, M. J.; Trucks, G. W.; Schlegel, H. B.; Scuseria, G. E.; Robb, M. A.; Cheeseman, J. R.; Scalmani, G.; Barone, V.; Mennucci, B.; Petersson, G. A.; et al. Gaussian 09. Gaussian, Inc.: Wallingford, CT 2013.
(109) Zhao, Y.; Truhlar, D. G. Density Functionals with Broad Applicability in Chemistry. *Acc. Chem. Res.* **2008**, *41* (2), 157–167. https://doi.org/10.1021/ar700111a.
(110) Cossi, M.; Rega, N.; Scalmani, G.; Barone, V. Energies, Structures, and Electronic Properties of Molecules in Solution with the C-PCM Solvation Model. *J. Comput. Chem.* **2003**, *24* (6), 669–681. https://doi.org/10.1002/jcc.10189.
(111) Tang, M. C.; Lin, H. C.; Li, D.; Zou, Y.; Li, J.; Xu, W.; Cacho, R. A.; Hillenmeyer, M. E.; Garg, N. K.; Tang, Y. Discovery of Unclustered Fungal Indole Diterpene Biosynthetic Pathways through Combinatorial Pathway Reassembly in Engineered Yeast. *J. Am. Chem. Soc.* **2015**, *137* (43), 13724–13727. https://doi.org/10.1021/jacs.5b06108.
(112) Zaghouani, M.; Nay, B. 3-Acylated Tetramic and Tetronic Acids as Natural Metal Binders: Myth or Reality? *Nat. Prod. Rep.* **2016**, *33* (4), 540–548.

https://doi.org/10.1039/c5np00144g.
(113) Tan, D.; Jamieson, C. S.; Ohashi, M.; Tang, M. C.; Houk, K. N.; Tang, Y. Genome-Mined Diels-Alderase Catalyzes Formation of the Cis-Octahydrodecalins of Varicidin A and B. *J. Am. Chem. Soc.* **2019**, *141* (2), 769–773. https://doi.org/10.1021/jacs.8b12010.
(114) Hayakawa, S.; Mlnato, H.; Katagiri, K. The Ilicicolins, Antibiotics from Cylindrocladium Ilicicola. *J. Antibiot. (Tokyo).* **1971**, *24* (9), 653–654. https://doi.org/10.7164/antibiotics.24.653.
(115) Matsumoto, M.; Minato, H. Structure of Ilicocolin H, an Antifungal Antibiotic. *Tetrahedron Lett.* **1976**, *17* (42), 3827–3830. https://doi.org/10.1016/S0040-4039(00)93121-6.
(116) Junker, B.; Zhang, J.; Mann, Z.; Reddy, J.; Greasham, R. Scale-Up Studies on a Defined Medium Process for Pilot Plant Production of Illicicolin by Gliocladiumroseum. *Biotechnol. Prog.* **2001**, *17* (2), 278–286. https://doi.org/https://doi.org/10.1021/bp0001718.
(117) Liu, X. Y.; Chen, X. C.; Qian, F.; Zhu, T. T.; Xu, J. W.; Li, Y. M.; Zhang, L. Q.; Jiao, B. H. Chlorinated Phenolic Sesquiterpenoids from the Arctic Fungus Nectria Sp. B-13. *Biochem. Syst. Ecol.* **2015**, *59*, 22–25. https://doi.org/10.1016/j.bse.2015.01.001.
(118) Kildgaard, S.; Subko, K.; Phillips, E.; Goidts, V.; De La Cruz, M.; Díaz, C.; Gotfredsen, C. H.; Andersen, B.; Frisvad, J. C.; Nielsen, K. F.; et al. A Dereplication and Bioguided Discovery Approach to Reveal New Compounds from a Marine-Derived Fungus Stilbella Fimetaria. *Mar. Drugs* **2017**, *15* (8), 253. https://doi.org/10.3390/md15080253.
(119) Singh, S. B.; Liu, W.; Li, X.; Chen, T.; Shafiee, A.; Card, D.; Abruzzo, G.; Flattery, A.; Gill, C.; Thompson, J. R.; et al. Antifungal Spectrum, in Vivo Efficacy, and Structure-Activity Relationship of Ilicicolin H. *ACS Med. Chem. Lett.* **2012**, *3* (10), 814–817. https://doi.org/10.1021/ml300173e.
(120) Singh, S. B.; Liu, W.; Li, X.; Chen, T.; Shafiee, A.; Dreikorn, S.; Hornak, V.; Meinz, M.; Onishi, J. C. Structure-Activity Relationship of Cytochrome Bc1 Reductase Inhibitor Broad Spectrum Antifungal Ilicicolin H. *Bioorg. Med. Chem. Lett.* **2013**, *23* (10), 3018–3022. https://doi.org/10.1016/j.bmcl.2013.03.023.
(121) Williams, D. R.; Bremmer, M. L.; Brown, D. L.; D'Antuono, J. Total Synthesis of (±)-Ilicicolin H. *J. Org. Chem.* **1985**, *50* (15), 2807–2809. https://doi.org/10.1021/jo00215a053.
(122) Williams, D. R.; Gaston, R. D.; Horton, I. B. Intramolecular Diels-Alder Cycloadditions of Bis-Diene Substrates. *Tetrahedron Lett.* **1985**, *26* (11), 1391–1394. https://doi.org/https://doi.org/10.1016/S0040-4039(00)99053-1.
(123) Mukherjee, D.; Watts, C. R.; Houk, K. N. Periselectivity in the [4 + 2] and [6 + 4] Cycloadditions of Diphenylnitrilimine to Tropone. *J. Org. Chem.* **1978**, *43* (5), 817–821. https://doi.org/10.1021/jo00399a006.
(124) Halo, L. M.; Heneghan, M. N.; Yakasai, A. A.; Song, Z.; Williams, K.; Bailey, A. M.; Cox, R. J.; Lazarus, C. M.; Simpson, T. J. Late Stage Oxidations during the Biosynthesis of the 2-Pyridone Tenellin in the Entomopathogenic Fungus Beauveria Bassiana. *J. Am. Chem. Soc.* **2008**, *130* (52), 17988–17996. https://doi.org/10.1021/ja807052c.
(125) He, X.; Zhang, Z.; Chen, Y.; Che, Q.; Zhu, T.; Gu, Q.; Li, D. Varitatin A, a Highly Modified Fatty Acid Amide from Penicillium Variabile Cultured with a DNA Methyltransferase Inhibitor. *J. Nat. Prod.* **2015**, *78* (11), 2841–2845. https://doi.org/10.1021/acs.jnatprod.5b00742.
(126) Schubert, H. L.; Blumenthal, R. M.; Cheng, X. Many Paths to Methyltransfer: A Chronicle of Convergence. *Trends Biochem. Sci.* **2003**, *28* (6), 329–335. https://doi.org/10.1016/S0968-0004(03)00090-2.
(127) Chai, J.-D.; Head-Gordon, M. Long-Range Corrected Hybrid Density Functionals with Damped Atom–Atom Dispersion Corrections. *Phys. Chem. Chem. Phys.* **2008**, *10* (44), 6615–6620. https://doi.org/10.1039/B810189B.
(128) Marenich, A. V; Cramer, C. J.; Truhlar, D. G. Universal Solvation Model Based on Solute Electron Density and on a Continuum Model of the Solvent Defined by the Bulk Dielectric

Constant and Atomic Surface Tensions. *J. Phys. Chem. B* **2009**, *113* (18), 6378–6396. https://doi.org/10.1021/jp810292n.
(129) Guarneri, A.; van Berkel, W. J.; Paul, C. E. Alternative Coenzymes for Biocatalysis. *Curr. Opin. Biotechnol.* **2019**, *60*, 63–71. https://doi.org/10.1016/j.copbio.2019.01.001.
(130) Dhambri, S.; Mohammad, S.; Van Buu, O. N.; Galvani, G.; Meyer, Y.; Lannou, M.-I.; Sorin, G.; Ardisson, J. Recent Advances in the Synthesis of Natural Multifunctionalized Decalins. *Nat. Prod. Rep.* **2015**, *32* (6), 841–864. https://doi.org/10.1039/c4np00142g.
(131) Zhang, Z.; Jamieson, C. S.; Zhao, Y.-L.; Li, D.; Ohashi, M.; Houk, K. N.; Tang, Y. Enzyme-Catalyzed Inverse-Electron Demand Diels–Alder Reaction in the Biosynthesis of Antifungal Ilicicolin H. *J. Am. Chem. Soc.* **2019**, *141* (14), 5659–5663. https://doi.org/10.1021/jacs.9b02204.
(132) Li, L.; Tang, M.-C.; Tang, S.; Gao, S.; Soliman, S.; Hang, L.; Xu, W.; Ye, T.; Watanabe, K.; Tang, Y. Genome Mining and Assembly-Line Biosynthesis of the UCS1025A Pyrrolizidinone Family of Fungal Alkaloids. *J. Am. Chem. Soc.* **2018**, *140* (6), 2067–2071. https://doi.org/10.1021/jacs.8b00056.
(133) Kusumi, T.; Ichikawa, A.; Kakisawa, H.; Tsunakawa, M.; Konishi, M.; Oki, T. The Structures of Quartromicins A1, A2, and A3: Novel Macrocyclic Antiviral Antibiotics Possessing Four Tetronic Acid Moieties. *J. Am. Chem. Soc.* **1991**, *113* (23), 8947–8948. https://doi.org/10.1021/ja00023a053.
(134) Li, C.-J.; Ma, J.; Sun, H.; Zhang, D.; Zhang, D.-M. Guajavadimer A, a Dimeric Caryophyllene-Derived Meroterpenoid with a New Carbon Skeleton from the Leaves of Psidium Guajava. *Org. Lett.* **2016**, *18* (2), 168–171. https://doi.org/10.1021/acs.orglett.5b03117.
(135) Yang, M.-H.; Gu, M.-L.; Han, C.; Guo, X.-J.; Yin, G.-P.; Yu, P.; Kong, L.-Y. Aureochaeglobosins A-C, Three [4 + 2] Adducts of Chaetoglobosin and Aureonitol Derivatives from Chaetomium Globosum. *Org. Lett.* **2018**, *20* (11), 3345–3348. https://doi.org/10.1021/acs.orglett.8b01243.
(136) El-Elimat, T.; Raja, H. A.; Ayers, S.; Kurina, S. J.; Burdette, J. E.; Mattes, Z.; Sabatelle, R.; Bacon, J. W.; Colby, A. H.; Grinstaff, M. W.; et al. Meroterpenoids from Neosetophoma Sp.: A Dioxa[4.3.3]Propellane Ring System, Potent Cytotoxicity, and Prolific Expression. *Org. Lett.* **2019**, *21* (2), 529–534. https://doi.org/10.1021/acs.orglett.8b03769.
(137) Cai, P.; Smith, D.; Cunningham, B.; Brown-Shimer, S.; Katz, B.; Pearce, C.; Venables, D.; Houck, D. Epolones: Novel Sesquiterpene-Tropolones from Fungus OS-F69284 That Induce Erythropoietin in Human Cells. *J. Nat. Prod.* **1998**, *61* (6), 791–795. https://doi.org/10.1021/np9800506.
(138) Mayerl, F.; Gao, Q.; Huang, S.; Klohr, S. E.; Matson, J. A.; Gustavson, D. R.; Pirnik, D. M.; Berry, R. L.; Fairchild, C.; Rose, W. C. Eupenifeldin, a Novel Cytotoxic Bistropolone from Eupenicillium Brefeldianum. *J. Antibiot. (Tokyo).* **1993**, *46* (7), 1082–1088. https://doi.org/10.7164/antibiotics.46.1082.
(139) Hsiao, C.-J.; Hsiao, S.-H.; Chen, W.-L.; Guh, J.-H.; Hsiao, G.; Chan, Y.-J.; Lee, T.-H.; Chung, C.-L. Pycnidione, a Fungus-Derived Agent, Induces Cell Cycle Arrest and Apoptosis in A549 Human Lung Cancer Cells. *Chem. Biol. Interact.* **2012**, *197* (1), 23–30. https://doi.org/10.1016/j.cbi.2012.03.004.
(140) Guo, H.; Roman, D.; Beemelmanns, C. Tropolone Natural Products. *Nat. Prod. Rep.* **2019**, *36* (8), 1137–1155. https://doi.org/10.1039/c8np00078f.
(141) Baldwin, J. E.; Mayweg, A. V; Neumann, K.; Pritchard, G. J. Studies toward the Biomimetic Synthesis of Tropolone Natural Products via a Hetero Diels-Alder Reaction. *Org. Lett.* **1999**, *1* (12), 1933–1935. https://doi.org/10.1021/ol991067y.
(142) Adlington, R. M.; Baldwin, J. E.; Mayweg, A. V. W.; Pritchard, G. J. Biomimetic Cycloaddition Approach to Tropolone Natural Products via a Tropolone Ortho-Quinone Methide. *Org. Lett.* **2002**, *4* (17), 3009–3011. https://doi.org/10.1021/ol026467r.

(143) Adlington, R. M.; Baldwin, J. E.; Pritchard, G. J.; Williams, A. J.; Watkin, D. J. A Biomimetic Synthesis of Lucidene. *Org. Lett.* **1999**, *1* (12), 1937–1939. https://doi.org/10.1021/ol991068q.
(144) Zhang, J.; Liu, L.; Wang, B.; Zhang, Y.; Wang, L.; Liu, X.; Che, Y. Phomanolides A and B from the Fungus Phoma Sp.: Meroterpenoids Derived from a Putative Tropolonic Sesquiterpene via Hetero-Diels-Alder Reactions. *J. Nat. Prod.* **2015**, *78* (12), 3058–3066. https://doi.org/10.1021/acs.jnatprod.5b00969.
(145) al Fahad, A.; Abood, A.; Simpson, T. J.; Cox, R. J. The Biosynthesis and Catabolism of the Maleic Anhydride Moiety of Stipitatonic Acid. *Angew. Chem. Int. Ed. Engl.* **2014**, *53* (29), 7519–7523. https://doi.org/10.1002/anie.201403450.
(146) Yan, D.; Chen, Q.; Gao, J.; Bai, J.; Liu, B.; Zhang, Y.; Zhang, L.; Zhang, C.; Zou, Y.; Hu, Y. Complexity and Diversity Generation in the Biosynthesis of Fumiquinazoline-Related Peptidyl Alkaloids. *Org. Lett.* **2019**, *21* (5), 1475–1479. https://doi.org/10.1021/acs.orglett.9b00260.
(147) Schor, R.; Schotte, C.; Wibberg, D.; Kalinowski, J.; Cox, R. J. Three Previously Unrecognised Classes of Biosynthetic Enzymes Revealed during the Production of Xenovulene A. *Nat. Commun.* **2018**, *9* (1), 1963. https://doi.org/10.1038/s41467-018-04364-9.
(148) Zhai, Y.; Li, Y.; Zhang, J.; Zhang, Y.; Ren, F.; Zhang, X.; Liu, G.; Liu, X.; Che, Y. Identification of the Gene Cluster for Bistropolone-Humulene Meroterpenoid Biosynthesis in Phoma Sp. *Fungal Genet. Biol.* **2019**, *129*, 7–15. https://doi.org/10.1016/j.fgb.2019.04.004.
(149) Cai, Y.; Hai, Y.; Ohashi, M.; Jamieson, C. S.; Garcia-Borras, M.; Houk, K. N.; Zhou, J.; Tang, Y. Structural Basis for Stereoselective Dehydration and Hydrogen-Bonding Catalysis by the SAM-Dependent Pericyclase LepI. *Nat. Chem.* **2019**, *11* (9), 812–820. https://doi.org/10.1038/s41557-019-0294-x.
(150) Adamo, C.; Barone, V. Toward Reliable Density Functional Methods without Adjustable Parameters: The PBE0 Model. *J. Chem. Phys.* **1999**, *110* (13), 6158–6170. https://doi.org/10.1063/1.478522.
(151) Grimme, S.; Antony, J.; Ehrlich, S.; Krieg, H. A Consistent and Accurate Ab Initio Parametrization of Density Functional Dispersion Correction (DFT-D) for the 94 Elements H-Pu. *J. Chem. Phys.* **2010**, *132* (15), 154104. https://doi.org/10.1063/1.3382344.
(152) Grimme, S.; Ehrlich, S.; Goerigk, L. Effect of the Damping Function in Dispersion Corrected Density Functional Theory. *J. Comput. Chem.* **2011**, *32* (7), 1456–1465. https://doi.org/10.1002/jcc.21759.
(153) Weigend, F.; Ahlrichs, R. Balanced Basis Sets of Split Valence, Triple Zeta Valence and Quadruple Zeta Valence Quality for H to Rn: Design and Assessment of Accuracy. *Phys. Chem. Chem. Phys.* **2005**, *7* (18), 3297–3305. https://doi.org/10.1039/B508541A.
(154) Frisch, M. J.; Trucks, G. W.; Schlegel, H. B.; Scuseria, G. E.; Robb, M. A.; Cheeseman, J. R.; Scalmani, G.; Barone, V.; Petersson, G. A.; Nakatsuji, H.; et al. Gaussian 16 Revision A.03. 2016.
(155) Ernzerhof, M.; Scuseria, G. E. Assessment of the Perdew–Burke–Ernzerhof Exchange-Correlation Functional. *J. Chem. Phys.* **1999**, *110* (11), 5029–5036. https://doi.org/10.1063/1.478401.
(156) Fage, C. D.; Isiorho, E. A.; Liu, Y.; Wagner, D. T.; Liu, H.; Keatinge-Clay, A. T. The Structure of SpnF, a Standalone Enzyme That Catalyzes [4 + 2] Cycloaddition. *Nat. Chem. Biol.* **2015**, *11* (4), 256–258. https://doi.org/10.1038/nchembio.1768.
(157) Chook, Y. M.; Ke, H.; Lipscomb, W. N. Crystal Structures of the Monofunctional Chorismate Mutase from Bacillus Subtilis and Its Complex with a Transition State Analog. *Proc. Natl. Acad. Sci.* **1993**, *90* (18), 8600 LP – 8603. https://doi.org/10.1073/pnas.90.18.8600.
(158) Zaitseva, J.; Lu, J.; Olechoski, K. L.; Lamb, A. L. Two Crystal Structures of the

Isochorismate Pyruvate Lyase from Pseudomonas Aeruginosa. *J. Biol. Chem.* **2006**, *281* (44), 33441–33449. https://doi.org/10.1074/jbc.M605470200.
(159) Zheng, Q.; Guo, Y.; Yang, L.; Zhao, Z.; Wu, Z.; Zhang, H.; Liu, J.; Cheng, X.; Wu, J.; Yang, H.; et al. Enzyme-Dependent [4 + 2] Cycloaddition Depends on Lid-like Interaction of the N-Terminal Sequence with the Catalytic Core in PyrI4. *Cell Chem. Biol.* **2016**, *23* (3), 352–360. https://doi.org/10.1016/j.chembiol.2016.01.005.
(160) Liscombe, D. K.; Louie, G. V; Noel, J. P. Architectures, Mechanisms and Molecular Evolution of Natural Product Methyltransferases. *Nat. Prod. Rep.* **2012**, *29* (10), 1238–1250. https://doi.org/10.1039/c2np20029e.
(161) Krissinel, E.; Henrick, K. Inference of Macromolecular Assemblies from Crystalline State. *J. Mol. Biol.* **2007**, *372* (3), 774–797. https://doi.org/10.1016/j.jmb.2007.05.022.
(162) Newmister, S. A.; Romminger, S.; Schmidt, J. J.; Williams, R. M.; Smith, J. L.; Berlinck, R. G. S.; Sherman, D. H. Unveiling Sequential Late-Stage Methyltransferase Reactions in the Meleagrin/Oxaline Biosynthetic Pathway. *Org. Biomol. Chem.* **2018**, *16* (35), 6450–6459. https://doi.org/10.1039/c8ob01565a.
(163) Holm, L.; Rosenström, P. Dali Server: Conservation Mapping in 3D. *Nucleic Acids Res.* **2010**, *38* (Web Server issue), W545–W549. https://doi.org/10.1093/nar/gkq366.
(164) Horowitz, S.; Dirk, L. M. A.; Yesselman, J. D.; Nimtz, J. S.; Adhikari, U.; Mehl, R. A.; Scheiner, S.; Houtz, R. L.; Al-Hashimi, H. M.; Trievel, R. C. Conservation and Functional Importance of Carbon-Oxygen Hydrogen Bonding in AdoMet-Dependent Methyltransferases. *J. Am. Chem. Soc.* **2013**, *135* (41), 15536–15548. https://doi.org/10.1021/ja407140k.
(165) Fick, R. J.; Clay, M. C.; Vander Lee, L.; Scheiner, S.; Al-Hashimi, H.; Trievel, R. C. Water-Mediated Carbon-Oxygen Hydrogen Bonding Facilitates S-Adenosylmethionine Recognition in the Reactivation Domain of Cobalamin-Dependent Methionine Synthase. *Biochemistry* **2018**, *57* (26), 3733–3740. https://doi.org/10.1021/acs.biochem.8b00375.
(166) Zheng, Q.; Gong, Y.; Guo, Y.; Zhao, Z.; Wu, Z.; Zhou, Z.; Chen, D.; Pan, L.; Liu, W. Structural Insights into a Flavin-Dependent [4 + 2] Cyclase That Catalyzes Trans-Decalin Formation in Pyrroindomycin Biosynthesis. *Cell Chem. Biol.* **2018**, *25* (6), 718-727.e3. https://doi.org/10.1016/j.chembiol.2018.03.007.
(167) Breslow, R. Hydrophobic Effects on Simple Organic Reactions in Water. *Acc. Chem. Res.* **1991**, *24* (6), 159–164. https://doi.org/10.1021/ar00006a001.
(168) Blokzijl, W.; Blandamer, M. J.; Engberts, J. B. F. N. Diels-Alder Reactions in Aqueous Solutions. Enforced Hydrophobic Interactions between Diene and Dienophile. *J. Am. Chem. Soc.* **1991**, *113* (11), 4241–4246. https://doi.org/10.1021/ja00011a029.
(169) Lee, A. Y.; Stewart, J. D.; Clardy, J.; Ganem, B. New Insight into the Catalytic Mechanism of Chorismate Mutases from Structural Studies. *Chem. Biol.* **1995**, *2* (4), 195–203. https://doi.org/10.1016/1074-5521(95)90269-4.
(170) Burschowsky, D.; van Eerde, A.; Ökvist, M.; Kienhöfer, A.; Kast, P.; Hilvert, D.; Krengel, U. Electrostatic Transition State Stabilization Rather than Reactant Destabilization Provides the Chemical Basis for Efficient Chorismate Mutase Catalysis. *Proc. Natl. Acad. Sci. U. S. A.* **2014**, *111* (49), 17516–17521. https://doi.org/10.1073/pnas.1408512111.
(171) Warshel, A.; Sharma, P. K.; Kato, M.; Xiang, Y.; Liu, H.; Olsson, M. H. M. Electrostatic Basis for Enzyme Catalysis. *Chem. Rev.* **2006**, *106* (8), 3210–3235. https://doi.org/10.1021/cr0503106.
(172) Smith, P. J.; Wilcox, C. S. The Chemistry of Functional Group Arrays. Electrostatic Catalysis and the “Intramolecular Salt Effect”. *Tetrahedron* **1991**, *47* (14), 2617–2628. https://doi.org/https://doi.org/10.1016/S0040-4020(01)81794-4.
(173) Fried, S. D.; Boxer, S. G. Electric Fields and Enzyme Catalysis. *Annu. Rev. Biochem.* **2017**, *86* (1), 387–415. https://doi.org/10.1146/annurev-biochem-061516-044432.
(174) Welborn, V. V.; Ruiz Pestana, L.; Head-Gordon, T. Computational Optimization of Electric

Fields for Better Catalysis Design. *Nat. Catal.* **2018**, *1* (9), 649–655. https://doi.org/10.1038/s41929-018-0109-2.
(175) Shaik, S.; Mandal, D.; Ramanan, R. Oriented Electric Fields as Future Smart Reagents in Chemistry. *Nat. Chem.* **2016**, *8*, 1091.
(176) Aragonès, A. C.; Haworth, N. L.; Darwish, N.; Ciampi, S.; Bloomfield, N. J.; Wallace, G. G.; Diez-Perez, I.; Coote, M. L. Electrostatic Catalysis of a Diels–Alder Reaction. *Nature* **2016**, *531*, 88.
(177) Dan, Q.; Newmister, S. A.; Klas, K. R.; Fraley, A. E.; McAfoos, T. J.; Somoza, A. D.; Sunderhaus, J. D.; Ye, Y.; Shende, V. V; Yu, F.; et al. Fungal Indole Alkaloid Biogenesis through Evolution of a Bifunctional Reductase/Diels–Alderase. *Nat. Chem.* **2019**, *11* (11), 972–980. https://doi.org/10.1038/s41557-019-0326-6.
(178) Gustin, D. J.; Mattei, P.; Kast, P.; Wiest, O.; Lee, L.; Cleland, W. W.; Hilvert, D. Heavy Atom Isotope Effects Reveal a Highly Polarized Transition State for Chorismate Mutase. *J. Am. Chem. Soc.* **1999**, *121* (8), 1756–1757. https://doi.org/10.1021/ja9841759.
(179) Wever, W. J.; Bogart, J. W.; Baccile, J. A.; Chan, A. N.; Schroeder, F. C.; Bowers, A. A. Chemoenzymatic Synthesis of Thiazolyl Peptide Natural Products Featuring an Enzyme-Catalyzed Formal [4 + 2] Cycloaddition. *J. Am. Chem. Soc.* **2015**, *137* (10), 3494–3497. https://doi.org/10.1021/jacs.5b00940.
(180) Bailey, S. S.; Payne, K. A. P.; Saaret, A.; Marshall, S. A.; Gostimskaya, I.; Kosov, I.; Fisher, K.; Hay, S.; Leys, D. Enzymatic Control of Cycloadduct Conformation Ensures Reversible 1,3-Dipolar Cycloaddition in a PrFMN-Dependent Decarboxylase. *Nat. Chem.* **2019**, *11* (11), 1049–1057. https://doi.org/10.1038/s41557-019-0324-8.
(181) Chen, Q.; Gao, J.; Jamieson, C.; Liu, J.; Ohashi, M.; Bai, J.; Yan, D.; Liu, B.; Che, Y.; Wang, Y.; et al. Enzymatic Intermolecular Hetero-Diels-Alder Reaction in the Biosynthesis of Tropolonic Sesquiterpenes. *J. Am. Chem. Soc.* **2019**, *141* (36), 14052–14056. https://doi.org/10.1021/jacs.9b06592.
(182) Little, R.; Paiva, F. C. R.; Jenkins, R.; Hong, H.; Sun, Y.; Demydchuk, Y.; Samborskyy, M.; Tosin, M.; Leeper, F. J.; Dias, M. V. B.; et al. Unexpected Enzyme-Catalysed [4+2] Cycloaddition and Rearrangement in Polyether Antibiotic Biosynthesis. *Nat. Catal.* **2019**. https://doi.org/10.1038/s41929-019-0351-2.
(183) Woodward, R. B.; Hoffmann, R. The Conservation of Orbital Symmetry. *Angew. Chemie Int. Ed. English* **1969**, *8* (11), 781–853. https://doi.org/10.1002/anie.196907811.
(184) Corey, E. J.; Cheng, X. M. *The Logic of Chemical Synthesis*; Wiley: New York, NY, USA, 1989.
(185) Hoffmann, H. M. R. The Ene Reaction. *Angew. Chemie Int. Ed. English* **1969**, *8* (8), 556–577. https://doi.org/10.1002/anie.196905561.
(186) Alder, K. Nobel Lectures, Chemistry 1942–1962; Elsevier Publishing Company: Amsterdam, 1964; pp 267–303.
(187) Niu, D.; Hoye, T. R. The Aromatic Ene Reaction. *Nat. Chem.* **2014**, *6* (1), 34–40. https://doi.org/10.1038/nchem.1797.
(188) Jensen, A. W.; Mohanty, D. K.; Dilling, W. L. The Growing Relevance of Biological Ene Reactions. *Bioorg. Med. Chem.* **2019**, *27* (5), 686–691. https://doi.org/https://doi.org/10.1016/j.bmc.2019.01.020.
(189) Lin, C.-I.; McCarty, R. M.; Liu, H. The Enzymology of Organic Transformations: A Survey of Name Reactions in Biological Systems. *Angew. Chemie Int. Ed.* **2017**, *56* (13), 3446–3489. https://doi.org/10.1002/anie.201603291.
(190) Snider, B. B.; Lu, Q. Total Synthesis of (.+-.)-Pyridoxatin. *J. Org. Chem.* **1994**, *59* (26), 8065–8070. https://doi.org/10.1021/jo00105a024.
(191) Snider, B. B.; Qing, L. A Two-Step Synthesis of Pyridoxatin Analogues. *Tetrahedron Lett.* **1994**, *35* (4), 531–534. https://doi.org/https://doi.org/10.1016/S0040-4039(00)75830-8.
(192) Jones, I. L.; Moore, F. K.; Chai, C. L. L. Total Synthesis of (±)-Cordypyridones A and B and

Related Epimers. *Org. Lett.* **2009**, *11* (23), 5526–5529. https://doi.org/10.1021/ol9023437.
(193) Appendino, G.; Cravotto, G.; Toma, L.; Annunziata, R.; Palmisano, G. The Chemistry of Coumarin Derivatives. Part VI. Diels-Alder Trapping of 3-Methylene-2,4-Chromandione. A New Entry to Substituted Pyrano[3,2-c]Coumarins. *J. Org. Chem.* **1994**, *59* (19), 5556–5564. https://doi.org/10.1021/jo00098a013.
(194) Qiao, Y.; Xu, Q.; Feng, W.; Tao, L.; Li, X.-N.; Liu, J.; Zhu, H.; Lu, Y.; Wang, J.; Qi, C.; et al. Asperpyridone A: An Unusual Pyridone Alkaloid Exerts Hypoglycemic Activity through the Insulin Signaling Pathway. *J. Nat. Prod.* **2019**, *82* (10), 2925–2930. https://doi.org/10.1021/acs.jnatprod.9b00188.
(195) McBrien, K. D.; Gao, Q.; Huang, S.; Klohr, S. E.; Wang, R. R.; Pirnik, D. M.; Neddermann, K. M.; Bursuker, I.; Kadow, K. F.; Leet, J. E. Fusaricide, a New Cytotoxic N-Hydroxypyridone from Fusarium Sp. *J. Nat. Prod.* **1996**, *59* (12), 1151–1153. https://doi.org/10.1021/np960521t.
(196) Li, C.; Sarotti, A. M.; Yang, B.; Turkson, J.; Cao, S. A New N-Methoxypyridone from the Co-Cultivation of Hawaiian Endophytic Fungi Camporesia Sambuci FT1061 and Epicoccum Sorghinum FT1062. *Molecules (Basel, Switzerland)*. Department of Pharmaceutical Sciences, Daniel K. Inouye College of Pharmacy, University of Hawai'i at Hilo, 200 West Kawili Street, Hilo, HI 96720, USA. chunshun@hawaii.edu. 2017. https://doi.org/10.3390/molecules22071166.
(197) Lee, H. J.; Chung, M. C.; Lee, C. H.; Chun, H. K.; Kim, H. M.; Kho, Y. H. Pyridoxatin, an Inhibitor of Gelatinase A with Cytotoxic Activity. *J. Microbiol. Biotechnol.* **1996**, *6* (6), 445–450.
(198) Singh, M. S.; Nagaraju, A.; Anand, N.; Chowdhury, S. Ortho-Quinone Methide (o-QM): A Highly Reactive, Ephemeral and Versatile Intermediate in Organic Synthesis. *RSC Adv.* **2014**, *4* (99), 55924–55959. https://doi.org/10.1039/C4RA11444B.
(199) Singh, S.; Chang, A.; Goff, R. D.; Bingman, C. A.; Grüschow, S.; Sherman, D. H.; Phillips Jr., G. N.; Thorson, J. S. Structural Characterization of the Mitomycin 7-O-Methyltransferase. *Proteins Struct. Funct. Bioinforma.* **2011**, *79* (7), 2181–2188. https://doi.org/10.1002/prot.23040.
(200) Hoffmann, R.; Woodward, R. B. Selection Rules for Concerted Cycloaddition Reactions. *J. Am. Chem. Soc.* **1965**, *87* (9), 2046–2048. https://doi.org/10.1021/ja01087a034.
(201) Hoffmann, R.; Woodward, R. B. Orbital Symmetries and Endo-Exo Relationships in Concerted Cycloaddition Reactions. *J. Am. Chem. Soc.* **1965**, *87* (19), 4388–4389. https://doi.org/10.1021/ja00947a033.
(202) Cookson, R. C.; Drake, B. V; Hudec, J.; Morrison, A. The Adduct of Tropone and Cyclopentadiene: A New Type of Cyclic Reaction. *Chem. Commun.* **1966**, No. 1, 15–16. https://doi.org/10.1039/C19660000015.
(203) Itô, S.; Fujise, Y.; Okuda, T.; Inoue, Y. Reaction of Tropone with Cyclopentadiene. *Bull. Chem. Soc. Jpn.* **1966**, *39* (6), 1351. https://doi.org/10.1246/bcsj.39.1351.
(204) Itô, S.; Sakan, K.; Fujise, Y. Cycloaddition Reaction of Tropone and Cyclopentadiene. *Tetrahedron Lett.* **1970**, *11* (33), 2873–2876. https://doi.org/10.1016/S0040-4039(01)98362-5.
(205) Houk, K. N.; Woodward, R. B. Cycloaddition Reactions of Tropone and 2,5-Dimethyl-3,4-Diphenylcyclopentadienone. *J. Am. Chem. Soc.* **1970**, *92* (13), 4145–4147. https://doi.org/10.1021/ja00716a074.
(206) Mcleod, D.; Thøgersen, M. K.; Jessen, N. I.; Jørgensen, K. A.; Jamieson, C. S.; Xue, X. S.; Houk, K. N.; Liu, F.; Hoffmann, R. Expanding the Frontiers of Higher-Order Cycloadditions. *Acc. Chem. Res.* **2019**, *52* (12), 3488–3501. https://doi.org/10.1021/acs.accounts.9b00498.
(207) Itô, S.; Fujise, Y.; Woods, M. C. Pentacyclo[7.5.0.02,7.05,13.06,12]Tetradeca-3,10-Dien-8-One. *Tetrahedron Lett.* **1967**, *8* (12), 1059–1064. https://doi.org/10.1016/S0040-

4039(00)90636-1.
(208) Itô, S.; Fujise, Y.; Sato, M. Structure Determination of 2-Methoxytropone-Cycloheptatriene Adducts by Mass Spectrometry. *Tetrahedron Lett.* **1969**, *10* (9), 691–694. https://doi.org/10.1016/S0040-4039(01)87784-4.
(209) Fukazawa, Y.; Ito, S.; Iitaka, Y. The Crystal and Molecular Structure of 2-Chlorotropone–Cycloheptatriene Adduct. *Acta Crystallogr. Sect. B* **1969**, *25* (4), 665–673. https://doi.org/10.1107/S0567740869002792.
(210) Fujise, Y.; Nakatsu, T.; Itô, S. Acetolysis of Pentacyclo[7.5.0.02,705,1306,12]Tetradeca-3, 10-Dien-8-Yl Toluene-p-Sulfonate. *Tetrahedron Lett.* **1975**, *16* (44), 3821–3824. https://doi.org/10.1016/S0040-4039(00)91284-X.
(211) Pham, H. V; Houk, K. N. Diels–Alder Reactions of Allene with Benzene and Butadiene: Concerted, Stepwise, and Ambimodal Transition States. *J. Org. Chem.* **2014**, *79* (19), 8968–8976. https://doi.org/10.1021/jo502041f.
(212) Caramella, P.; Quadrelli, P.; Toma, L.; Romano, S.; Khuong, K. S.; Northrop, B.; Houk, K. N. The Three Corrugated Surfaces of 1,4-Divinyltetramethylene Diradical Intermediates and Their Connections to 1,2-Divinylcyclobutane, 4-Vinylcyclohexene, 1,5-Cyclooctadiene, and Two Butadienes. *J. Org. Chem.* **2005**, *70* (8), 2994–3008. https://doi.org/10.1021/jo0501947.
(213) Wang, Z.; Hirschi, J. S.; Singleton, D. A. Recrossing and Dynamic Matching Effects on Selectivity in a Diels-Alder Reaction. *Angew. Chem. Int. Ed. Engl.* **2009**, *48* (48), 9156–9159. https://doi.org/10.1002/anie.200903293.
(214) Gonzalez-James, O. M.; Kwan, E. E.; Singleton, D. A. Entropic Intermediates and Hidden Rate-Limiting Steps in Seemingly Concerted Cycloadditions. Observation, Prediction, and Origin of an Isotope Effect on Recrossing. *J. Am. Chem. Soc.* **2012**, *134* (4), 1914–1917. https://doi.org/10.1021/ja208779k.
(215) Xue, X. S.; Jamieson, C. S.; Garcia-Borràs, M.; Dong, X.; Yang, Z.; Houk, K. N. Ambimodal Trispericyclic Transition State and Dynamic Control of Periselectivity. *J. Am. Chem. Soc.* **2019**, *141* (3), 1217–1221. https://doi.org/10.1021/jacs.8b12674.
(216) Guo, Y.; Riplinger, C.; Becker, U.; Liakos, D. G.; Minenkov, Y.; Cavallo, L.; Neese, F. Communication: An Improved Linear Scaling Perturbative Triples Correction for the Domain Based Local Pair-Natural Orbital Based Singles and Doubles Coupled Cluster Method [DLPNO-CCSD(T)]. *J. Chem. Phys.* **2018**, *148* (1), 11101. https://doi.org/10.1063/1.5011798.
(217) Dunning, T. H. Gaussian Basis Sets for Use in Correlated Molecular Calculations. I. The Atoms Boron through Neon and Hydrogen. *J. Chem. Phys.* **1989**, *90* (2), 1007–1023. https://doi.org/10.1063/1.456153.
(218) Neese, F. The ORCA Program System. *Wiley Interdiscip. Rev. Comput. Mol. Sci.* **2012**, *2* (1), 73–78. https://doi.org/10.1002/wcms.81.
(219) Neese, F. Software Update: The ORCA Program System, Version 4.0. *WIREs Comput. Mol. Sci.* **2018**, *8* (1), e1327. https://doi.org/10.1002/wcms.1327.
(220) Goldstein, E.; Beno, B. R.; Houk, K. N. Transition Structures and Exo/Endo Stereoselectivities of Concerted [6 + 4] Cycloadditions with Density Functional Theory. *Theor. Chem. Acc.* **1999**, *103* (1), 81–84. https://doi.org/10.1007/s002140050517.
(221) Houk, K. N.; Gonzalez, J.; Li, Y. Pericyclic Reaction Transition States: Passions and Punctilios, 1935-1995. *Acc. Chem. Res.* **1995**, *28* (2), 81–90. https://doi.org/10.1021/ar00050a004.
(222) Leach, A. G.; Goldstein, E.; Houk, K. N. A Cornucopia of Cycloadducts: Theoretical Predictions of the Mechanisms and Products of the Reactions of Cyclopentadiene with Cycloheptatriene. *J. Am. Chem. Soc.* **2003**, *125* (27), 8330–8339. https://doi.org/10.1021/ja029694x.
(223) Yu, P.; Chen, T. Q.; Yang, Z.; He, C. Q.; Patel, A.; Lam, Y.; Liu, C.-Y.; Houk, K. N.

Mechanisms and Origins of Periselectivity of the Ambimodal {$[$}6 + 4{$]$} Cycloadditions of Tropone to Dimethylfulvene. *J. Am. Chem. Soc.* **2017**, *139* (24), 8251–8258. https://doi.org/10.1021/jacs.7b02966.

(224) Singh, V. Periselective Reactions of Tropone: A Novel Tandem Π6s + Π4s, Π4s + Π2s Reaction with Cycloheptatriene and Π4s + Π2s Cycloaddition with Cyclohexa-2,4-Dienone. *Indian J. Chem. Sect. B* **1995**, *34B* (10), 847–850.

(225) Burns, J. M. Computational Evidence for a Reaction Pathway Bifurcation in Sasaki-Type (4 + 3)-Cycloadditions. *Org. Biomol. Chem.* **2018**, *16* (11), 1828–1836. https://doi.org/10.1039/C8OB00075A.

(226) Chen, S.; Yu, P.; Houk, K. N. Ambimodal Dipolar/Diels–Alder Cycloaddition Transition States Involving Proton Transfers. *J. Am. Chem. Soc.* **2018**, *140* (51), 18124–18131. https://doi.org/10.1021/jacs.8b11080.

(227) Singleton, D. A.; Hang, C.; Szymanski, M. J.; Greenwald, E. E. A New Form of Kinetic Isotope Effect. Dynamic Effects on Isotopic Selectivity and Regioselectivity. *J. Am. Chem. Soc.* **2003**, *125* (5), 1176–1177. https://doi.org/10.1021/ja027221k.

(228) Bailey, J. O.; Singleton, D. A. Failure and Redemption of Statistical and Nonstatistical Rate Theories in the Hydroboration of Alkenes. *J. Am. Chem. Soc.* **2017**, *139* (44), 15710–15723. https://doi.org/10.1021/jacs.7b07175.